Saliency-based sensorless control for AC induction machines in wind applications

by

Geber Villa Fernández

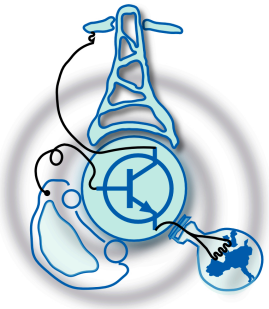

Submitted to the Department of Electrical Engineering, Electronics, Computers and Systems
in partial fulfillment of the requirements for the degree of

Master of Science in Electrical Energy Conversion and Power Systems

at the

UNIVERSIDAD DE OVIEDO

July 2016

Author .....

Certified by .....

Pablo García Fernández
Associate Professor
Thesis Supervisor

Saliency-based sensorless control for AC induction machines in wind applications

by

Geber Villa Fernández

Submitted to the Department of Electrical Engineering, Electronics, Computers and Systems
on July 22, 2016, in partial fulfillment of the
requirements for the degree of
Master of Science in Electrical Energy Conversion and Power Systems

Abstract

The master thesis explores the uses of saliency-tracking methods for the sensorless control of induction machines in wind applications in the low speed region. The study is focused on a feasibility analysis of the technique under the typical speed/load conditions. In order to improve the system accuracy as well as extended load operation, decoupling of saturation-induced saliencies is also considered.

Thesis Supervisor: Pablo García Fernández
Title: Associate Professor

Contents

List of Figures

List of Tables

List of Symbols

Acronyms

AC	Alternating Current
BPF	Band-Pass Filter
FFT	Fast Fourier Transform
FOC	Field Oriented Control
HPF	High-Pass Filter
LPF	Low-Pass Filter
PLL	Phase-Locked Loop
PWM	Pulse-Width Modulation
VSC	Voltage Source Converter

Frame references

e	saliency synchronous reference frame
r	rotor synchronous reference frame
rf	rotor flux synchronous reference frame
s	stationary reference frame
neg	negative sequence synchronous reference frame
pos	positive sequence synchronous reference frame

Functions

max maximum

min minimum

Subscripts

q, d qd reference frame components

r rotor

s stator

Superscripts

$\wedge$ estimated value

$*$ reference value

Variables

F friction

h harmonic number of saliency

i current

i^s_{qdr} qd rotor current in stationary reference frame

$i^s_{qdr\_c}$ qd carrier rotor current in stationary reference frame

$i^{neg}_{qds\_c}$ qd carrier stator current in negative sequence synchronous reference frame

$i^{pos}_{qds\_c}$ qd carrier stator current in positive sequence synchronous reference frame

$i^{pos}_{qds\_c\_filt}$ filtered qd carrier stator current in positive sequence synchronous reference frame

i^r_{qds} qd stator current in rotor synchronous reference frame

i^{rf}_{qds} qd stator current in rotor flux synchronous reference frame

i^s_{qds} qd stator current in stationary reference frame

$i^s_{qds\_c}$	qd carrier stator current in stationary reference frame
I_{sc_n}	magnitude of positive sequence carrier stator current
I_{sc_p}	magnitude of positive sequence carrier stator current
J	inertia
j	imaginary unit
K_i	integral gain
K_p	proportional gain
L	inductance
λ	flux linkage
λ^r_{qdr}	rotor flux linkage in rotor synchronous reference frame
λ^s_{qdr}	rotor flux linkage in stationary reference frame
λ^s_{qds}	stator flux linkage in stationary reference frame
λ_r	magnitude of rotor flux linkage
L_m	magnetizing inductance
$L_{\sigma s}$	stator transient inductance
$\Delta L_{\sigma s}$	differential stator transient inductance
$\Sigma L_{\sigma s}$	average stator transient inductance
L_r	rotor inductance
L_s	stator inductance
ΔL_{sal}	saliency inductance
N_r	number of rotor slots
N_s	number of stator slots
ω	angular speed/frequency
ω_{agp}	airgap permeance variation speed

ω_{br}	complex speed variable
ω_c	carrier frequency
ω_e	saliency frequency (rotor or flux dependant)
ω_r	electrical rotor speed
ω_{rm}	mechanical rotor speed
p	differential operator
ϕ	phase shift
ϕ_e	electrical saliency phase shift (rotor or flux dependant)
p_p	pole pairs
R	resistance
R_r	rotor resistance
R_s	stator resistance
R'_s	stator transient resistance
T	torque
t	time
θ	angular position
θ_c	electrical carrier signal position
θ_e	electrical saliency position (rotor or flux dependant)
θ_r	electrical rotor position
T_m	load torque
v	voltage
V_{DC}	DC bus voltage
v^s_{qds}	qd stator voltage in stationary reference frame
$v^s_{qds\_c}$	qd carrier stator voltage in stationary reference frame

V_{sc}	magnitude of carrier stator voltage

Chapter 1

Introduction

The control of AC induction machines is a key aspect in industry since a lot of industrial applications require some kind of rotational motion and induction machines are widely extended to carry out this purpose. While it is true that permanent magnet machines are replacing induction machines for new applications, the high cost of magnetic materials implies that induction machines remain important for some applications, such as wind energy generation.

A commonly used technique in order to carry out the control of AC machines is known as Field Oriented Control (FOC). The main objective of FOC is to transform the three-phase magnitudes of the machine (voltage, current and fluxes) into a reference frame in synchronization with the rotor flux (qd synchronous reference frame). In this way, the magnitudes are going to be represented by two components, one aligned (d axis) and the other one orthogonal (q axis) to the rotor flux. Therefore, both flux and torque of the machine can be controlled independently by injecting current in the qd synchronous reference frame: d-axis current for controlling the flux and q-axis current for controlling the torque.

The main challenge of FOC in induction machines is to perform the synchronization with the rotor flux since its position cannot be directly known. Unlike in synchronous machines, in which the operating/mechanical speed is equal to the synchronous/electrical speed, they are not synchronized in induction machines so that there is some slip between them. Therefore, the rotor flux has to be estimated by

measuring several electrical magnitudes (stator voltages and/or currents) and, in most cases, the mechanical rotor position.

The mechanical rotor position is usually measured by using encoders, which are quite accurate but also quite expensive. In addition, encoders are electro-mechanical sensors so that they require more maintenance than pure electronic devices. Consequently, sensorless control techniques are designed in order to remove the dependence on electro-mechanical devices by estimating the rotor position/speed with only electrical measurements.

This thesis will be focused on a sensorless control technique in the low speed region based on the manufacturing asymmetries of induction machines. These asymmetries produce several saliencies, which can be tracked in order to estimate the rotor position/speed of the machine.

Chapter 2

Objectives of the Master Thesis

As commented during Chapter 1, the main objective of this thesis is the estimation of the speed/position in the low speed region using saliency-based control techniques. This goal will be addressed by the following tasks:

- Brief analysis of some sensorless control techniques: Some sensorless control techniques will be briefly analyzed in order to see their characteristics and why they are not suitable for implementing a sensorless control at low/zero speeds.

- Modelling of the induction machine with saliencies: A mathematical model of the effect of the saliencies into the machine inductance will be determined in order to be able to perform several simulations of the machine with saliencies.

- Analysis of the carrier high frequency excitation into induction machines with saliencies: The high frequency excitation will allow to perform the saliency tracking of the machine at low/zero speeds. Therefore, an analysis of its effect into the machine with saliencies will be discussed in order to achieve the saliency tracking and hence the sensorless control.

- Simulation of the carrier frequency excitation effect into the machine model: Several simulations will be performed to validate the expected behavior of the machine when high frequency excitation is applied.

- Implementation of the Field Oriented Control in an induction machine: In order to be able to control the induction machine and achieve the sensorless control, the implementation of the Field Oriented Control will be discussed.

- Estimation of the rotor position of the machine via saliency tracking: Once the basic simulations were performed, the saliency tracking will be validated in order to check that its implementation is suitable.

- Implementation of the Sensorless Control: Finally, the sensorless control will be fully implemented and then tested in order to check its feasibility and performance.

Chapter 3

State of the Art

3.1 Induction Machine Model

The electrical model of the squirrel cage induction machine in the dq stationary reference frame is shown in equations (3.1) to (3.5) [3, 4, 9, 10].

$$v^s_{qds} = R_s\, i^s_{qds} + p\, \lambda^s_{qds} \qquad \text{stator voltage} \tag{3.1}$$

$$0 = R_r\, i^s_{qdr} + (p - j\,\omega_r)\, \lambda^s_{qdr} \qquad \text{rotor voltage} \tag{3.2}$$

$$\lambda^s_{qds} = L_s\, i^s_{qds} + L_m\, i^s_{qdr} \qquad \text{stator flux linkage} \tag{3.3}$$

$$\lambda^s_{qdr} = L_m\, i^s_{qds} + L_r\, i^s_{qdr} \qquad \text{rotor flux linkage} \tag{3.4}$$

$$x_{qd} = x_q - j\, x_d \qquad \text{complex vector notation} \tag{3.5}$$

These equations can be adapted to a state-space model in which the stator current and the rotor flux are system states and the stator voltage is the system input. The result is shown in equations (3.6) to (3.10) [3, 4, 9, 10].

$$p\, i^s_{qds} = \frac{1}{L_{\sigma s}} \left(v^s_{qds} - R'_s\, i^s_{qds} + \frac{L_m}{L_r}\, \omega_{br}\, \lambda^s_{qdr} \right) \tag{3.6}$$

$$p\, \lambda^s_{qdr} = \frac{L_m}{L_r}\, R_r\, i^s_{qds} - \omega_{br}\, \lambda^s_{qdr} \tag{3.7}$$

$$L_{\sigma s} = L_s - \frac{{L_m}^2}{L_r} \qquad \text{stator transient inductance} \qquad (3.8)$$

$$R'_s = R_s + \left(\frac{L_m}{L_r}\right)^2 R_r \qquad \text{stator transient resistance} \qquad (3.9)$$

$$\omega_{br} = \frac{R_r}{L_r} - j\,\omega_r \qquad \text{complex speed variable} \qquad (3.10)$$

3.2 Current Model Open-Loop Rotor Flux Observer

A rotor flux observer is necessary to perform the Field Oriented Control (FOC) in induction machines. In this way, the rotor flux magnitude and position can be estimated in order to perform a properly control of the machine. There are several open-loop implementations in order to build a rotor flux observer, which are derived from the following basic topologies [3, 9]:

- Current model open-loop flux observer.
- Voltage model open-loop flux observer.
- Full-order open-loop flux observer.
- Cancellation method open-loop flux estimator.

From these open-loop topologies, it is also possible to build closed-loop flux observers, so that the parameter sensitivity and hence the accuracy of the resultant flux observer is improved [3, 9].

The selected topology of flux observer is the current model open-loop flux observer because its implementation is quite simple and it operates properly at low speeds (unlike the voltage model). From (3.7) and (3.10), it is possible to obtain the equation that explains the behavior of this flux observer as shown in (3.11) [3, 9].

$$p\,\widehat{\lambda^s_{qdr}} = \frac{\widehat{R_r}}{\widehat{L_r}}\left(\widehat{L_m}\,i^s_{qds} - \widehat{\lambda^s_{qdr}} + j\,\omega_r\,\frac{\widehat{L_r}}{\widehat{R_r}}\,\widehat{\lambda^s_{qdr}}\right) \qquad (3.11)$$

Nevertheless, this expression can be simplified by transforming it into a rotor synchronous reference frame. In this way, the term which depends on the rotor speed

is eliminated. The resultant equation is shown in (3.12) [3, 9].

$$p\,\widehat{\lambda^r_{qdr}} = \frac{\widehat{R_r}}{\widehat{L_r}}\left(\widehat{L_m}\,i^r_{qds} - \widehat{\lambda^r_{qdr}}\right) \tag{3.12}$$

From (3.12), it is possible to obtain the block diagram of the current model open-loop rotor flux observer as shown in Figure 3-1. Note that the rotor position has to be known in order to perform the transformation from the stationary reference frame to the rotor synchronous reference frame and vice versa. This flux observer requires the measurement of the stator current in the stationary reference frame and the measurement/estimation of the rotor position. The final result is the rotor flux in stationary reference frame, from which the magnitude and position of the rotor flux can be obtained in order to perform the FOC.

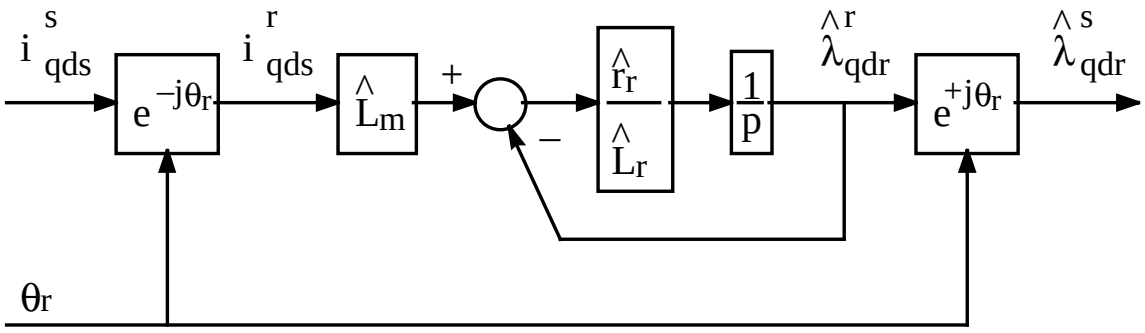

Figure 3-1: Block diagram of the current model open-loop rotor flux observer [3].

3.3 Sensorless Control Techniques

There are several sensorless control techniques that can be used in order to perform the sensorless control of an induction machine. Some sensorless control techniques are briefly explained below: [3, 4]:

- Speed estimation based in the fundamental back-emf: This technique uses a flux observer combined with a mechanical model of the machine in order to estimate the rotor speed/position. The drawback is that it is based on the fundamental

excitation, so it is not suitable for low/zero speeds since the fundamental back-emf is very low at these speeds. In addition, a good mechanical model, in which mechanical disturbances are considered, is required to perform adequate estimations [8].

- FFT saliency tracking: This technique performs the FFT of the voltage/current of the machine. If there is some kind of saliency in the machine, the voltage/current will have several harmonics at frequencies other than the fundamental excitation frequency. If these harmonics correspond to a rotating saliency, they provide spatial information and the rotor speed/position can be estimated. The drawback is that the FFT computation is relatively slow and hence the resultant bandwidth is low. In addition, this technique is based on the fundamental excitation, so it is not suitable for low/zero speeds [6].

- Phase voltage saliency tracking: This technique analyzes the effect in the zero sequence voltage of a machine due to a saliency in the machine. If the zero sequence voltage corresponds to a rotating saliency, it provides spatial information and the rotor speed/position can be estimated. The drawback is that this technique is based on the fundamental excitation, so it is not suitable for low/zero speeds [7].

- di/dt and inductance measurement saliency tracking: This technique is based on the fact that the inductance of a machine with a saliency varies with the saliency position. One possibility for measuring the machine inductance consists of measuring the current ripple produced due to the inverter switching. Although this technique does not rely on the fundamental excitation and hence it is suitable for low/zero speeds, its implementation is complicated since it can require special inverter switching modulation to acquire proper information [11].

As can be seen, the sensorless techniques which rely on the fundamental excitation in order to estimate the rotor position/speed do not operate properly at low/zero speeds since the fundamental excitation is also low/zero at these speeds. To solve

this problem, instead of using the fundamental excitation, it is possible to inject a high frequency carrier voltage/current into the machine. In this way, the induced high frequency voltage/current can be used to perform the saliency tracking but the fundamental behavior of the machine is not affected since the high frequency carrier voltage/current is low compared to the fundamental frequency voltage/current. In addition, this technique is valid for low and zero speed since the high frequency excitation is continuously forced. Figure 3-2 shows a diagram of high frequency excitation with carrier voltage to estimate the rotor position [1, 3, 4].

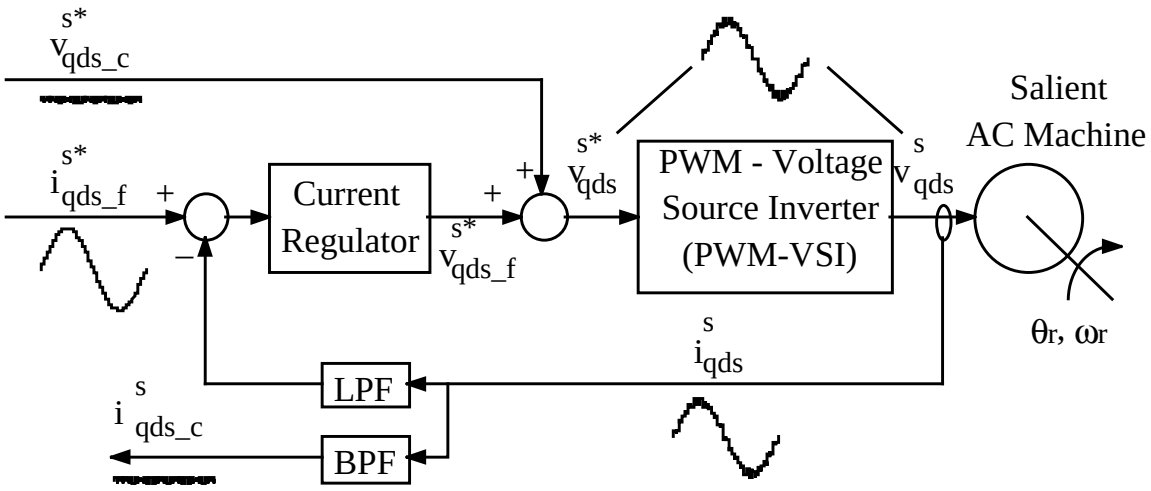

Figure 3-2: Diagram of high frequency excitation with carrier voltage to estimate the rotor position [3].

3.4 Harmonic Saliency Inductance Modeling

In order to perform a proper saliency tracking of the induction machine, it is necessary to analyze the different saliencies of the machine and create the corresponding inductance model of the machine. Once the inductance model of the machine is known, the saliency tracking will focus on the most powerful saliency which provides spatial information. There are three main sources which produce saliencies in the machine [2–4]:

- Rotor and stator slotting: Either rotor and stator slotting produces an airgap

permeance variation in the machine. Typically, a machine has several rotor/stator slots per pole, which implies that the airgap permeance variation due to rotor/stator slotting alone has a short period and hence it is not significant. Nevertheless, when a machine has both rotor and stator slotting, the joint effect produces a significant airgap permeance variation that provides spatial information in the resultant inductance of the machine. It can be demonstrated that the airgap permeance variation is related to the mechanical rotor speed as shown in (3.13).

$$\omega_{agp} = \frac{N_r}{N_r - N_s}\,\omega_{rm} \tag{3.13}$$

- Rotor eccentricity: Rotor eccentricity also produces an airgap permeance variation in the machine. However, the rotor eccentricity exists due to manufacturing errors or machine wear, which implies that the airgap permeance variation due to rotor eccentricity is not useful but it disturbs the resultant inductance of the machine in an undesirable way. Static eccentricity generates an airgap permeance variation which does not rotate with the rotor whereas dynamic eccentricity generates an airgap permeance variation which rotates at the same speed as the rotor. If the manufacturing process is suitable, the rotor eccentricity effect can be neglected.

- Saturation: Saturation also produces an airgap permeance variation in the machine (airgap permeance decreases in points in which the saturation occurs). Although saturation is an undesirable effect, it commonly appears in machines since they operate near saturation to take full advantage of the machine. Saturation is caused by the flux of the machine, so the consequent airgap permeance variation rotates at the same speed as the flux. Nevertheless, the saturation is a non-linear phenomenon, so that several harmonics are generated due to saturation, which have to be taken into account.

Saliencies can be modeled by including an inductance variation into the induc-

tance matrix of the machine model. Note that saliencies can be classified into two main groups: position-dependent saliencies and stationary saliencies. Regarding the position-dependent saliencies, such as rotor/stator slotting, the corresponding inductance matrices are shown in (3.14) and (3.15). Nevertheless, (3.15) corresponds only to the special case in which the number of rotor and stator slots are the same, so that it is not interesting since this slotting design is commonly avoided. Regarding the stationary saliencies, such as static eccentricity, the corresponding inductance matrix is shown in (3.16). Nevertheless, this kind of saliency is not useful since it does not provide any spatial information but disturbs the resultant saliency inductance [3, 4].

$$L_{qd} = \Delta L_{sal} \begin{bmatrix} \cos\left(h\left(\theta_e + \phi_e\right)\right) & -\sin\left(h\left(\theta_e + \phi_e\right)\right) \\ -\sin\left(h\left(\theta_e + \phi_e\right)\right) & -\cos\left(h\left(\theta_e + \phi_e\right)\right) \end{bmatrix} \tag{3.14}$$

$$L_{qd} = \Delta L_{sal} \begin{bmatrix} \cos\left(h\left(\theta_e + \phi_e\right)\right) & -\sin\left(h\left(\theta_e + \phi_e\right)\right) \\ \sin\left(h\left(\theta_e + \phi_e\right)\right) & \cos\left(h\left(\theta_e + \phi_e\right)\right) \end{bmatrix} \tag{3.15}$$

$$L_{qd} = \begin{bmatrix} \Delta L_{sal,qq} & \Delta L_{sal,qd} \\ \Delta L_{sal,dq} & \Delta L_{sal,dd} \end{bmatrix} \tag{3.16}$$

Chapter 4

Carrier Frequency Excitation

As stated in Chapter 3, the best solution for estimating the rotor position/speed at low and zero speed is to inject a high frequency carrier signal in addition to the fundamental frequency excitation signal. In this particular case, the machine will be supplied with a Voltage Source Converter (VSC) and hence the high frequency excitation can be performed in closed loop with a current regulator or in open loop by directly injecting a high frequency voltage. The implemented injection will be the second one (open-loop voltage injection). This chapter will be focused on understanding the behavior of the machine due to high frequency excitation by analyzing the high frequency model of the machine.

4.1 High Frequency Machine Model

Although the effect of the high frequency resistance can be considered in order to perform the saliency tracking [5], the effect of the resistive terms in the machine model are not considered in this particular case. Therefore, from equations (3.1) to (3.4), it is possible to obtain the equations (4.1) and (4.2) [1–4].

$$v^s_{qds\_c} \simeq p\left(L_s\, i^s_{qds\_c} + L_m\, i^s_{qdr\_c}\right) \tag{4.1}$$

$$0 \simeq (p - j\,\omega_r)\left(L_m\, i^s_{qds\_c} + L_r\, i^s_{qdr\_c}\right) \tag{4.2}$$

It is supposed that the carrier frequency (ω_c) is fixed, so that the differential operator (p) is equal to $j\,\omega_c$. In this way, equation (4.3) is obtained from (4.2) [1–4].

$$i^s_{qdr\_c} \simeq -\frac{L_m}{L_r}\, i^s_{qds\_c} \tag{4.3}$$

By substituting (4.3) into (4.1) and taking into account (3.8), equation (4.4) is obtained [1–4].

$$v^s_{qds\_c} \simeq j\,\omega_c\, L_{\sigma s}\, i^s_{qds\_c} \tag{4.4}$$

As can be seen, the behavior of the machine at high frequency carrier excitation is determined by the stator transient inductance. Therefore, in order to be able to perform a saliency tracking with high frequency carrier excitation, the stator transient inductance has to vary depending on the rotor/flux position. The stator transient inductance matrix in the saliency synchronous reference frame is shown in (4.5) [1–4].

$$L^e_{os} = \begin{bmatrix} L^e_{oqs} & 0 \\ 0 & L^e_{ods} \end{bmatrix} \qquad\qquad L^e_{oqs} \neq L^e_{ods} \tag{4.5}$$

The stator transient inductance matrix has to be transformed to the stationary reference frame in order to use it in the high frequency machine model. Before performing the transformation, it is interesting to define the average stator transient inductance and the differential stator transient inductance as shown in (4.6) and (4.7) [1–4].

$$\Sigma L_{\sigma s} = \frac{1}{2}\left(L^e_{oqs} + L^e_{ods}\right) \qquad \text{average stator transient inductance} \tag{4.6}$$

$$\Delta L_{\sigma s} = \frac{1}{2}\left(L^e_{oqs} - L^e_{ods}\right) \qquad \text{differential stator transient inductance} \tag{4.7}$$

If the stator transient inductance model corresponds to (3.14), its value in the stationary reference frame can be represented by (4.8). If the stator transient inductance model corresponds to (3.15), its value in the stationary reference frame can be

represented by (4.9) [1–4].

$$L_{\sigma s} = \Sigma L_{\sigma s} \begin{bmatrix} 1 & 0 \\ 0 & 1 \end{bmatrix} + \Delta L_{\sigma s} \begin{bmatrix} \cos(h\,\theta_e) & -\sin(h\,\theta_e) \\ -\sin(h\,\theta_e) & -\cos(h\,\theta_e) \end{bmatrix} \tag{4.8}$$

$$L_{\sigma s} = \Sigma L_{\sigma s} \begin{bmatrix} 1 & 0 \\ 0 & 1 \end{bmatrix} + \Delta L_{\sigma s} \begin{bmatrix} \cos(h\,\theta_e) & -\sin(h\,\theta_e) \\ \sin(h\,\theta_e) & \cos(h\,\theta_e) \end{bmatrix} \tag{4.9}$$

In this thesis, the inductance model to study is given by (3.14) because it corresponds to the rotor/stator slotting when the number of rotor slots and stator slots are different. Therefore, the final high frequency machine model is given by equations (4.10) and (4.11).

$$i^s_{qds\_c} \simeq \frac{1}{j\,\omega_c}\, {L_{\sigma s}}^{-1}\, v^s_{qds\_c} \tag{4.10}$$

$${L_{\sigma s}}^{-1} = \frac{1}{\Sigma {L_{\sigma s}}^2 - \Delta {L_{\sigma s}}^2} \left[\Sigma L_{\sigma s} \begin{bmatrix} 1 & 0 \\ 0 & 1 \end{bmatrix} - \Delta L_{\sigma s} \begin{bmatrix} \cos(h\,\theta_e) & -\sin(h\,\theta_e) \\ -\sin(h\,\theta_e) & -\cos(h\,\theta_e) \end{bmatrix} \right] \tag{4.11}$$

The parameters that will be used to compute the high frequency model are shown in Table 4.1.

Table 4.1: High frequency model parameters.

L^e_{oqs}	0.14mH
L^e_{ods}	0.1mH
V_{sc}	1V
h	8
ω_c	2π500rad/s

4.2 Excitation in stationary reference frame

The carrier frequency excitation consists on injecting a three-phase balance voltage at high frequency (carrier frequency) in addition to the fundamental frequency excitation signal. In this way, a high frequency rotating vector is generated as shown in (4.12) [1–4].

$$\begin{aligned} v^{s}_{qds\_c} &= V_{sc} \begin{bmatrix} \cos(\omega_c t) \\ -\sin(\omega_c t) \end{bmatrix} \\ &= V_{sc}\, e^{j\,\omega_c t} \end{aligned} \tag{4.12}$$

Applying this voltage to the high frequency machine model defined in (4.10) and (4.11), it can be demonstrated that the induced current is determined by equations (4.13), (4.14) and (4.15) [1–4].

$$\begin{aligned} i^{s}_{qds\_c} &= I_{sc\_p} \begin{bmatrix} \sin(\omega_c t) \\ \cos(\omega_c t) \end{bmatrix} - I_{sc\_n} \begin{bmatrix} \sin(h\,\theta_e - \omega_c t) \\ \cos(h\,\theta_e - \omega_c t) \end{bmatrix} \\ &= -j\, I_{sc\_p}\, e^{j\,\omega_c t} + j\, I_{sc\_n}\, e^{j(h\,\theta_e - \omega_c t)} \end{aligned} \tag{4.13}$$

$$I_{sc\_p} = \left(\frac{\Sigma L_{\sigma s}}{\Sigma {L_{\sigma s}}^2 - \Delta {L_{\sigma s}}^2} \right) \frac{V_{sc}}{\omega_c} \tag{4.14}$$

$$I_{sc\_n} = \left(\frac{\Delta L_{\sigma s}}{\Sigma {L_{\sigma s}}^2 - \Delta {L_{\sigma s}}^2} \right) \frac{V_{sc}}{\omega_c} \tag{4.15}$$

As can be seen, the induced current consists of two different components: a positive sequence component and a negative sequence component. The positive sequence component rotates in the same direction as the carrier voltage and does not provide any spatial information. However, the negative sequence component rotates in the opposite direction to the carrier voltage and provides spatial information. This is because the current value is modulated by the differential stator transient inductance, which depends on the position [1–4].

Figure 4-1, Figure 4-2, Figure 4-3 and Figure 4-4 show the results of carrier fre-

quency excitation with fixed saliency position in stationary reference frame. The saliency position (θ_e) is equal to 30°. The computation was performed in MATLAB by executing the script in Appendix A.1. As can be seen, while the injected voltage is balanced, the induced current is unbalanced due to the saliency, so it has a negative sequence component. Therefore, the current polar trajectory is elliptical with the major axis oriented to $(h/2)\,\theta_e$. Consequently, this ellipsis will rotate as the saliency rotates. The instantaneous polar position is given by the carrier voltage angle. In the frequency domain, the FFT of the current shows the positive sequence component at ω_c and the negative sequence component at $-\omega_c$ since the machine is not rotating (fixed saliency position).

Figure 4-5, Figure 4-6, Figure 4-7 and Figure 4-8 show the results of carrier frequency excitation with rotating saliency in stationary reference frame. The saliency frequency (ω_e) is equal to $2\pi 5$rad/s. The computation was performed in MATLAB by executing the script in Appendix A.2. As can be seen, while the injected voltage is balanced, the induced current is unbalanced due to the saliency, so it has a negative sequence component. Therefore, the current polar trajectory is not circular and the instantaneous polar position is given by both the carrier voltage angle and the saliency position. In the frequency domain, the FFT of the current shows the positive sequence component at ω_c and the negative sequence component at $h\,\omega_e - \omega_c$ since the machine is rotating at ω_e.

4.3 Excitation in negative sequence synchronous reference frame

As stated in Section 4.2, the induced current due to the high frequency excitation has two components: a positive sequence which does not provide spatial information and a negative sequence which provides spatial information. The final objective of the carrier frequency excitation is to track the saliency position in order to estimate the rotor position. Therefore, since only the negative sequence component provides

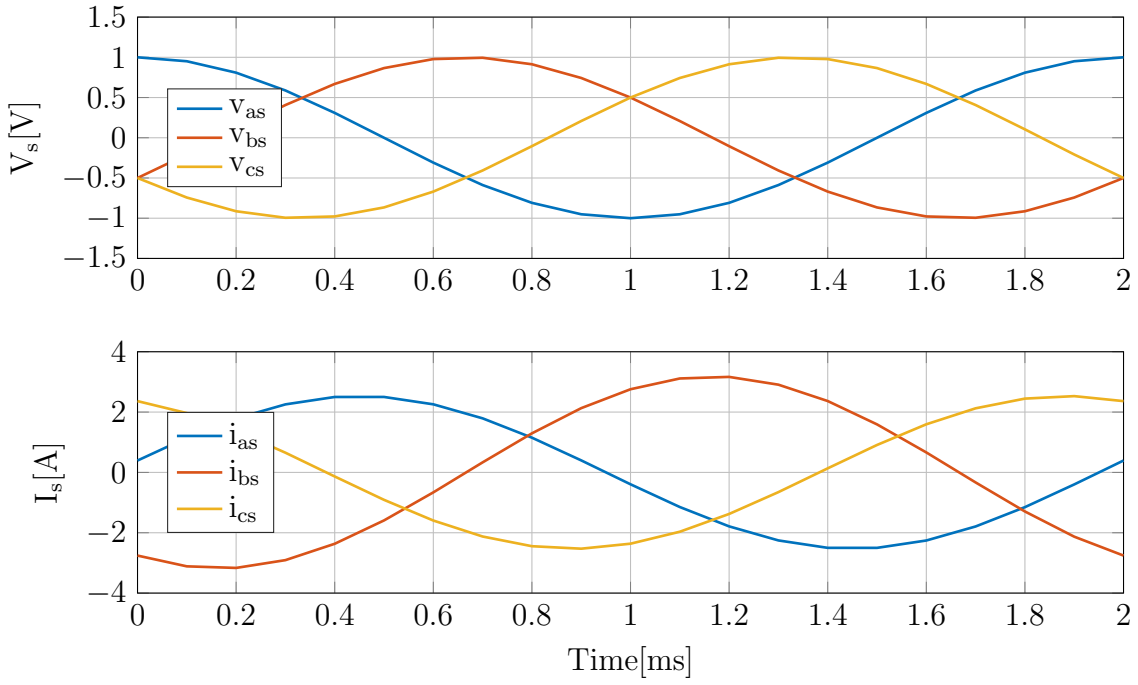

Figure 4-1: Carrier frequency excitation with fixed saliency position in stationary reference frame: three-phase voltage/current evolution. $L^e_{oqs} = 0.14$mH, $L^e_{ods} = 0.1$mH, $V_{sc} = 1$V, $h = 8$, $\theta_e = 30°$, $\omega_c = 2\pi 500$rad/s.

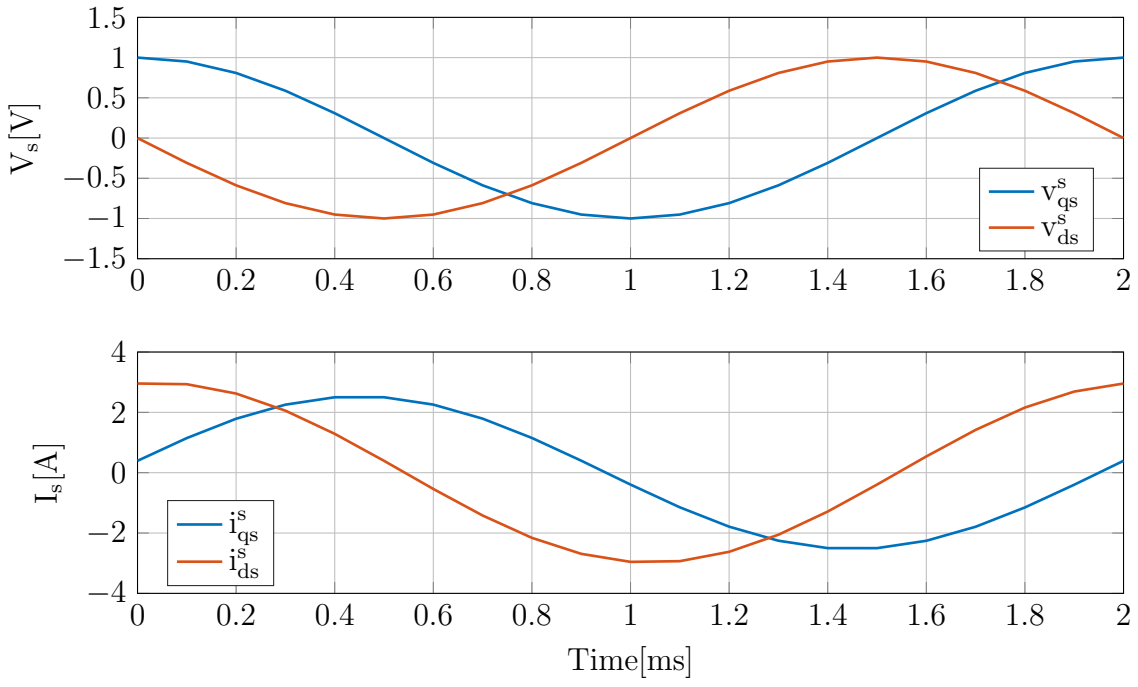

Figure 4-2: Carrier frequency excitation with fixed saliency position in stationary reference frame: qd voltage/current evolution. $L^e_{oqs} = 0.14$mH, $L^e_{ods} = 0.1$mH, $V_{sc} = 1$V, $h = 8$, $\theta_e = 30°$, $\omega_c = 2\pi 500$rad/s.

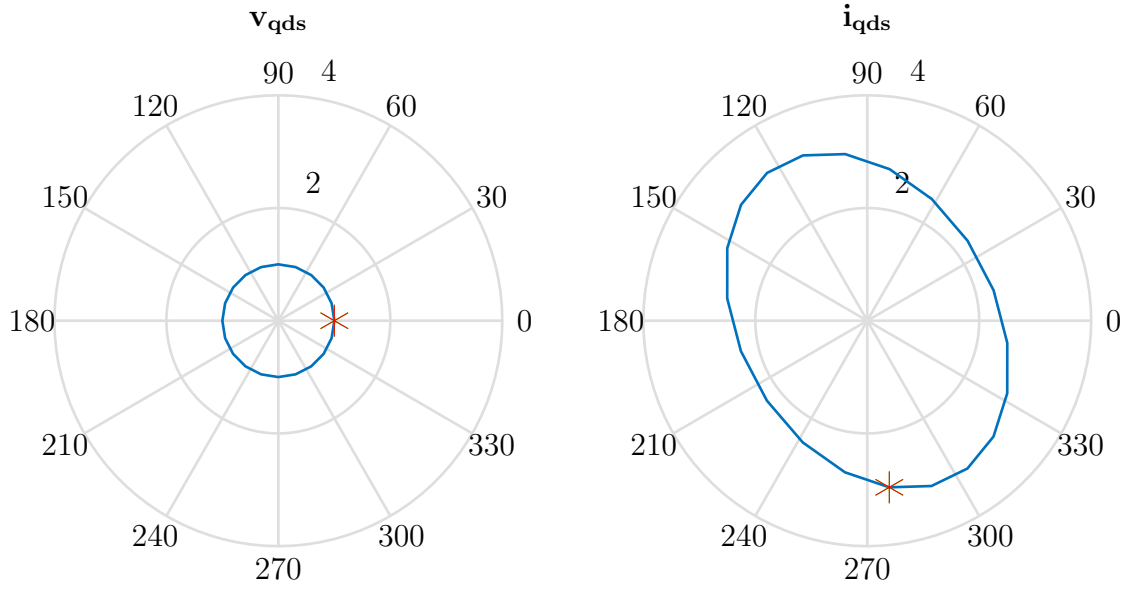

Figure 4-3: Carrier frequency excitation with fixed saliency position in stationary reference frame: voltage/current polar trajectory. Green mark: starting point, red mark: ending point. $L^e_{oqs} = 0.14\text{mH}$, $L^e_{ods} = 0.1\text{mH}$, $V_{sc} = 1\text{V}$, $h = 8$, $\theta_e = 30°$, $\omega_c = 2\pi 500\text{rad/s}$.

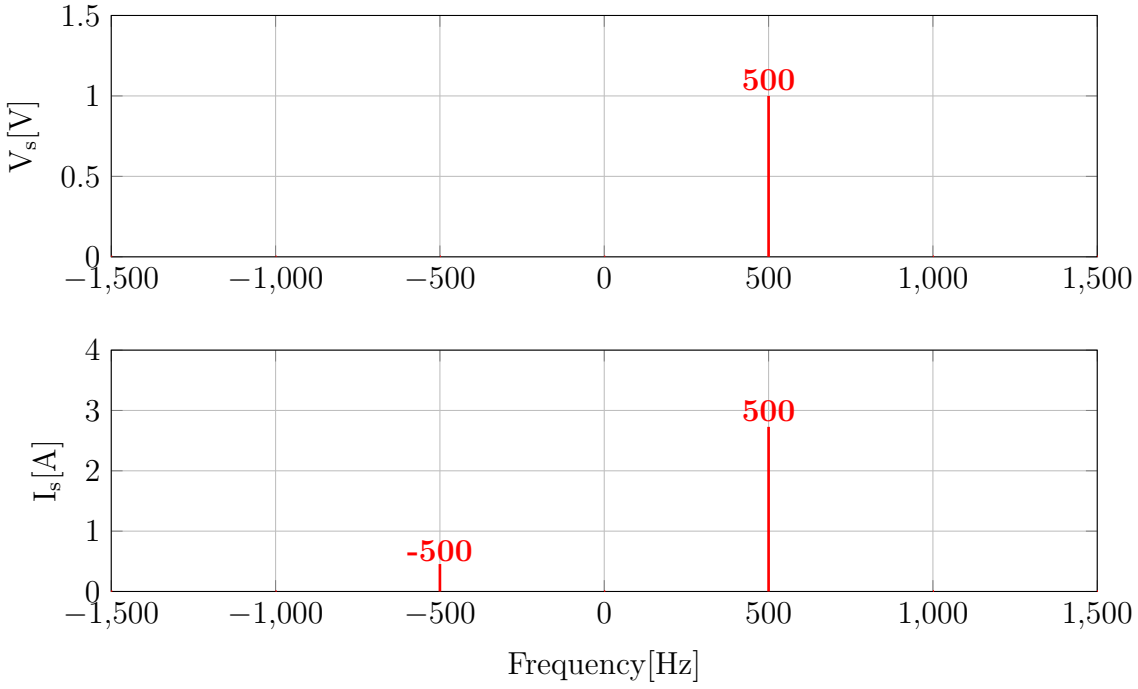

Figure 4-4: Carrier frequency excitation with fixed saliency position in stationary reference frame: voltage/current FFT. $L^e_{oqs} = 0.14\text{mH}$, $L^e_{ods} = 0.1\text{mH}$, $V_{sc} = 1\text{V}$, $h = 8$, $\theta_e = 30°$, $\omega_c = 2\pi 500\text{rad/s}$.

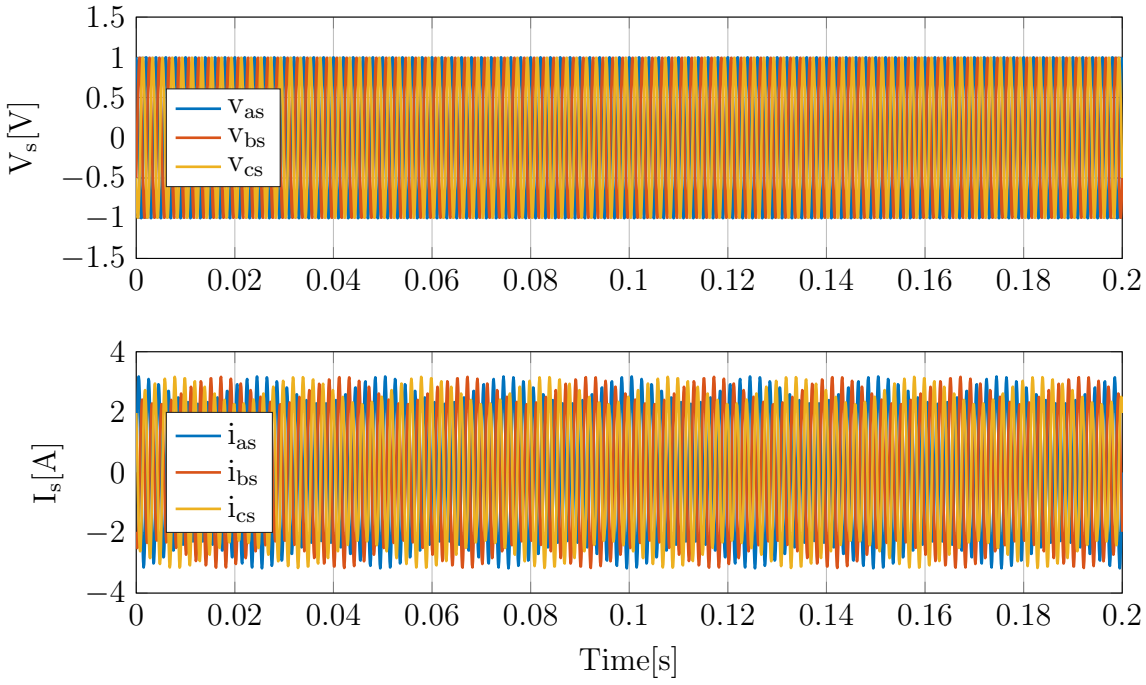

Figure 4-5: Carrier frequency excitation with rotating saliency in stationary reference frame: three-phase voltage/current evolution. $L^e_{oqs} = 0.14$mH, $L^e_{ods} = 0.1$mH, $V_{sc} = 1$V, $h = 8$, $\omega_e = 2\pi 5$rad/s, $\omega_c = 2\pi 500$rad/s.

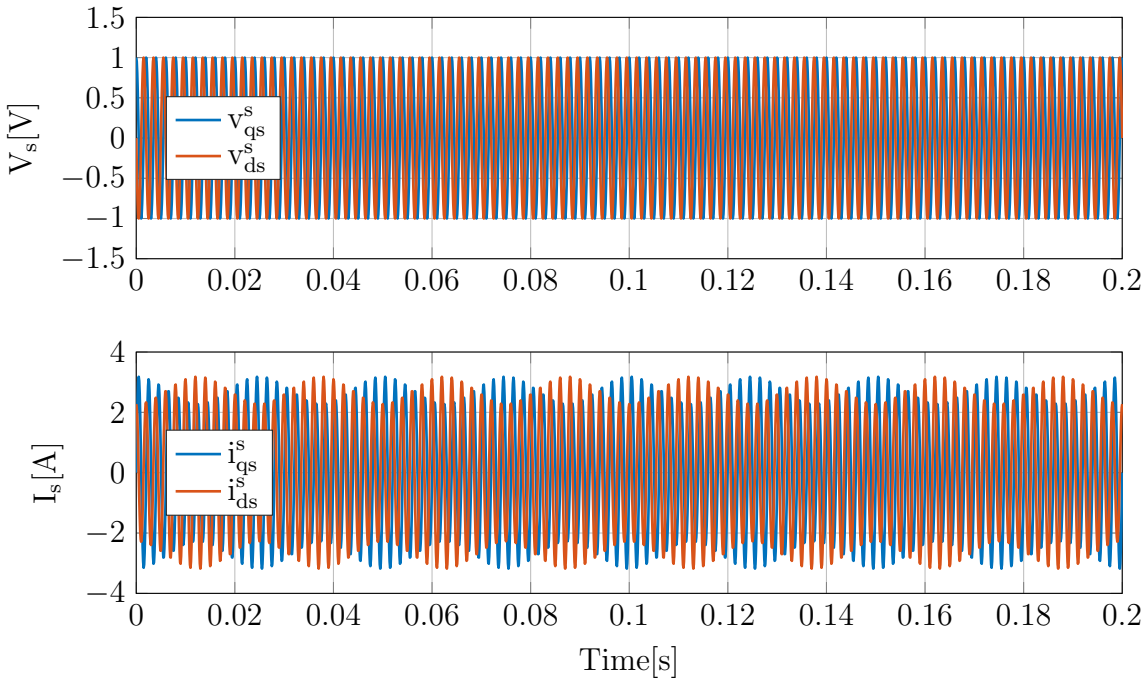

Figure 4-6: Carrier frequency excitation with rotating saliency in stationary reference frame: qd voltage/current evolution. $L^e_{oqs} = 0.14$mH, $L^e_{ods} = 0.1$mH, $V_{sc} = 1$V, $h = 8$, $\omega_e = 2\pi 5$rad/s, $\omega_c = 2\pi 500$rad/s.

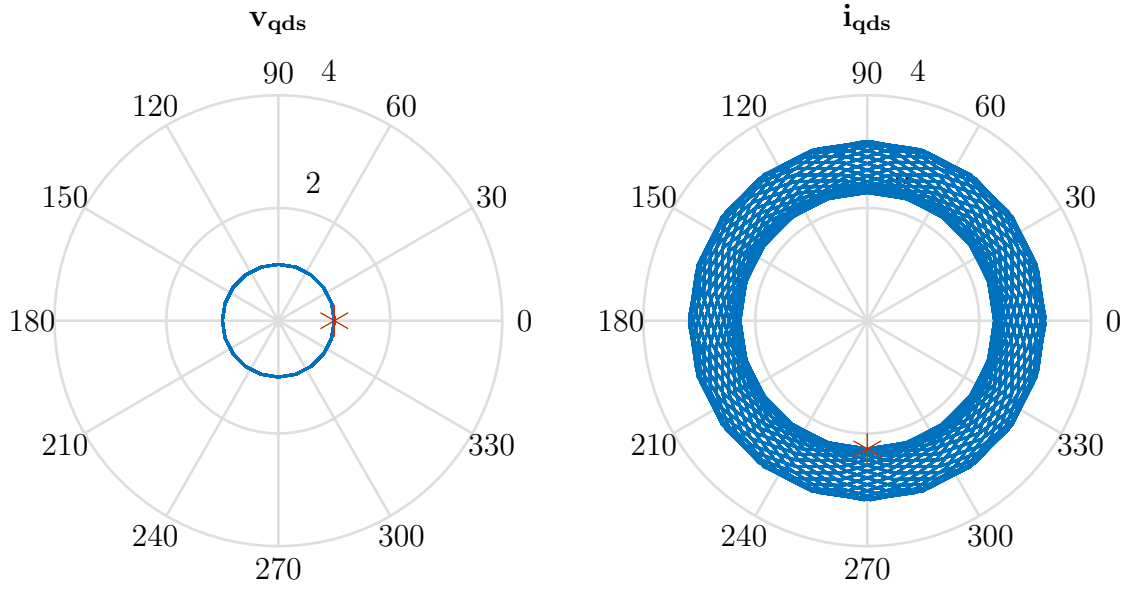

Figure 4-7: Carrier frequency excitation with rotating saliency in stationary reference frame: voltage/current polar trajectory. Green mark: starting point, red mark: ending point. $L^e_{oqs} = 0.14\text{mH}$, $L^e_{ods} = 0.1\text{mH}$, $V_{sc} = 1\text{V}$, $h = 8$, $\omega_e = 2\pi 5\text{rad/s}$, $\omega_c = 2\pi 500\text{rad/s}$.

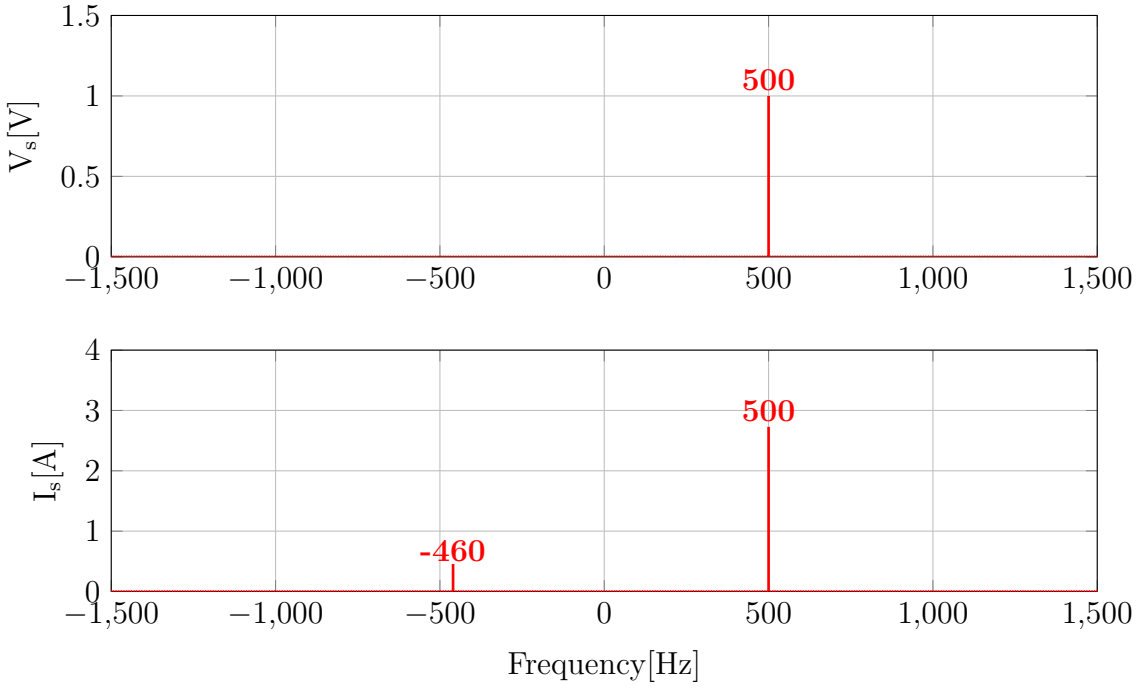

Figure 4-8: Carrier frequency excitation with rotating saliency in stationary reference frame: voltage/current FFT. $L^e_{oqs} = 0.14\text{mH}$, $L^e_{ods} = 0.1\text{mH}$, $V_{sc} = 1\text{V}$, $h = 8$, $\omega_e = 2\pi 5\text{rad/s}$, $\omega_c = 2\pi 500\text{rad/s}$.

spatial information, it is advisable to operate in a negative sequence synchronous reference frame to track the saliency position [1–4].

Nevertheless, although the positive sequence component does not provide spatial information, it disturbs the saliency tracking since it is a noticeable harmonic. Therefore, it is mandatory to filter the positive sequence component before performing the saliency tracking. Note that the positive and the negative sequence components are quite separated in the frequency domain so the filtering is relatively easy. There are two options to carry out the transformation to negative sequence synchronous reference frame with positive sequence component filtering:

- Transformation to negative sequence synchronous reference frame and filtering of positive sequence component with a low-pass filter.
- Transformation to positive sequence synchronous reference frame, filtering of positive sequence component with a high-pass filter and transformation to negative sequence synchronous reference frame.

The first option is more simple because it requires only one reference frame transformation but the LPF bandwidth selection is not arbitrary. In negative sequence synchronous reference frame, the negative sequence component is a DC magnitude. Therefore, the LPF has to attenuate significantly the positive sequence component but trying to not introduce a phase shift in the angular position of the negative sequence component. Consequently, the LPF bandwidth selection is not straightforward and has to be analyzed properly. In addition, the positive sequence component cannot be fully filtered with this option due to the inherent behavior of the LPF.

The second option is more complex because it requires two reference frame transformations but the HPF bandwidth selection is relatively arbitrary. In positive sequence synchronous reference frame, the positive sequence component is a DC magnitude. Therefore, the HPF will attenuate totally the positive sequence component regardless of the HPF bandwidth. Consequently, the HPF bandwidth selection is relatively straightforward and the only restriction is to not modify the negative sequence component.

The selected option is the second one because the positive sequence component position is perfectly known (ω_c) and the HPF allows a perfect filtering of this component. The steps of the selected option are:

- Transformation to positive sequence synchronous reference frame: (4.16).

$$i_{qds\_c}^{pos} = i_{qds\_c}^{s}\, e^{-j\,\omega_c\, t} \tag{4.16}$$

- High-pass filtering to remove positive sequence component: (4.17).

$$i_{qds\_c\_filt}^{pos} = \text{HPF}\left\{i_{qds\_c}^{pos}\right\} \tag{4.17}$$

- Transformation to negative sequence synchronous reference frame: (4.18).

$$i_{qds\_c}^{neg} = i_{qds\_c\_filt}^{pos}\, e^{j\,\omega_c\, t}\, e^{-j(h\,\theta_e - \omega_c\, t)} = i_{qds\_c\_filt}^{pos}\, e^{-j(h\,\theta_e - 2\,\omega_c\, t)} \tag{4.18}$$

Figure 4-9, Figure 4-10 and Figure 4-11 show the results of carrier frequency excitation with rotating saliency in positive sequence synchronous reference frame. The saliency frequency (ω_e) is equal to 2π5rad. The computation was performed in MATLAB by executing the script in Appendix A.3. In this reference frame, the positive sequence component is a DC magnitude, which is totally filtered with a second-order HPF with a bandwidth of 5Hz. Figure 4-12, Figure 4-13 and Figure 4-14 show the results of carrier frequency excitation with rotating saliency in negative sequence synchronous reference frame. The saliency frequency (ω_e) is equal to 2π5rad. The computation was performed in MATLAB by executing the script in Appendix A.3. Note that the positive sequence component was previously filtered. In this reference frame, the negative sequence component is a DC magnitude, which makes easier to perform the saliency tracking. As can be seen, the resultant vector has an angle of 90 degrees and hence its q-axis component is zero.

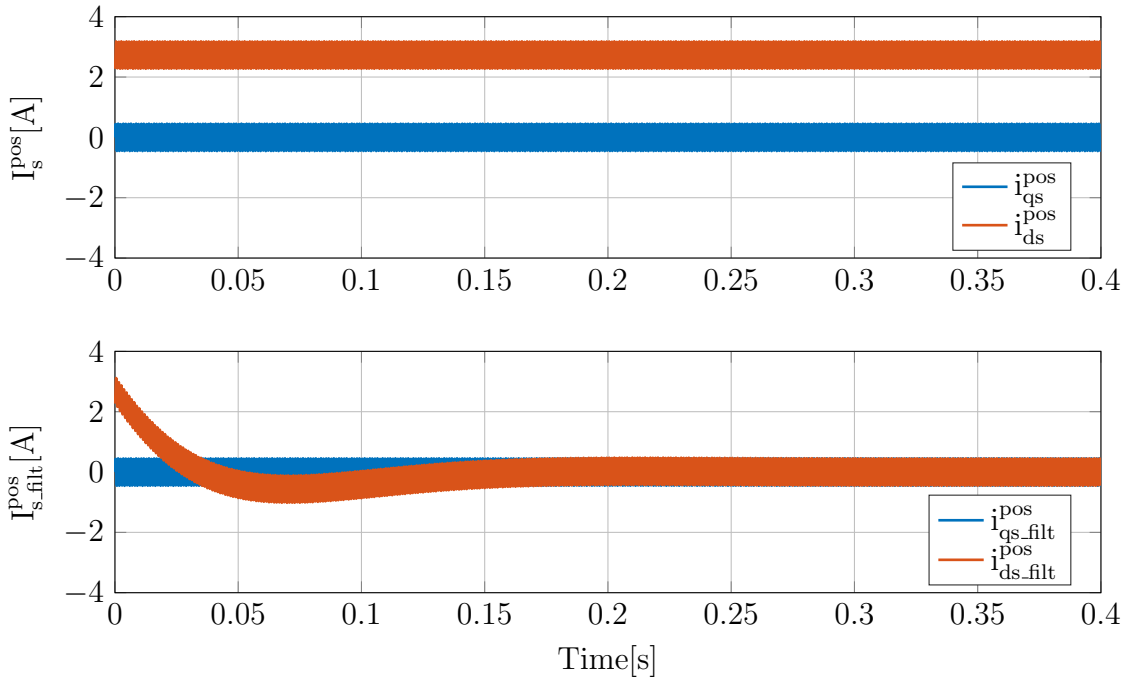

Figure 4-9: Carrier frequency excitation with rotating saliency in positive sequence synchronous reference frame: qd current evolution. $L^e_{oqs} = 0.14$mH, $L^e_{ods} = 0.1$mH, $V_{sc} = 1$V, $h = 8$, $\omega_e = 2\pi 5$rad/s, $\omega_c = 2\pi 500$rad/s, second-order HPF at 5Hz.

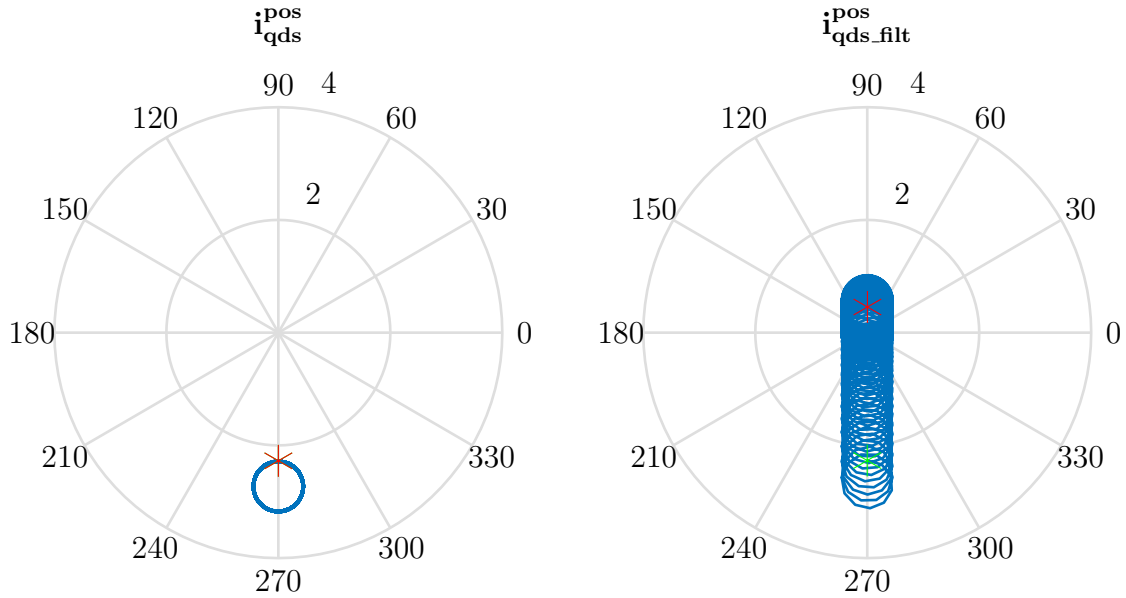

Figure 4-10: Carrier frequency excitation with rotating saliency in positive sequence synchronous reference frame: current polar trajectory. Green mark: starting point, red mark: ending point. $L^e_{oqs} = 0.14$mH, $L^e_{ods} = 0.1$mH, $V_{sc} = 1$V, $h = 8$, $\omega_e = 2\pi 5$rad/s, $\omega_c = 2\pi 500$rad/s, second-order HPF at 5Hz.

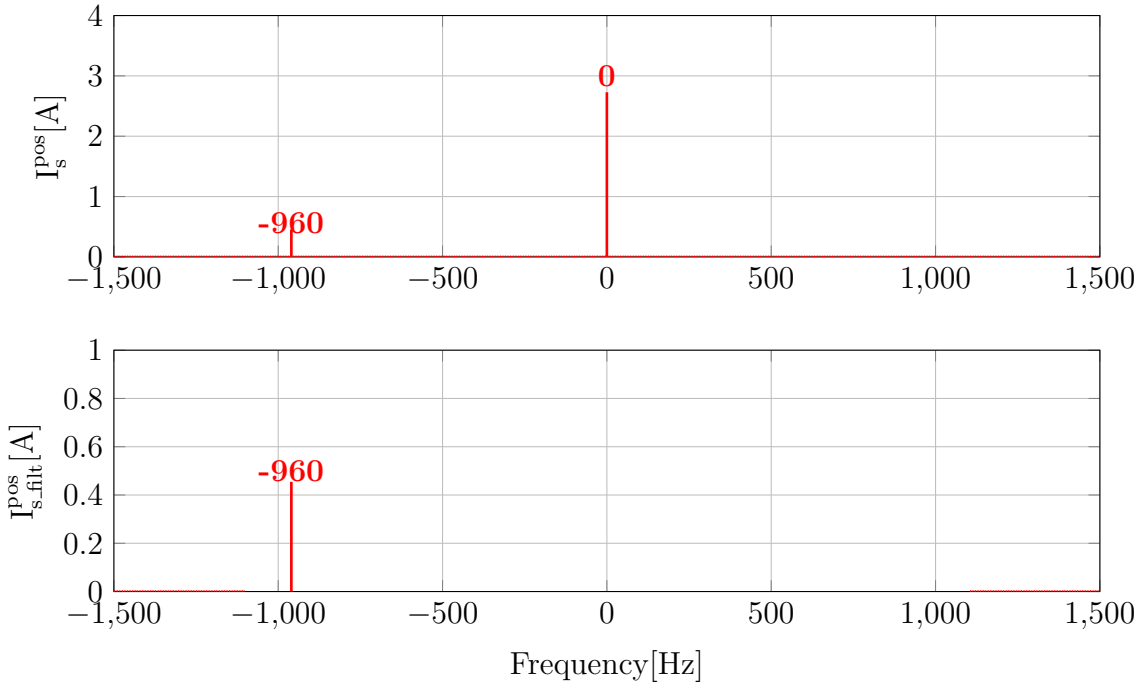

Figure 4-11: Carrier frequency excitation with rotating saliency in positive sequence synchronous reference frame: current FFT. $L^e_{oqs} = 0.14$mH, $L^e_{ods} = 0.1$mH, $V_{sc} = 1$V, $h = 8$, $\omega_e = 2\pi 5$rad/s, $\omega_c = 2\pi 500$rad/s, second-order HPF at 5Hz.

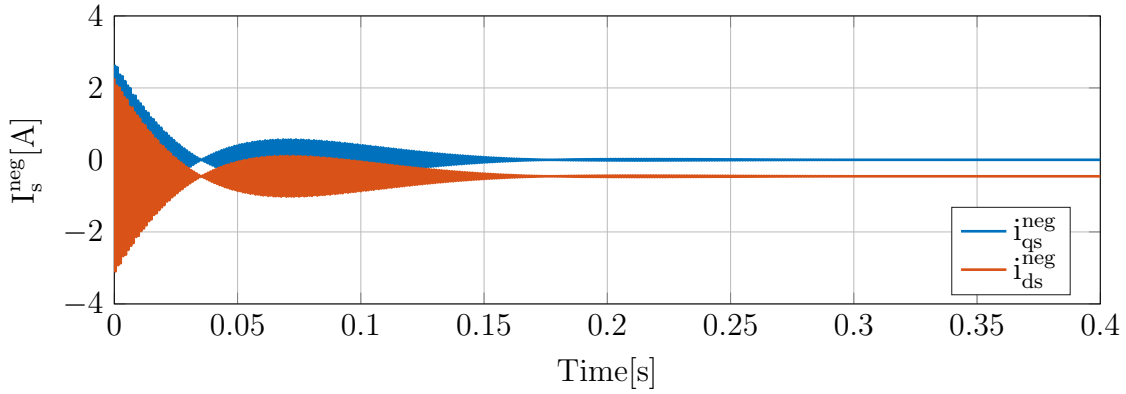

Figure 4-12: Carrier frequency excitation with rotating saliency in negative sequence synchronous reference frame: qd current evolution. $L^e_{oqs} = 0.14$mH, $L^e_{ods} = 0.1$mH, $V_{sc} = 1$V, $h = 8$, $\omega_e = 2\pi 5$rad/s, $\omega_c = 2\pi 500$rad/s, second-order HPF at 5Hz.

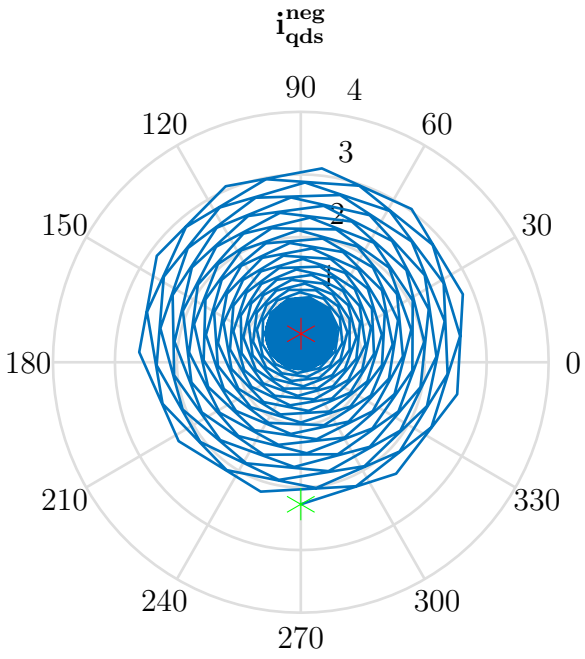

Figure 4-13: Carrier frequency excitation with rotating saliency in negative sequence synchronous reference frame: current polar trajectory. Green mark: starting point, red mark: ending point. $L^e_{oqs} = 0.14$mH, $L^e_{ods} = 0.1$mH, $V_{sc} = 1$V, $h = 8$, $\omega_e = 2\pi 5$rad/s, $\omega_c = 2\pi 500$rad/s, second-order HPF at 5Hz.

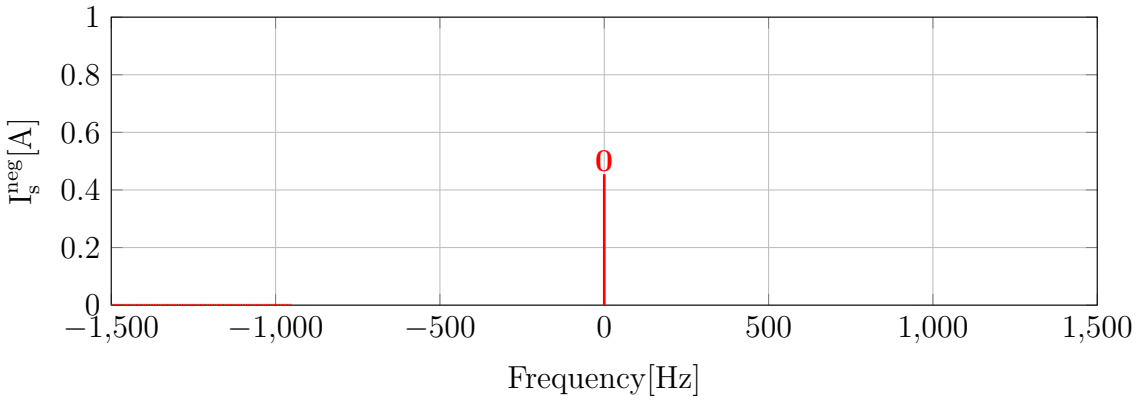

Figure 4-14: Carrier frequency excitation with rotating saliency in negative sequence synchronous reference frame: current FFT. $L^e_{oqs} = 0.14$mH, $L^e_{ods} = 0.1$mH, $V_{sc} = 1$V, $h = 8$, $\omega_e = 2\pi 5$rad/s, $\omega_c = 2\pi 500$rad/s, second-order HPF at 5Hz.

4.4 Saliency tracking

As stated in Section 4.3, the negative sequence component is a DC vector in the negative sequence synchronous reference frame with an angle of 90 degrees and hence its q-axis component is zero. Therefore, it is possible to perform the saliency tracking by using a PLL. Consequently, the needed steps to perform the saliency tracking are:

- Injecting a three-phase balance voltage at high frequency (carrier frequency). (4.12).
- Measuring the induced current, which will have a positive sequence component (without spatial information) and a negative sequence component (with spatial information). (4.13).
- Transformation to positive sequence synchronous reference frame. $\omega_c\, t = \theta_c$ is known since it depends on the injected carrier voltage. (4.16).
- High-pass filtering to remove positive sequence component. (4.17).
- Transformation to negative sequence synchronous reference frame. θ_e is not known so it is necessary to use a estimated saliency position ($\widehat{\theta_e}$). Therefore, it is necessary to establish an initial estimated saliency position, e.g., 0 rad. (4.18).
- Computation of the error in the current in negative sequence synchronous reference frame. In this particular case, the q-axis component of the current is forced to zero. (4.19).

$$\text{error} = -i_{qs\_c}^{neg} \tag{4.19}$$

- Computation of the estimated saliency frequency ($\widehat{\omega_e}$) with the PI controller of the PLL (PI_PLL). (4.20).

$$\widehat{\omega_e} = \text{PI\_PLL}\left\{\text{error}\right\} \tag{4.20}$$

- Computation of the estimated saliency position ($\widehat{\theta_e}$) with an integrator. (4.21).

$$\widehat{\theta_e} = \frac{1}{p}\widehat{\omega_e} \tag{4.21}$$

The selected proportional gain (K_{p_PLL}) and integral gain (K_{i_PLL}) of the PLL PI controller are shown in (4.22) and (4.23).

$$K_{p\_PLL} = 20 \tag{4.22}$$

$$K_{i\_PLL} = 10 \tag{4.23}$$

In this way, the PI forces the q-axis component of the current in negative sequence synchronous to be zero by estimating the saliency frequency/position. Figure 4-15, Figure 4-16, Figure 4-17 and Figure 4-18 show the results of the saliency tracking in negative sequence synchronous reference frame. The computation was performed in MATLAB by executing the script in Appendix A.4. The control of the PLL is enabled at 0.4s. As can be seen, the estimated saliency frequency/position is practically equal to the real saliency frequency/position when the control is enabled. In addition, the PLL is capable to follow changes in the saliency frequency really fast and accurate.

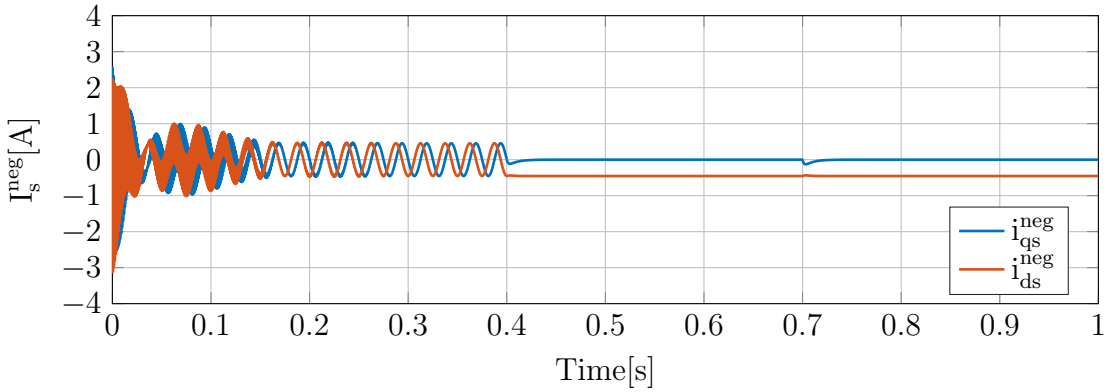

Figure 4-15: Saliency tracking in negative sequence synchronous reference frame: qd current evolution. $L^e_{oqs} = 0.14$mH, $L^e_{ods} = 0.1$mH, $V_{sc} = 1$V, $h = 8$, $\omega_c = 2\pi 500$rad/s, second-order HPF at 5Hz.

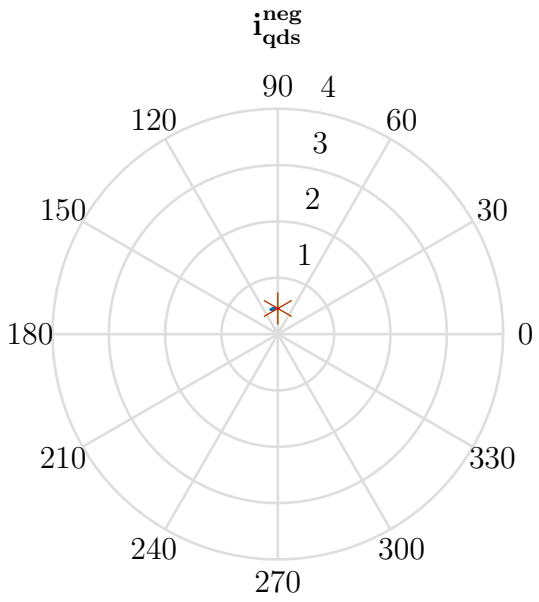

Figure 4-16: Saliency tracking in negative sequence synchronous reference frame: current polar trajectory. Green mark: starting point, red mark: ending point. $L^e_{oqs} = 0.14$mH, $L^e_{ods} = 0.1$mH, $V_{sc} = 1$V, $h = 8$, $\omega_c = 2\pi 500$rad/s, second-order HPF at 5Hz.

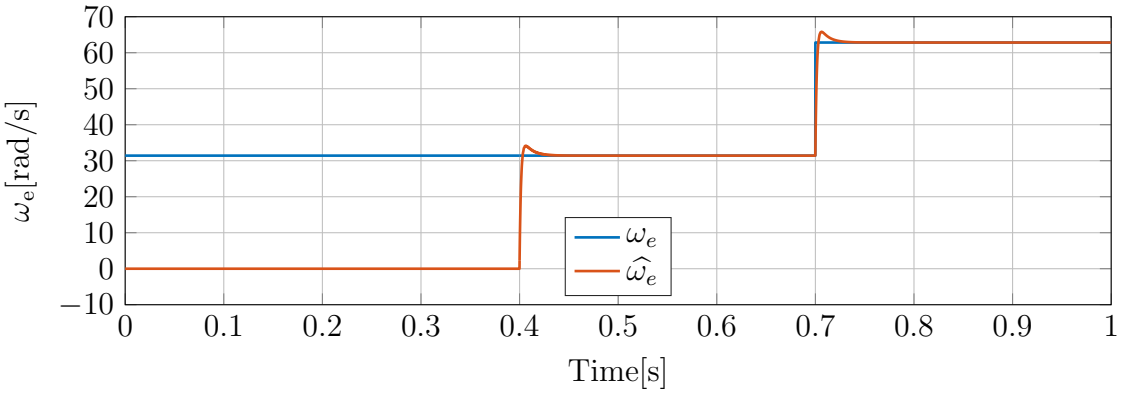

Figure 4-17: Saliency tracking in negative sequence synchronous reference frame: saliency frequency evolution. $L^e_{oqs} = 0.14$mH, $L^e_{ods} = 0.1$mH, $V_{sc} = 1$V, $h = 8$, $\omega_c = 2\pi 500$rad/s, second-order HPF at 5Hz.

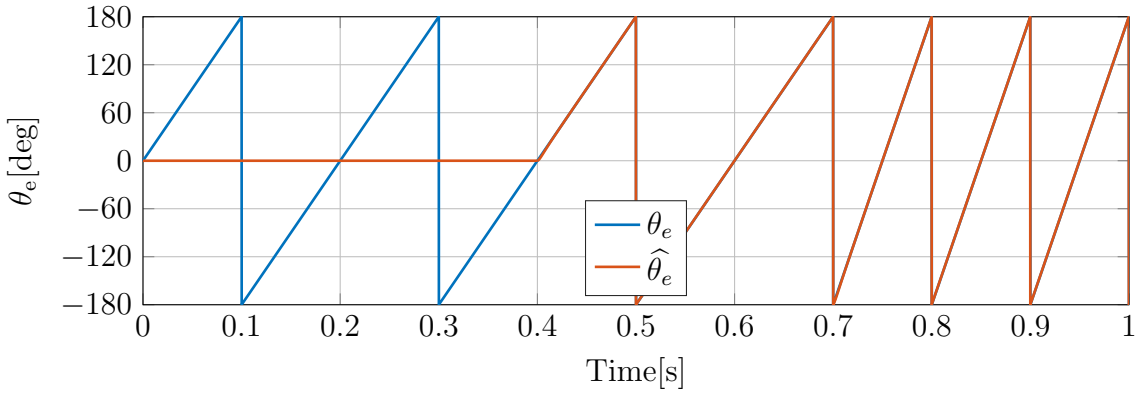

Figure 4-18: Saliency tracking in negative sequence synchronous reference frame: saliency position evolution. $L^e_{oqs} = 0.14$mH, $L^e_{ods} = 0.1$mH, $V_{sc} = 1$V, $h = 8$, $\omega_c = 2\pi 500$rad/s, second-order HPF at 5Hz.

Chapter 5

Open Loop Simulations

Once the carrier frequency excitation is analyzed (Chapter 4), it is necessary to develop a complete model of the induction machine with the saliency in order to be able to simulate its behavior. This chapter will be focused on obtaining the induction machine model with saliency and performing simple open loop simulations in order to test the carrier frequency excitation of the machine. Both the machine model and the corresponding simulations will be performed in Simulink.

5.1 Machine Model with Saliency

In order to obtain the machine model with saliency, the Simulink model "Asynchronous Machine SI Units" will be used as a basis. The machine model will be a discrete-time model since all the simulations will be performed in discrete time. In addition, the machine model will be performed in stationary reference frame since it is a generic reference frame that can be easily transformed into another reference frame.

The block diagram of the custom machine model with saliency is shown in Figure B-1 in Appendix B. The main difference between the Simulink basis model and the custom machine model is the matrices computation since it is necessary to add the saliency inductance into the custom machine model. The matrices computation of the custom machine model is shown in Appendix B. As can be seen the saliency

inductance matrix (LsalM) is added to both the stator inductance matrix (LsM) and the rotor inductance matrix (LrM). The machine parameters are shown in Table 5.1.

Table 5.1: Machine parameters.

L^e_{oqs}	0.14mH
L^e_{ods}	0.1mH
R_s	0.01Ω
R_r	0.005Ω
L_m	5mH
J	2.9kg.mˆ2
F	0.05658N.m.s
p_p	2
h	8
ϕ_e	15°
Rated power	160kW
Rated voltage	400V
Rated speed	1487rpm

5.2 Simulation with Pure Carrier Frequency Excitation

The first simulation to be carried out is an open loop simulation in which the induction machine is supplied only with a voltage at the carrier frequency. Since there is not fundamental frequency excitation, the rotor speed (ω_r) is externally fixed. The rotor angle (θ_r) will be estimated by performing saliency tracking as explained in Section 4.4. The HPF bandwidth and the PI proportional/integral gains will maintain the same values (5Hz, 20/10). The block diagram of the simulation is shown in Figure B-2 in Appendix B. The rotor speed (ω_r) is initially fixed at 2π5rad/s and the magnitude of the voltage will be 7V at 500Hz (carrier frequency). The saliency tracking control is enabled at 0.4s and the rotor speed (ω_r) is changed several times to check the performance.

Figure 5-1, Figure 5-2, Figure 5-3 and Figure 5-4 show the results of the open loop simulation with pure carrier frequency excitation. As can be seen, the negative sequence component of the current corresponds to a saliency with an harmonic number of 8: $8 \cdot 5 - 500 = -460$. The positive sequence component of the current (ω_c) is filtered by synchronizing with it and using a HPF since it does not provide any useful information. In this way, the saliency tracking is working properly and the estimated rotor frequency/position is practically equal to the real saliency frequency/position.

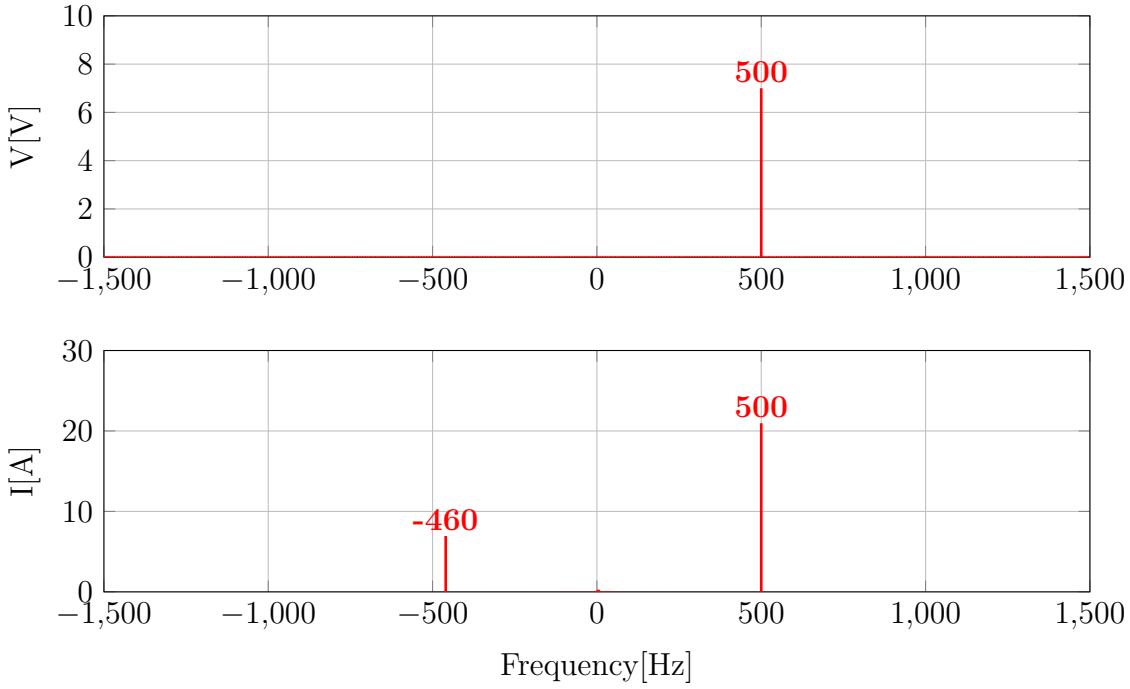

Figure 5-1: Results of open loop simulation with pure carrier frequency excitation: voltage/current FFT for ω_r equal to $2\pi 5$rad/s.

5.3 Simulation including Fundamental Excitation

The second simulation to be carried out is an open loop simulation in which the induction machine is supplied with a voltage at the fundamental frequency and a voltage at the carrier frequency. Now, the rotor speed (ω_r) will be determined by the fundamental frequency excitation. The rotor angle (θ_r) will be estimated by performing saliency tracking as explained in Section 4.4. The HPF bandwidth and the

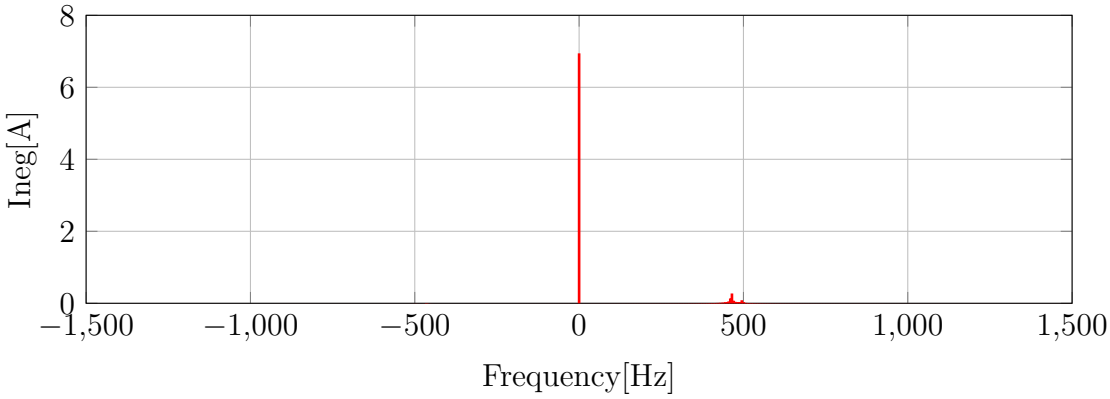

Figure 5-2: Results of open loop simulation with pure carrier frequency excitation: final filtered current for ω_r equal to $2\pi 5$rad/s in negative sequence synchronous reference frame.

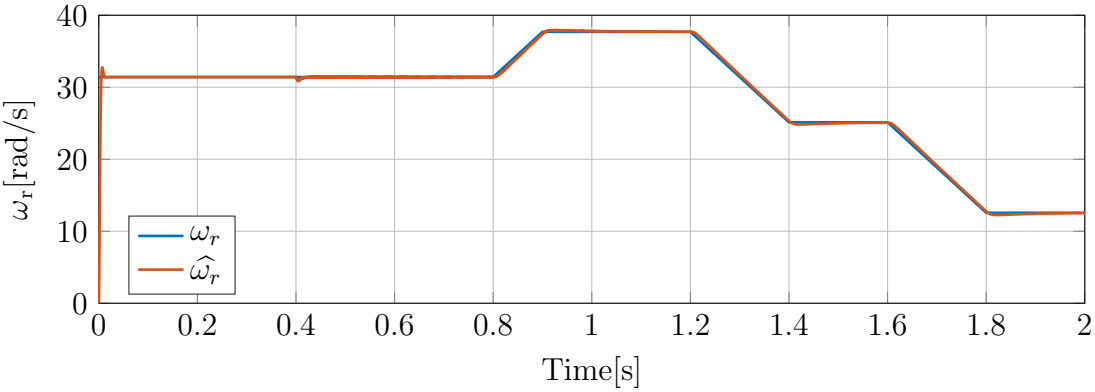

Figure 5-3: Results of open loop simulation with pure carrier frequency excitation: electrical rotor speed (with LPF at 100Hz).

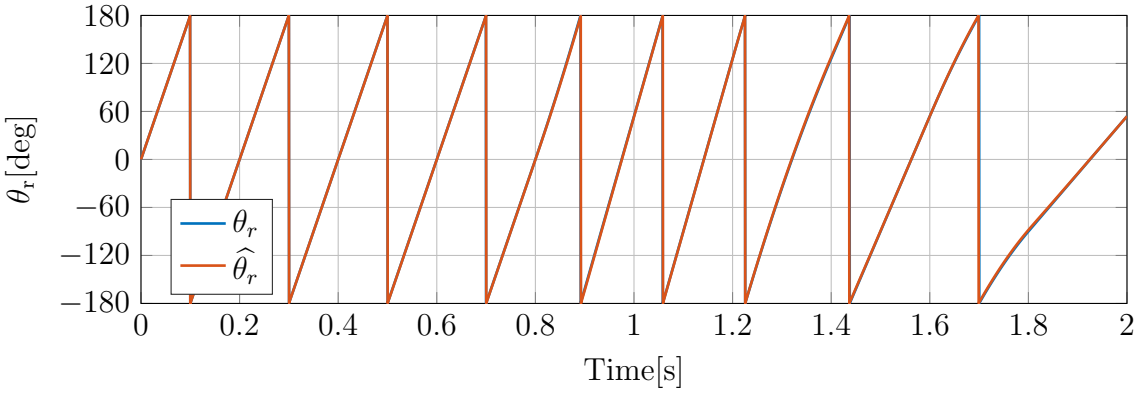

Figure 5-4: Results of open loop simulation with pure carrier frequency excitation: electrical rotor position.

PI proportional/integral gains will maintain the same values (5Hz, 20/10). The block diagram of the simulation is similar to the block diagram of the previous simulation in Figure B-2 but modifying the filtering process as shown in Figure B-3. Note that now the fundamental frequency is also filtered in a similar way to the carrier frequency. Nevertheless, the HPF bandwidth for the fundamental frequency filtering is 100Hz in order to filter the secondary harmonics around the fundamental one. The magnitude of the voltage will be 35V at 5Hz (fundamental frequency) and 7V (0.2pu) at 500Hz (carrier frequency). The saliency tracking control is enabled at 2s.

Figure 5-5, Figure 5-6, Figure 5-7 and Figure 5-8 show the results of the open loop simulation including fundamental excitation. As can be seen, the carrier negative sequence component of the current corresponds to a saliency with an harmonic number of 8: $8 \cdot 5 - 500 = -460$. There are several frequency components that are going to be filtered by synchronizing with them and using a HPF since they do not provide any useful information:

- Fundamental frequency (ω_e: 5Hz) and secondary harmonics with a 100Hz HPF.
- Carrier frequency (ω_c: 500Hz) with a 5Hz HPF.

In this way, the saliency tracking is working properly and the estimated rotor position is practically equal to the real saliency position. Note that now the saliency frequency is not perfectly estimated since there are some harmonics that are not being filtered and disturb the PLL control. Nevertheless, the estimated rotor position is not practically affected.

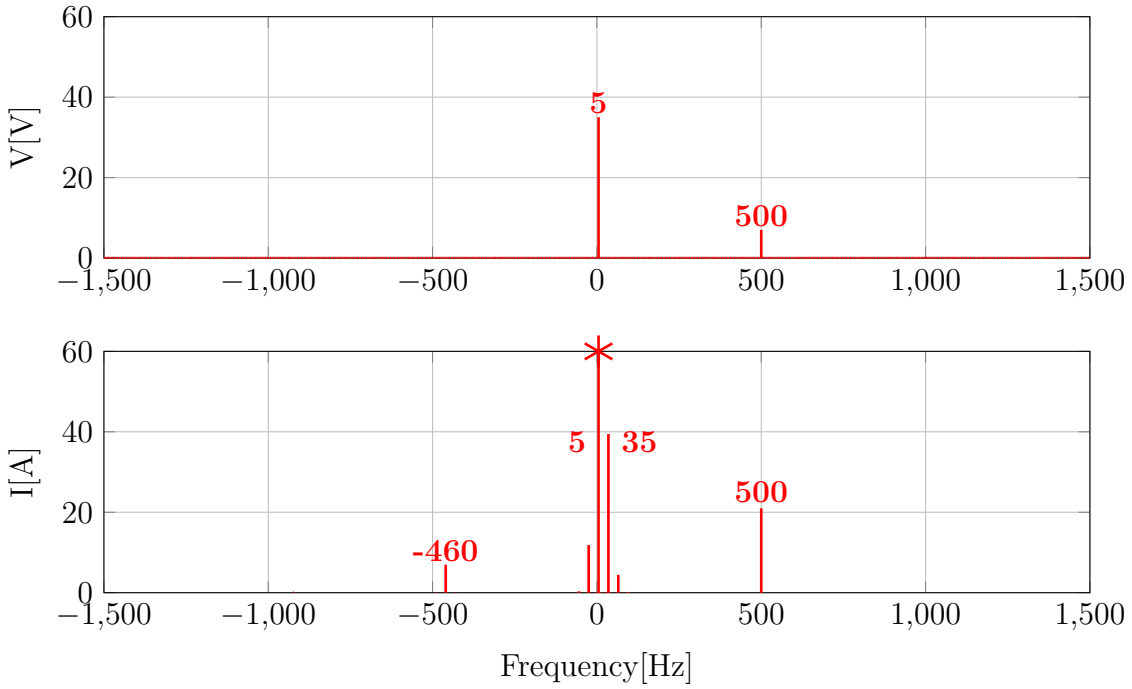

Figure 5-5: Results of open loop simulation including fundamental excitation: voltage/current FFT with fundamental capped.

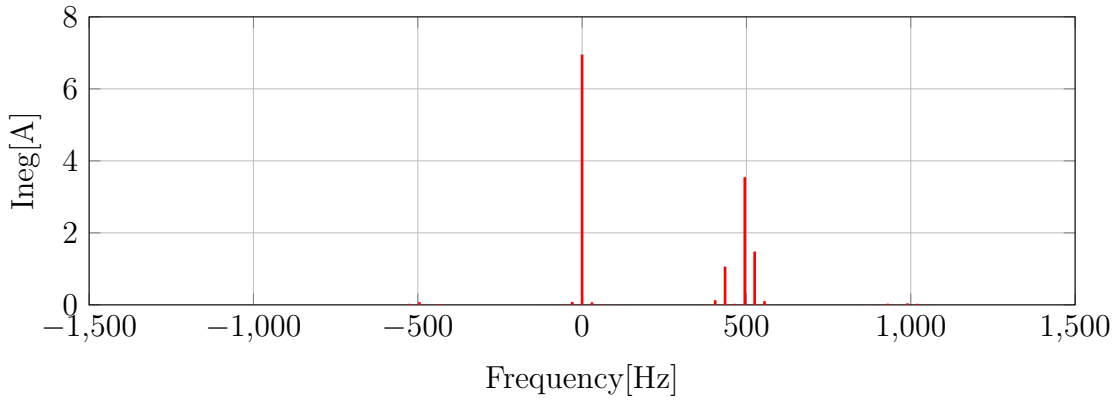

Figure 5-6: Results of open loop simulation including fundamental excitation: final filtered current in negative sequence synchronous reference frame.

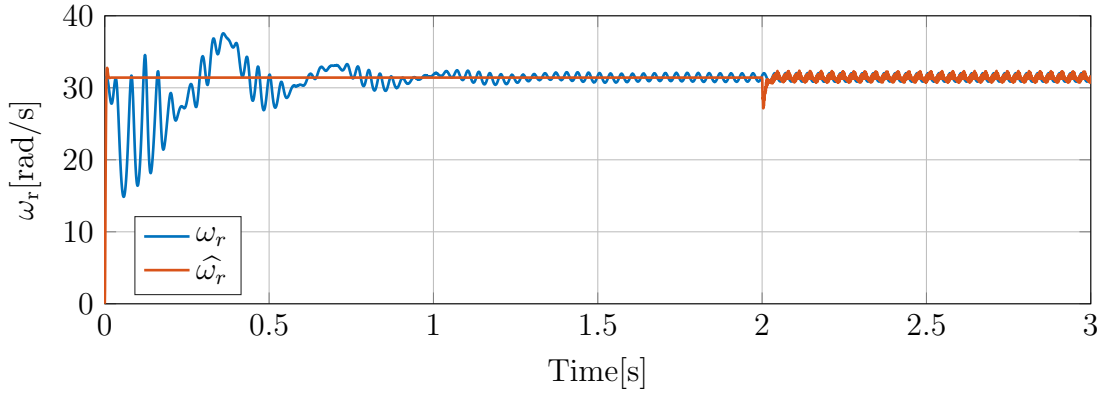

Figure 5-7: Results of open loop simulation including fundamental excitation: electrical rotor speed (with LPF at 100Hz).

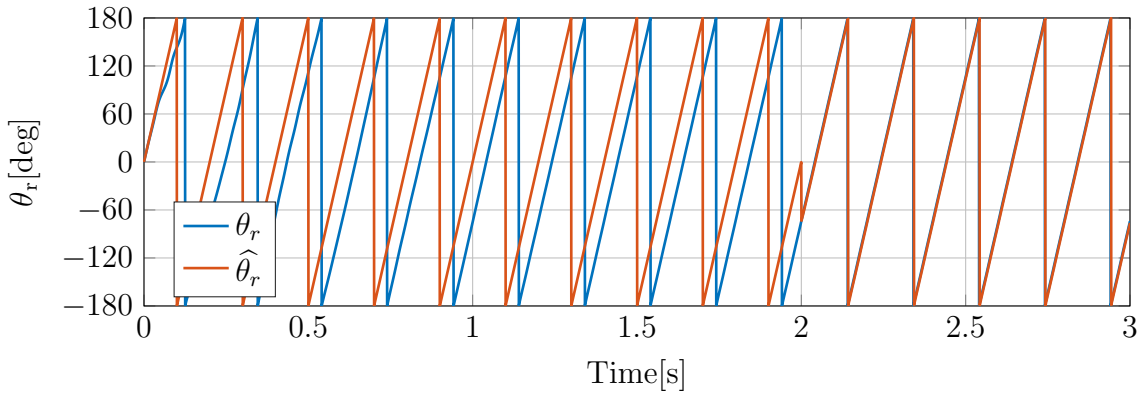

Figure 5-8: Results of open loop simulation including fundamental excitation: electrical rotor position.

Chapter 6

Field Oriented Control

Once the open loop simulations of the machine are performed (Chapter 5), it is necessary to carry out the control of the machine in order to operate in the desired operating conditions. The kind of control to be used in order to manage the induction machine is known as Field Oriented Control (FOC). It consists of transforming the machine three-phase magnitudes into a qd rotor flux synchronous reference frame. In this way, the magnitudes are going to be represented by two components, one aligned (d axis) and the other one orthogonal (q axis) to the rotor flux. Therefore, both flux and torque of the machine can be controlled independently by injecting current in the qd synchronous reference frame: d-axis current for controlling the flux and q-axis current for controlling the torque [10].

The following aspects will be analyzed in this chapter in order to complete the FOC:

- Power system.
- Measurements and rotor flux observer.
- Current control loop.
- Flux/speed control loop.
- Pulses generator.
- Validation.

6.1 Power System

The induction machine will be supplied by a three-phase inverter connected to a DC bus. The gate pulses are generated by the control system via Pulse-Width Modulation (PWM). The switching frequency of the inverter will be 10kHz. In order to take full advantage of the DC bus, third harmonic injection is included, so that the DC bus voltage (V_{DC}) is $\sqrt{2}$ times the rated voltage (400V).

The block diagram of the power system is shown in Figure B-4 in Appendix B.

6.2 Measurements and rotor flux observer

In order to close the control loop, it is necessary to perform some measurements. In particular, it is necessary to measure the stator current of two different phases and the rotor position/speed. The current measurements has to be transformed first into the stationary reference frame and subsequently into the rotor flux synchronous reference frame. Therefore, a rotor flux observer is needed in order to estimate the angular position of the rotor flux. The rotor position/speed has to be transformed from mechanical units into electrical units by using the number of pole pairs.

The implementation used for the rotor flux observer will be the current model open-loop rotor flux observer, which was explained in Section 3.2. In this way, both the rotor flux magnitude and the rotor flux position are estimated, so that the rotor flux synchronization can be achieved.

The block diagram of the measurements and rotor flux observer is shown in Figure B-5 in Appendix B. As can be seen, there is a filtering of the carrier frequency current before performing the transformation into the rotor flux synchronous reference frame. This is to reduce the influence of the carrier frequency excitation into the control system. Note that the computation of the measurements and the rotor flux observer will be performed with a frequency of 10kHz.

6.3 Current control loop

The control loop of the induction machine will be a cascade control loop in which the inner control loop will be the current control loop. In the current control loop, both d-axis and q-axis current will be controlled independently by using two different PI controllers. Nevertheless, the gains of both controllers will be the same since both currents have the same dynamics. The output of the controllers (control action) will be the d-axis and q-axis reference voltages that have to be generated by the inverter. It should be recalled that the control system operates in the rotor flux synchronous reference frame whereas the inverter generates three-phase voltages. Therefore, the d-axis and q-axis reference voltages are transformed into three-phase voltages to feed the inverter. Note that the reference voltages are saturated to $\pm V_{DC}/\sqrt{3}$, which is the minimum/maximum voltage that the inverter can supply (third harmonic injection).

The selected proportional gain (K_{p_I}) and integral gain (K_{i_I}) of the current PI controllers are shown in (6.1) and (6.2).

$$K_{p\_I} = 0.5 \tag{6.1}$$

$$K_{i\_I} = 100 \tag{6.2}$$

The block diagram of the current control loop is shown in Figure B-6 in Appendix B. Note that the computation of the current control loop will be performed with a frequency of 10kHz.

6.4 Flux/speed control loop

The outer control loop of the cascade control loop of the induction machine will be the flux/speed control loop.

In the flux control loop, the rotor flux is controlled by using a PI controller. The output of the rotor flux PI controller (control action) will be the d-axis reference current, since the d-axis current produces flux (d-axis aligned with the rotor flux).

The selected proportional gain (K_{p_rf}) and integral gain (K_{i_rf}) of the rotor flux

PI controller are shown in (6.3) and (6.4).

$$K_{p\_rf} = 2000 \tag{6.3}$$

$$K_{i\_rf} = 10 \tag{6.4}$$

In the speed control loop, the rotor speed is controlled by using a PI controller. The output of the speed PI controller (control action) will be the reference torque, which will be transformed into the q-axis reference current as shown in (6.5), since the q-axis current produces torque (q-axis orthogonal to the rotor flux).

$$i_{qs}^{rf*} = \frac{T^*}{3/2\, p_p\, \lambda_r} \tag{6.5}$$

The selected proportional gain (K_{p_speed}) and integral gain (K_{i_speed}) of the speed PI controller are shown in (6.6) and (6.7).

$$K_{p\_\text{speed}} = 4 \tag{6.6}$$

$$K_{i\_\text{speed}} = 5 \tag{6.7}$$

The output of the controllers (control action) will be the d-axis and q-axis reference currents, which have to be controlled by the current control loop. Note that the reference currents are saturated to the minimum/maximum current of the machine to avoid overcurrents.

The block diagram of the flux/speed control loop is shown in Figure B-7 in Appendix B. Note that the computation of the flux/speed control loop will be performed with a frequency of 10kHz.

6.5 Pulses generator

In order to generate the desired three-phase voltage, it is necessary to generate the pulses which drive the inverter. Note that the output of the current control loop is the three-phase reference voltage. The third homopolar injection is applied to this

three-phase reference voltage (V^*_{abc}) in order to obtain the final three-phase reference voltage ($V^*_{abc\_thi}$) as shown in (6.8).

$$V^*_{abc\_thi} = V^*_{abc} - \frac{1}{2}\left(\max\left\{V^*_{abc}\right\} + \min\left\{V^*_{abc}\right\}\right) \tag{6.8}$$

After that, the three-phase reference voltage is transformed into the duty cycle (per unit voltage) by dividing it by $V_{DC}/2$. It can be selected to have only fundamental excitation, only carrier frequency excitation or both of them. In order to generate the pulses, a PWM generator with sine-triangle modulation is used.

The block diagram of the pulses generator is shown in Figure B-8 in Appendix B. Note that the switching frequency is 10kHz.

6.6 Validation

Once the FOC is completed, it is necessary to validate its performance. The following simulation profile will be tested:

- Initial rotor speed reference (n^*_{rm}): 150rpm
- Rotor flux reference (λ^*_r): 1 Wb
- Change of rotor speed reference (n^*_{rm}) to 1000rpm at 1s.
- Change of rotor speed reference (n^*_{rm}) to 200rpm at 2s.
- Change of rotor speed reference (n^*_{rm}) to 100rpm at 3s.

Figure 6-1, Figure 6-2, Figure 6-3 and Figure 6-4 show the results of the validation of the FOC. As can be seen, the estimation of the rotor flux is quite accurate, so the rotor flux observer is working properly and the rotor flux alignment is suitable. In addition, it can be seen that both the rotor flux and the rotor speed follow the references quite fast and accurate by controlling the d-axis and q-axis current. The current regulation is much faster than the rotor flux/speed as expected in a cascade control loop.

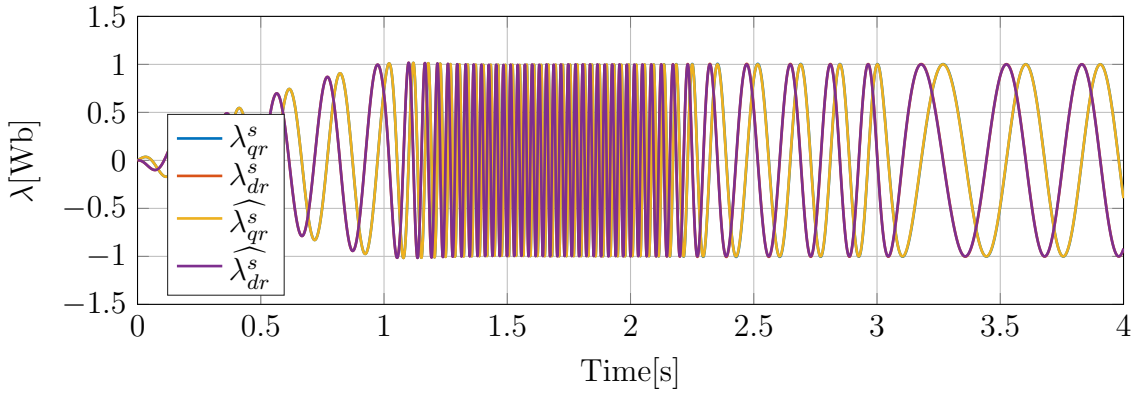

Figure 6-1: Validation of Field Oriented Control: Real rotor flux vs estimated rotor flux.

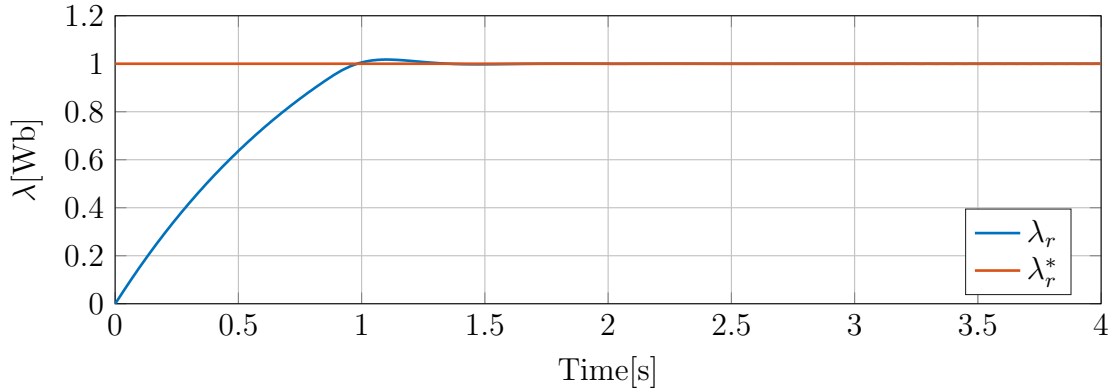

Figure 6-2: Validation of Field Oriented Control: Rotor flux evolution.

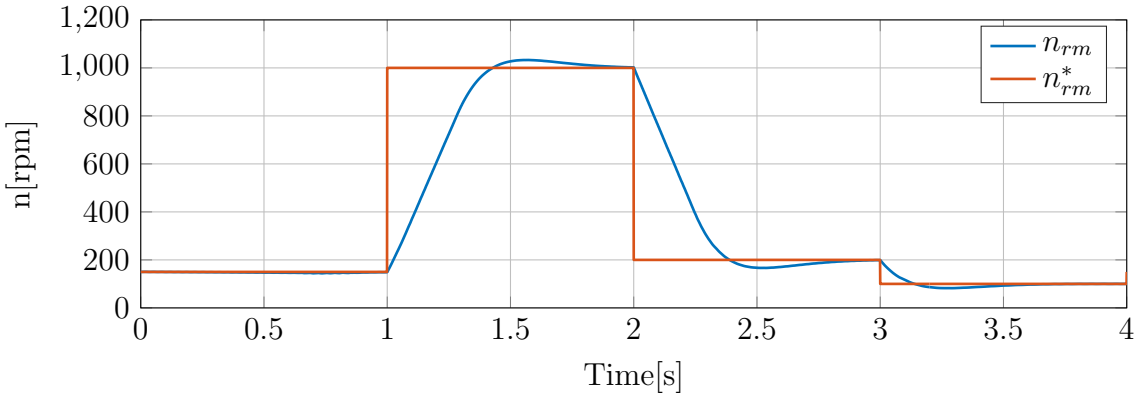

Figure 6-3: Validation of Field Oriented Control: Mechanical rotor speed evolution.

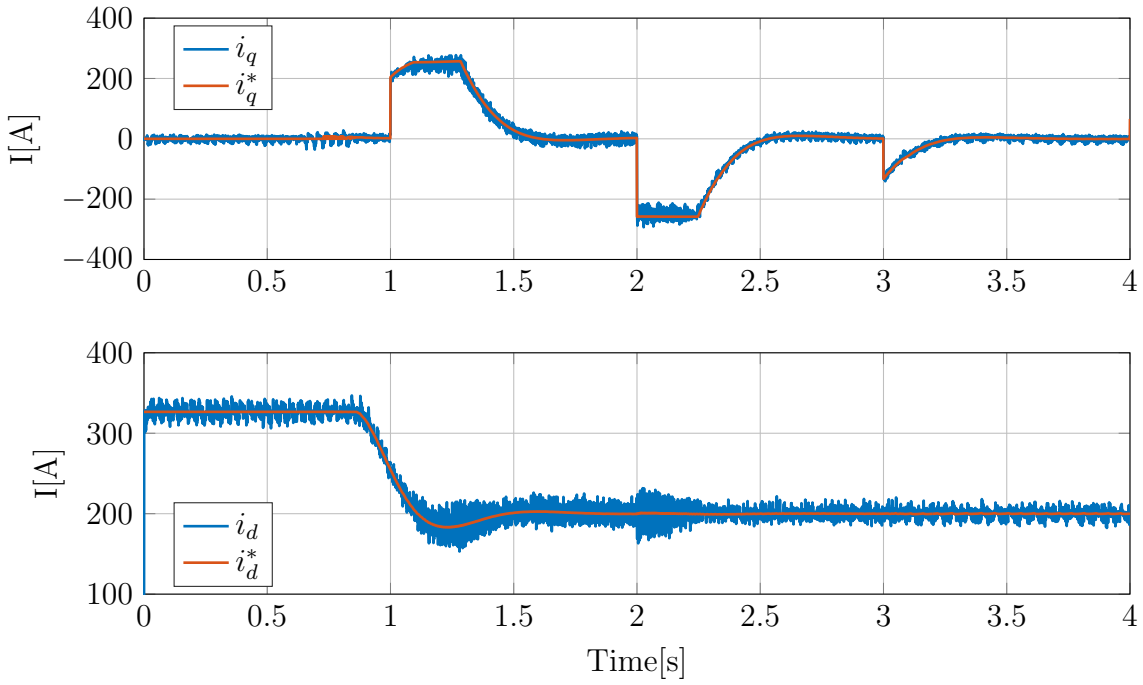

Figure 6-4: Validation of Field Oriented Control: Current evolution.

Chapter 7

FOC Simulations

Once the field oriented control is performed (Chapter 6), it is necessary to perform several simulations in order to test the carrier frequency excitation of the machine with the field oriented control. This chapter will be focused on performing these simulations in order to validate the carrier frequency excitation when the machine is controlled.

7.1 Simulation with Pure Carrier Frequency Excitation

The first simulation to be carried out is a FOC simulation in which the induction machine is supplied only with a voltage at the carrier frequency. Since there is not fundamental frequency excitation, the rotor speed (ω_r) is externally fixed. The rotor angle (θ_r) will be estimated by performing saliency tracking as explained in Section 4.4. The HPF bandwidth and the PI proportional/integral gains will maintain the same values (5Hz, 20/10). The block diagram of the rotor angle estimator is shown in Figure B-9 in Appendix B. The rotor speed (ω_r) is initially fixed at 2π5rad/s and the magnitude of the voltage will be 20V at 500Hz (carrier frequency). The rotor angle estimator is enabled at 0.4s and the rotor speed (ω_r) is changed several times to check the performance.

Figure 7-1, Figure 7-2, Figure 7-3 and Figure 7-4 show the results of the FOC simulation with pure carrier frequency excitation. As can be seen, the negative sequence component of the current corresponds to a saliency with an harmonic number of 8: $8 \cdot 5 - 500 = -460$. The positive sequence component of the current (ω_c) is filtered by synchronizing with it and using a HPF since it does not provide any useful information. In this way, the saliency tracking is working properly and the estimated rotor frequency/position is practically equal to the real saliency frequency/position. The obtained results are very similar to the results in Section 5.2. Only the estimated frequency is more noisy due to the FOC and power converter effects.

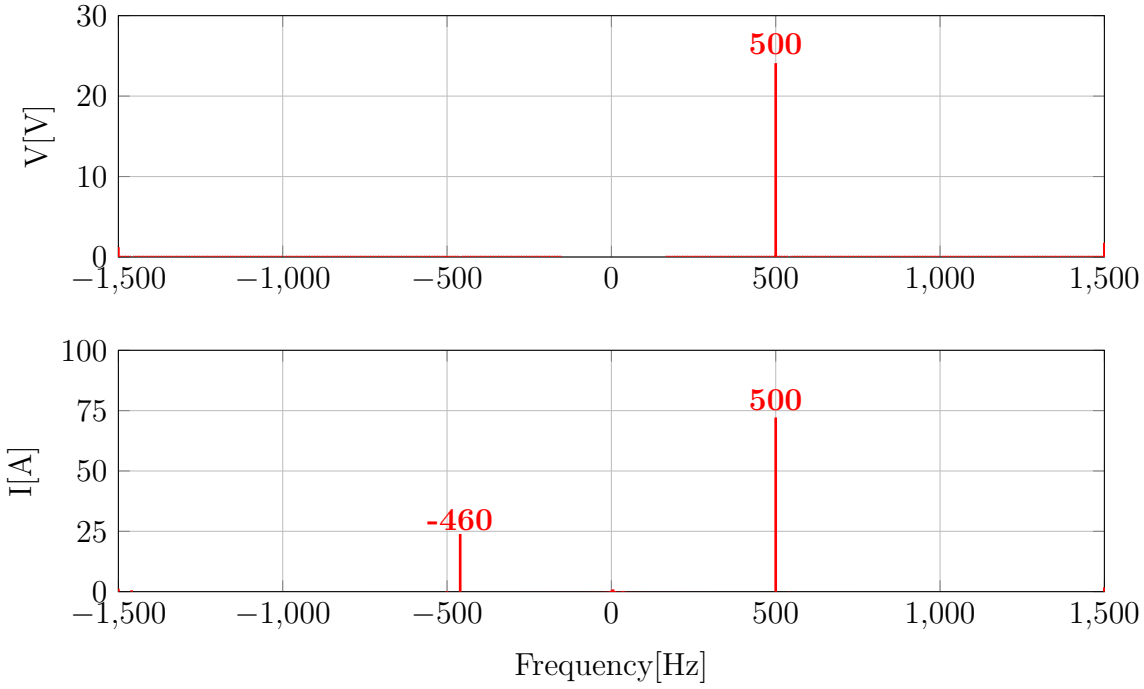

Figure 7-1: Results of FOC simulation with pure carrier frequency excitation: voltage/current FFT for ω_r equal to $2\pi 5$rad/s.

7.2 Simulation including Fundamental Excitation

The second simulation to be carried out is a FOC simulation in which the induction machine is supplied with a voltage at the fundamental frequency and a voltage at the carrier frequency. Now, the rotor speed (ω_r) will be determined by the fundamental

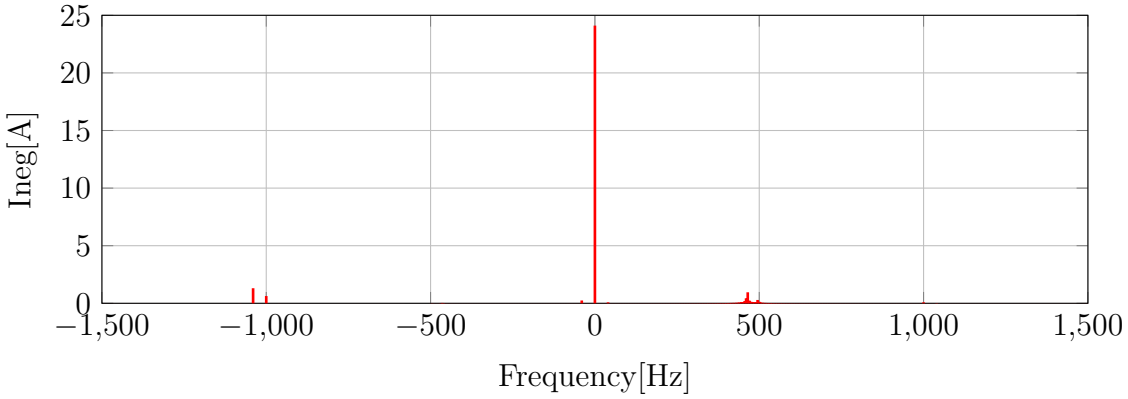

Figure 7-2: Results of FOC simulation with pure carrier frequency excitation: final filtered current for ω_r equal to $2\pi 5$rad/s in negative sequence synchronous reference frame.

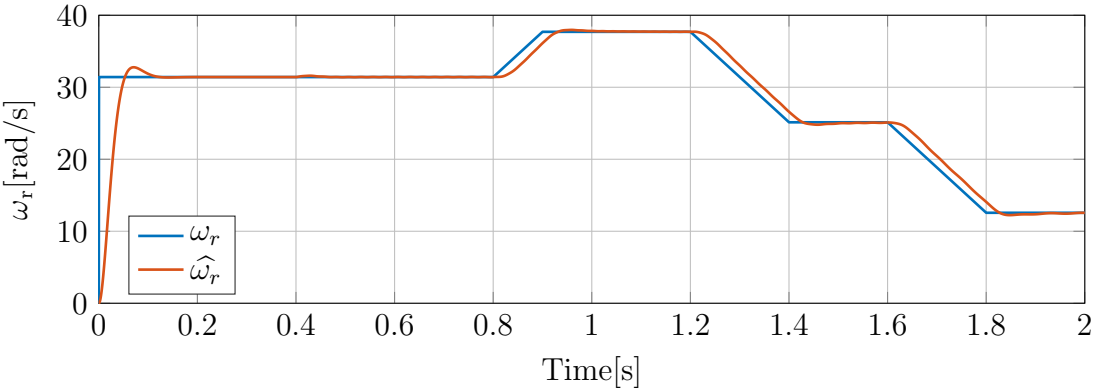

Figure 7-3: Results of FOC simulation with pure carrier frequency excitation: electrical rotor speed (with LPF at 10Hz).

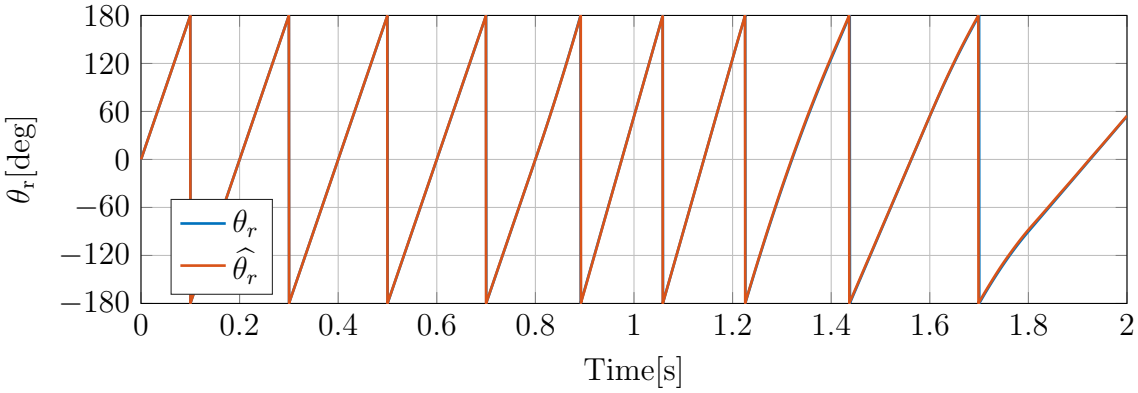

Figure 7-4: Results of FOC simulation with pure carrier frequency excitation: electrical rotor position.

frequency excitation. The rotor angle (θ_r) will be estimated by performing saliency tracking as explained in Section 4.4. The HPF bandwidth and the PI proportional/integral gains will maintain the same values (5Hz, 20/10). The block diagram of the simulation is similar to the block diagram of the previous simulation in Figure B-9 but modifying the filtering process as shown in Figure B-10. Note that now the fundamental frequency is also filtered in a similar way to the carrier frequency. Nevertheless, the HPF bandwidth for the fundamental frequency filtering is 100Hz in order to filter the secondary harmonics around the fundamental one. The magnitude of the carrier voltage will be 7V at 500Hz (carrier frequency). The initial rotor speed reference is 150rpm (5Hz) and is changed several times to check the performance. The saliency tracking control is enabled at 1s. The fundamental frequency position is estimated with the rotor flux position in order to perform the fundamental frequency filtering.

Figure 7-5, Figure 7-6, Figure 7-7 and Figure 7-8 show the results of the FOC simulation including fundamental excitation. As can be seen, the carrier negative sequence component of the current corresponds to a saliency with an harmonic number of 8: $8 \cdot 5 - 500 = -460$. There are several frequency components that are going to be filtered by synchronizing with them and using a HPF since they do not provide any useful information:

- Fundamental frequency (ω_e: 5Hz) and secondary harmonics with a 100Hz HPF.

- Carrier frequency (ω_c: 500Hz) with a 5Hz HPF.

In this way, the saliency tracking is working properly and the estimated rotor position is practically equal to the real saliency position. Note that now the saliency frequency is not perfectly estimated since there are some harmonics that are not being filtered and disturb the PLL control. Nevertheless, the estimated rotor position is not practically affected and the saliency tracking is suitable, even though the rotor speed is changed.

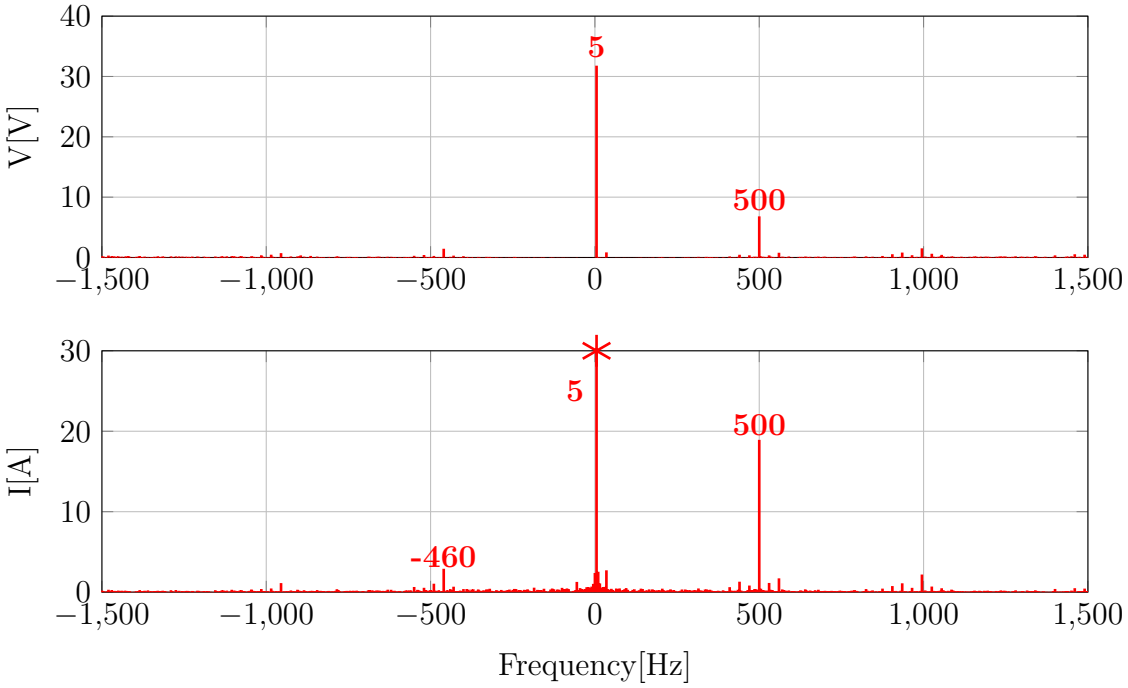

Figure 7-5: Results of FOC simulation including fundamental excitation: voltage/current FFT with fundamental capped for 150rpm.

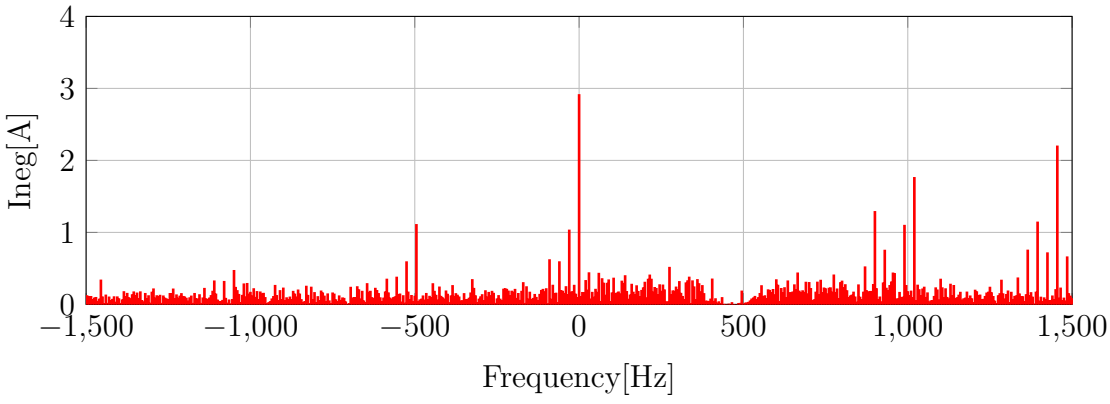

Figure 7-6: Results of FOC simulation including fundamental excitation: final filtered current in negative sequence synchronous reference frame for 150rpm.

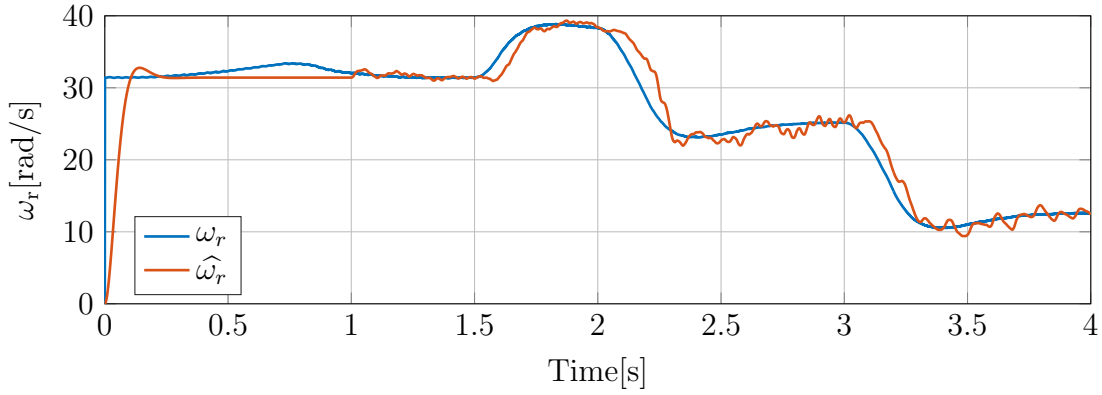

Figure 7-7: Results of FOC simulation including fundamental excitation: electrical rotor speed (with LPF at 5Hz).

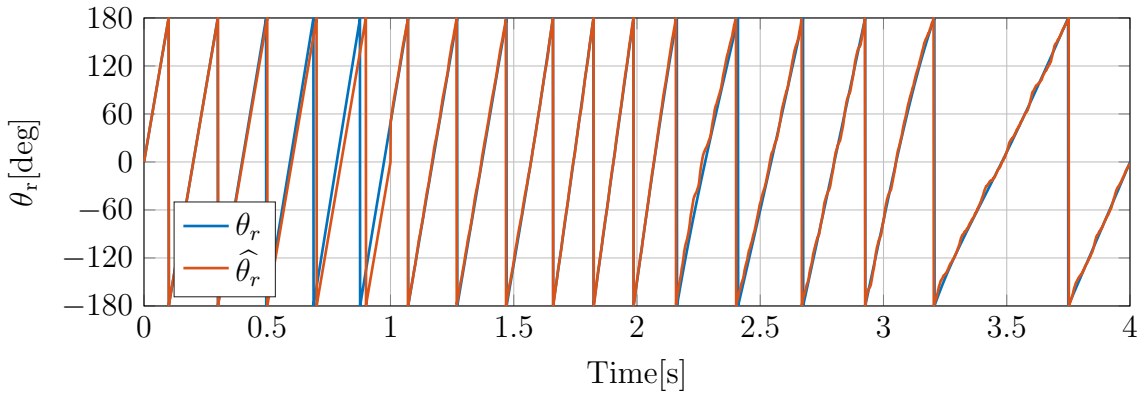

Figure 7-8: Results of FOC simulation including fundamental excitation: electrical rotor position.

7.3 Final Simulation with Sensorless Control

In the previous sections, it was demonstrated that the saliency tracking via high frequency excitation is suitable for induction machines with saliencies, so that the estimation of both rotor speed and position is quite accurate, even though the operating conditions of the machine changes. Therefore, the last step is to use the estimated measurements of speed and position for performing the Field Oriented Control (FOC) instead of the real mechanical measurements of speed and position. In this way, the dependence on electro-mechanical sensors is suppressed and the sensorless control is achieved. The estimated rotor position is necessary to estimate the rotor flux magnitude and position (the current model open-loop flux observer requires the rotor position), whereas the estimated rotor speed is necessary to close the speed control loop.

Figure 7-9, Figure 7-10, Figure 7-11 and Figure 7-12 show the results of the final simulation with sensorless control. Both the rotor speed reference and the load torque are changed in order to check the dynamic and static performance of the sensorless control. As can be seen, the estimation of the rotor flux is quite accurate, so the rotor flux observer is working properly. In addition, it can be seen that the rotor speed follows the references quite fast and accurate and it can compensate the perturbations in the form of load torque. To conclude, the saliency tracking is working properly and the estimated rotor position is practically equal to the real saliency position. The saliency frequency is not perfectly estimated since there are some harmonics that are not being filtered and disturb the PLL control. Nevertheless, the estimated rotor speed is quite accurate, so that it allows a good sensorless control of the rotor speed.

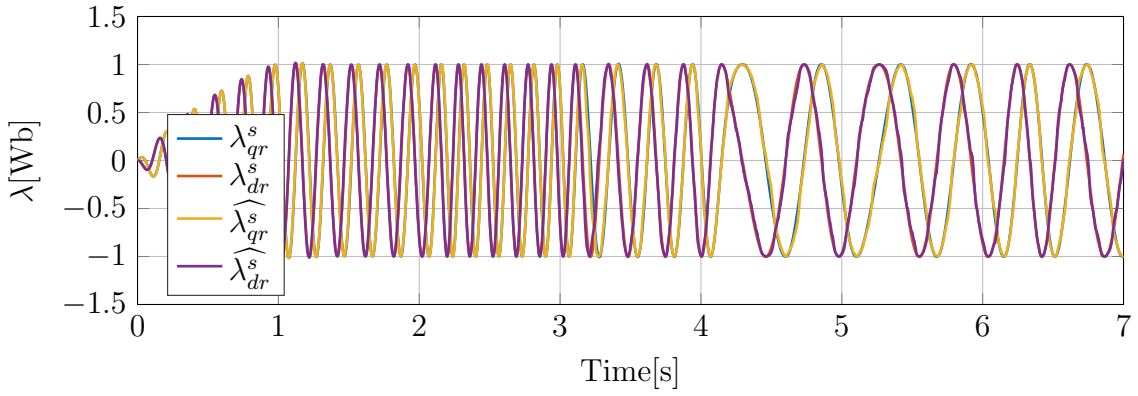

Figure 7-9: Sensorless control: Real rotor flux vs estimated rotor flux.

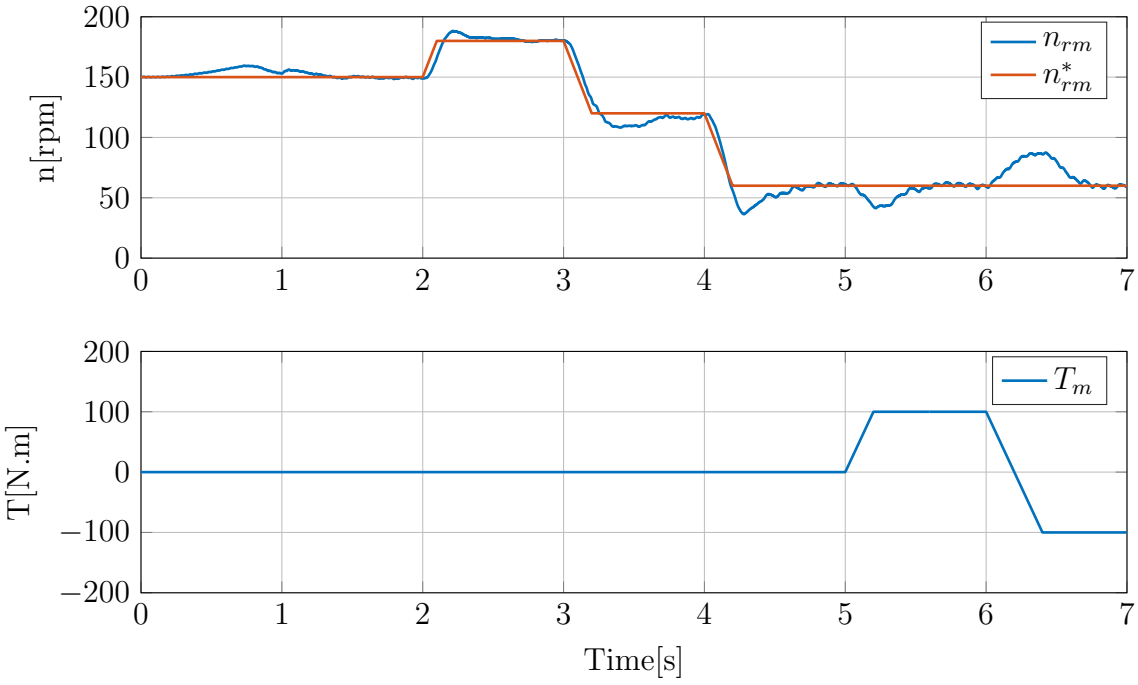

Figure 7-10: Sensorless control: Mechanical rotor speed evolution and load torque.

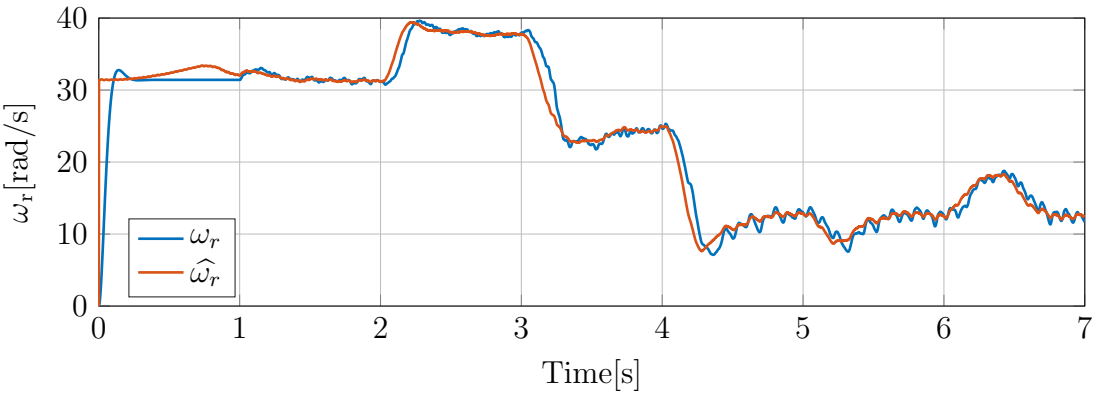

Figure 7-11: Sensorless control: Electrical rotor speed (with LPF at 5Hz).

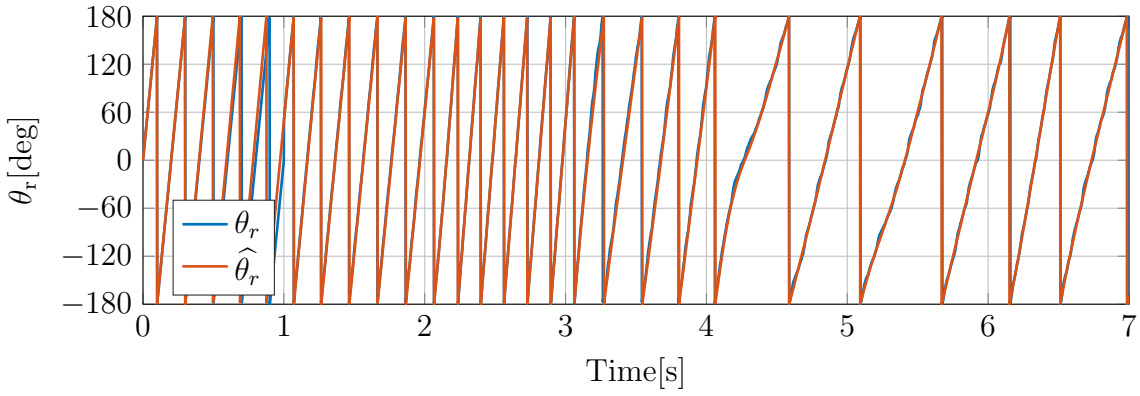

Figure 7-12: Sensorless control: Electrical rotor position.

Chapter 8

Conclusions

As stated in the previous chapters, sensorless control techniques are suitable in order to perform the control of induction machines. The sensorless control technique implemented in this thesis is based on the injection of high frequency voltage into the machine in order to induce current harmonics that can provide spatial information. Nevertheless, it is a prerequisite that the machine has some kind of saliency, e.g., due to stator/rotor slotting. The continuous injection of high frequency voltage allows the saliency tracking at low and zero speeds.

In this particular thesis, the carrier frequency excitation was used in order to estimate the rotor position of an induction machine with Field Oriented Control (FOC). After that, the sensorless control was implemented and tested, which works properly since it follows the references and rejects the disturbances fast and accurate. This is because the estimation of the rotor position and speed (saliency tracking) is fast and accurate under steady-state and transient conditions.

A further analysis of the harmonics that disturb the saliency tracking might be done when a power converter with field oriented control is used to manage the machine. In this way, these harmonics can also be filtered in order to improve the saliency tracking even more.

Another possibility of improvement is to modify the algorithm used to perform the saliency tracking. In this particular case, a Phase-Locked Loop (PLL) is implemented to carry out the saliency tracking. The PLL is only focused on one component of

the filtered dq current, the q-axis component. A more complex controller in which both components of the filtered dq current are controlled might improve the saliency tracking performance during transients.

In addition, when the induction machine is overloaded, saturation of the machine core can be produced. Saturation phenomenon implies a non-linear operation of the machine and hence it generates several harmonics that can also disturb the saliency tracking. A further analysis of the harmonics generation due to saturation and its consequent decoupling can be done in order to increase the operation range of the sensorless control.

Chapter 9

Future Developments

In order to improve the performance of the sensorless control analyzed in this thesis, the following issues can be considered:

- Further analysis of the harmonics that disturb the saliency tracking and the consequent filtering.
- Modification/improvement of the algorithm used to perform the saliency tracking.
- Analysis of the saturation effect into the saliency tracking due to overload.

Chapter 10

Quality Report

During the development of this Master Thesis, there was some technical issues that hindered its completion:

- Lack of a Simulink model of an induction machine with saliencies: This thesis was focused on the analysis of an induction machine with saliencies when it is excited with high frequency. Nevertheless, the sensorless control of the machine also requires the excitation of the machine at fundamental frequency. Therefore, a complete model of the induction machine with saliencies had to be done in order to perform the sensorless control.

- Lack of information about the parameters of wind generators: Since electrical wind generation is a strategic sector, it is complicated to obtain detailed information about the machine parameters in order to perform the simulations.

- Large induction generators symmetry: Large induction generators are practically symmetrical because both the stator and the rotor are formed by conductor bars instead of windings. Therefore, it is more complicated to analyze the saliencies in this kind of generators.

Appendix A

MATLAB Scripts

A.1 Excitation in stationary reference frame (fixed saliency)

```
%% Clear workspace
close all;
clear;
clc;

%% Parameters
Loqs = 0.14e-3; % q-axis stator transient inductance [H]
Lods = 0.10e-3; % d-axis stator transient inductance [H]
h = 8; % Harmonic number of saliency
Oe = pi/6; % Electrical rotor position [rad]
fc = 500; % Carrier frequency [Hz]
fs = 10e3; % Sample frequency [Hz]

%% Time vector computation
wc = 2*pi*fc; % Carrier frequency [rad/s]
Ts = 1/fs; % Sample period [s]
Tc = 1/fc; % Carrier period [s]
t = 0:Ts:Tc; % Time vector [s]

%% Voltage computation
vas = cos(wc*t);        % Phase a
vbs = cos(wc*t-2*pi/3); % Phase b
vcs = cos(wc*t+2*pi/3); % Phase c

a = exp(1j*2*pi/3);            % 2*pi/3 rotation
vs = 2/3*(vas+a*vbs+a^2*vcs);  % Complex voltage
vqds_s = [real(vs);-imag(vs)]; % Voltage in stationary qd axis

%% Inductance matrix with saliency
sum_Los = (Loqs+Lods)/2;   % Mean stator transient inductance
delta_Los = (Loqs-Lods)/2; % Differential stator transient inductance
% Inductance matrix
Los = sum_Los*eye(2)...
    + delta_Los*[ cos(h*Oe)   -sin(h*Oe) ;...
                  -sin(h*Oe)  -cos(h*Oe) ];
% Inverse inductance matrix
```

```
Los_inv = 1/(sum_Los^2-delta_Los^2) *...
    ( sum_Los*eye(2)...
      - delta_Los*[ cos(h*Oe)   -sin(h*Oe) ;...
                    -sin(h*Oe)  -cos(h*Oe) ] );

%% Current computation
is = 1/(1j*wc) *...
    complex( Los_inv(1,:)*vqds_s ,...
             -Los_inv(2,:)*vqds_s ); % Complex current
iqds_s = [real(is);-imag(is)]; % Current in stationary qd axis

ias = real(is);                          % Phase a
ibs = -1/2*real(is)+sqrt(3)/2*imag(is); % Phase b
ics = -1/2*real(is)-sqrt(3)/2*imag(is); % Phase c

%% Complex FFT computation
f1 = -1500; % Minimum frequency
f2 = 1500;  % Maximum frequency
[fft_vs,vec_frec_vs] = FFT_Complex_Norm(vs(1:end-1),Ts,f1,f2,0); % Voltage
[fft_is,vec_frec_is] = FFT_Complex_Norm(is(1:end-1),Ts,f1,f2,0); % Current

%% Plot results
figure('Name','3ph magnitudes','NumberTitle','off');
subplot(211);
plot(t*1e3,vas,t*1e3,vbs,t*1e3,vcs,'LineWidth',1);
grid on;
set(gca,'XLim',[0 2]);
set(gca,'XTick',0:0.2:2);
set(gca,'YLim',[-1.5 1.5]);
set(gca,'YTick',-1.5:0.5:1.5);
legend('v_{as}','v_{bs}','v_{cs}','Location','West');
ylabel('V_s[V]');
subplot(212);
plot(t*1e3,ias,t*1e3,ibs,t*1e3,ics,'LineWidth',1);
grid on;
set(gca,'XLim',[0 2]);
set(gca,'XTick',0:0.2:2);
set(gca,'YLim',[-4 4]);
set(gca,'YTick',-4:2:4);
legend('i_{as}','i_{bs}','i_{cs}','Location','West');
ylabel('I_s[A]');
xlabel('Time[ms]');

figure('Name','Stationary qd magnitudes','NumberTitle','off');
subplot(211);
plot(t*1e3,vqds_s(1,:),t*1e3,vqds_s(2,:),'LineWidth',1);
grid on;
set(gca,'XLim',[0 2]);
set(gca,'XTick',0:0.2:2);
set(gca,'YLim',[-1.5 1.5]);
set(gca,'YTick',-1.5:0.5:1.5);
legend('v_{qs}^s','v_{ds}^s','Location','SouthEast');
ylabel('V_s[V]');
subplot(212);
plot(t*1e3,iqds_s(1,:),t*1e3,iqds_s(2,:),'LineWidth',1);
grid on;
set(gca,'XLim',[0 2]);
set(gca,'XTick',0:0.2:2);
set(gca,'YLim',[-4 4]);
set(gca,'YTick',-4:2:4);
legend('i_{qs}^s','i_{ds}^s','Location','SouthWest');
ylabel('I_s[A]');
xlabel('Time[ms]');

figure('Name','Polar trajectory','NumberTitle','off');
subplot(121);
polarplot(vs,'LineWidth',1);
grid on;
```

```
hold on;
polarplot(vs(1),'g*','MarkerSize',12);
polarplot(vs(end),'r*','MarkerSize',12);
ax = gca;
ax.RLim = [0 ceil(max(abs([vs is])))];
ax.ThetaTick = 0:15:360;
title('v_{qds}');
subplot(122);
polarplot(is,'LineWidth',1);
grid on;
hold on;
polarplot(is(1),'g*','MarkerSize',12);
polarplot(is(end),'r*','MarkerSize',12);
ax = gca;
ax.RLim = [0 ceil(max(abs([vs is])))];
ax.ThetaTick = 0:15:360;
title('i_{qds}');

figure('Name','FFT','NumberTitle','off');
[~,ind_fft_vs]=sort(abs(fft_vs));
[~,ind_fft_is]=sort(abs(fft_is));
subplot(211);
stem(vec_frec_vs,abs(fft_vs),'r','LineWidth',1,'Marker','none');
grid on;
hold on;
text(vec_frec_vs(ind_fft_vs(end)),...
    1.1*abs(fft_vs(ind_fft_vs(end))),...
    sprintf('%d',vec_frec_vs(ind_fft_vs(end))),...
    'Color',[1 0 0],'HorizontalAlignment','center','FontWeight','bold');
set(gca,'XLim',[-1500 1500]);
set(gca,'XTick',-1500:500:1500);
set(gca,'YLim',[0 1.5]);
set(gca,'YTick',0:0.5:1.5);
ylabel('V_s[V]');
subplot(212);
stem(vec_frec_is,abs(fft_is),'r','LineWidth',1,'Marker','none');
grid on;
hold on;
text(vec_frec_is(ind_fft_is(end)),...
    1.1*abs(fft_is(ind_fft_is(end))),...
    sprintf('%d',vec_frec_is(ind_fft_is(end))),...
    'Color',[1 0 0],'HorizontalAlignment','center','FontWeight','bold');
text(vec_frec_is(ind_fft_is(end-1)),...
    1.5*abs(fft_is(ind_fft_is(end-1))),...
    sprintf('%d',vec_frec_is(ind_fft_is(end-1))),...
    'Color',[1 0 0],'HorizontalAlignment','center','FontWeight','bold');
set(gca,'XLim',[-1500 1500]);
set(gca,'XTick',-1500:500:1500);
set(gca,'YLim',[0 4]);
set(gca,'YTick',0:1:4);
ylabel('I_s[A]');
xlabel('Frequency[Hz]');
```

A.2 Excitation in stationary reference frame (rotating saliency)

```
%% Clear workspace
close all;
clear;
clc;

%% Parameters
```

```
Loqs = 0.14e-3; % q-axis stator transient inductance [H]
Lods = 0.10e-3; % d-axis stator transient inductance [H]
h = 8; % Harmonic number of saliency
fe = 5; % Rotor electrical frequency
fc = 500; % Carrier frequency [Hz]
fs = 10e3; % Sample frequency [Hz]

%% Time vector computation
we = 2*pi*fe; % Rotor electrical frequency [rad/s]
wc = 2*pi*fc; % Carrier frequency [rad/s]
Te = 1/fe; % Rotor electrical period [s]
Ts = 1/fs; % Sample period [s]
Tc = 1/fc; % Carrier period [s]
t = 0:Ts:Te; % Time vector [s]
Oe_vec = we*t; % Rotor electrical position vector [rad]

%% Voltage computation
vas = cos(wc*t);        % Phase a
vbs = cos(wc*t-2*pi/3); % Phase b
vcs = cos(wc*t+2*pi/3); % Phase c

a = exp(1j*2*pi/3);            % 2*pi/3 rotation
vs = 2/3*(vas+a*vbs+a^2*vcs);  % Complex voltage
vqds_s = [real(vs);-imag(vs)]; % Voltage in stationary qd axis

%% Inductance matrix with saliency and current computation
sum_Los = (Loqs+Lods)/2;   % Mean stator transient inductance
delta_Los = (Loqs-Lods)/2; % Differential stator transient inductance

is = complex(zeros(1,length(Oe_vec))); % Reserve memory for complex current

% Current computation
for cc = 1:length(Oe_vec)
    % Actual rotor electrical position
    Oe = Oe_vec(cc);

    % Inductance matrix
    Los = sum_Los*eye(2)...
        + delta_Los*[ cos(h*Oe)   -sin(h*Oe) ;...
                     -sin(h*Oe)  -cos(h*Oe) ];
    % Inverse inductance matrix
    Los_inv = 1/(sum_Los^2-delta_Los^2) *...
        ( sum_Los*eye(2)...
          - delta_Los*[ cos(h*Oe)   -sin(h*Oe) ;...
                       -sin(h*Oe)  -cos(h*Oe) ] );
    % Complex current
    is(cc) = 1/(1j*wc) *...
        complex( Los_inv(1,:)*vqds_s(:,cc) ,...
                -Los_inv(2,:)*vqds_s(:,cc) );
end

iqds_s = [real(is);-imag(is)]; % Current in stationary qd axis

ias = real(is);                          % Phase a
ibs = -1/2*real(is)+sqrt(3)/2*imag(is); % Phase b
ics = -1/2*real(is)-sqrt(3)/2*imag(is); % Phase c

%% Complex FFT computation
f1 = -1500; % Minimum frequency
f2 = 1500;  % Maximum frequency
[fft_vs,vec_frec_vs] = FFT_Complex_Norm(vs(1:end-1),Ts,f1,f2,0); % Voltage
[fft_is,vec_frec_is] = FFT_Complex_Norm(is(1:end-1),Ts,f1,f2,0); % Current

%% Plot results
figure('Name','3ph magnitudes','NumberTitle','off');
subplot(211);
plot(t,vas,t,vbs,t,vcs,'LineWidth',1);
grid on;
```

```
set(gca,'XLim',[0 0.2]);
set(gca,'XTick',0:0.02:2);
set(gca,'YLim',[-1.5 1.5]);
set(gca,'YTick',-1.5:0.5:1.5);
legend('v_{as}','v_{bs}','v_{cs}','Location','West');
ylabel('V_s[V]');
subplot(212);
plot(t,ias,t,ibs,t,ics,'LineWidth',1);
grid on;
set(gca,'XLim',[0 0.2]);
set(gca,'XTick',0:0.02:2);
set(gca,'YLim',[-4 4]);
set(gca,'YTick',-4:2:4);
legend('i_{as}','i_{bs}','i_{cs}','Location','West');
ylabel('I_s[A]');
xlabel('Time[s]');

figure('Name','Stationary qd magnitudes','NumberTitle','off');
subplot(211);
plot(t,vqds_s(1,:),t,vqds_s(2,:),'LineWidth',1);
grid on;
set(gca,'XLim',[0 0.2]);
set(gca,'XTick',0:0.02:2);
set(gca,'YLim',[-1.5 1.5]);
set(gca,'YTick',-1.5:0.5:1.5);
legend('v_{qs}^s','v_{ds}^s','Location','West');
ylabel('V_s[V]');
subplot(212);
plot(t,iqds_s(1,:),t,iqds_s(2,:),'LineWidth',1);
grid on;
set(gca,'XLim',[0 0.2]);
set(gca,'XTick',0:0.02:2);
set(gca,'YLim',[-4 4]);
set(gca,'YTick',-4:2:4);
legend('i_{qs}^s','i_{ds}^s','Location','West');
ylabel('I_s[A]');
xlabel('Time[s]');

figure('Name','Polar trajectory','NumberTitle','off');
subplot(121);
polarplot(vs,'LineWidth',1);
grid on;
hold on;
polarplot(vs(1),'g*','MarkerSize',12);
polarplot(vs(end),'r*','MarkerSize',12);
ax = gca;
ax.RLim = [0 ceil(max(abs([vs is])))];
ax.ThetaTick = 0:15:360;
title('v_{qds}');
subplot(122);
polarplot(is,'LineWidth',1);
grid on;
hold on;
polarplot(is(1),'g*','MarkerSize',12);
polarplot(is(end),'r*','MarkerSize',12);
ax = gca;
ax.RLim = [0 ceil(max(abs([vs is])))];
ax.ThetaTick = 0:15:360;
title('i_{qds}');

figure('Name','FFT','NumberTitle','off');
[~,ind_fft_vs]=sort(abs(fft_vs));
[~,ind_fft_is]=sort(abs(fft_is));
subplot(211);
stem(vec_frec_vs,abs(fft_vs),'r','LineWidth',1,'Marker','none');
grid on;
hold on;
text(vec_frec_vs(ind_fft_vs(end)),...
```

```
    1.1*abs(fft_vs(ind_fft_vs(end))),...
    sprintf('%d',vec_frec_vs(ind_fft_vs(end))),...
    'Color',[1 0 0],'HorizontalAlignment','center','FontWeight','bold');
set(gca,'XLim',[-1500 1500]);
set(gca,'XTick',-1500:500:1500);
set(gca,'YLim',[0 1.5]);
set(gca,'YTick',0:0.5:1.5);
ylabel('V_s[V]');
subplot(212);
stem(vec_frec_is,abs(fft_is),'r','LineWidth',1,'Marker','none');
grid on;
hold on;
text(vec_frec_is(ind_fft_is(end)),...
    1.1*abs(fft_is(ind_fft_is(end))),...
    sprintf('%d',vec_frec_is(ind_fft_is(end))),...
    'Color',[1 0 0],'HorizontalAlignment','center','FontWeight','bold');
text(vec_frec_is(ind_fft_is(end-1)),...
    1.5*abs(fft_is(ind_fft_is(end-1))),...
    sprintf('%d',vec_frec_is(ind_fft_is(end-1))),...
    'Color',[1 0 0],'HorizontalAlignment','center','FontWeight','bold');
set(gca,'XLim',[-1500 1500]);
set(gca,'XTick',-1500:500:1500);
set(gca,'YLim',[0 4]);
set(gca,'YTick',0:1:4);
ylabel('I_s[A]');
xlabel('Frequency[Hz]');
```

A.3 Excitation in negative sequence synchronous reference frame

```
%% Clear workspace
close all;
clear;
clc;

%% Parameters
Loqs = 0.14e-3; % q-axis stator transient inductance [H]
Lods = 0.10e-3; % d-axis stator transient inductance [H]
h = 8; % Harmonic number of saliency
fe = 5; % Rotor electrical frequency
fc = 500; % Carrier frequency [Hz]
fs = 10e3; % Sample frequency [Hz]
ffilter = 5; % Filter frequency [Hz]

%% Time vector computation
we = 2*pi*fe; % Rotor electrical frequency [rad/s]
wc = 2*pi*fc; % Carrier frequency [rad/s]
Te = 1/fe; % Rotor electrical period [s]
Ts = 1/fs; % Sample period [s]
Tc = 1/fc; % Carrier period [s]
t = 0:Ts:3*Te; % Time vector [s]
Oe_vec = we*t; % Rotor electrical position vector [rad]

%% Voltage computation
vas = cos(wc*t);        % Phase a
vbs = cos(wc*t-2*pi/3); % Phase b
vcs = cos(wc*t+2*pi/3); % Phase c

a = exp(1j*2*pi/3);           % 2*pi/3 rotation
vs = 2/3*(vas+a*vbs+a^2*vcs);  % Complex voltage
vqds_s = [real(vs);-imag(vs)]; % Voltage in stationary qd axis
```

```
%% Inductance matrix with saliency and current computation
sum_Los = (Loqs+Lods)/2;   % Mean stator transient inductance
delta_Los = (Loqs-Lods)/2; % Differential stator transient inductance

is = complex(zeros(1,length(Oe_vec))); % Reserve memory for complex current

% Current computation
for cc = 1:length(Oe_vec)
    % Actual rotor electrical position
    Oe = Oe_vec(cc);

    % Inductance matrix
    Los = sum_Los*eye(2)...
        + delta_Los*[ cos(h*Oe)   -sin(h*Oe) ;...
                     -sin(h*Oe)  -cos(h*Oe) ];
    % Inverse inductance matrix
    Los_inv = 1/(sum_Los^2-delta_Los^2) *...
        ( sum_Los*eye(2)...
          - delta_Los*[ cos(h*Oe)   -sin(h*Oe) ;...
                       -sin(h*Oe)  -cos(h*Oe) ] );
    % Complex current
    is(cc) = 1/(1j*wc) *...
        complex( Los_inv(1,:)*vqds_s(:,cc) ,...
                -Los_inv(2,:)*vqds_s(:,cc) );
end

iqds_s = [real(is);-imag(is)]; % Current in stationary qd axis

ias = real(is);                          % Phase a
ibs = -1/2*real(is)+sqrt(3)/2*imag(is); % Phase b
ics = -1/2*real(is)-sqrt(3)/2*imag(is); % Phase c

%% Filtering of positive sequence component
% Positive synchronous reference frame current
is_pos = is.*exp(-1j*(wc*t));
iqds_pos = [real(is_pos);-imag(is_pos)];

% High-pass filter function
[b_filter,a_filter] = butter(2,2*ffilter/fs,'high');
%b_filter = fir1(20,2*ffilter/fs,'high'); a_filter = 1;

% Filtering of positive sequence component
is_pos_filt = filter(b_filter,a_filter,is_pos);
iqds_pos_filt = [real(is_pos_filt);-imag(is_pos_filt)];

%% Negative synchronous reference frame current computation
% Negative synchronous reference frame current
is_neg = is_pos_filt.*exp(-1j*(h*Oe_vec-2*wc*t));
iqds_neg = [real(is_neg);-imag(is_neg)];

%% Complex FFT computation
f1 = -1500; % Minimum frequency
f2 = 1500;  % Maximum frequency
% Voltage
[fft_vs,vec_frec_vs] = FFT_Complex_Norm(vs(2*Te/Ts+1:end-1),Ts,f1,f2,0);
% Current
[fft_is,vec_frec_is] = FFT_Complex_Norm(is(2*Te/Ts+1:end-1),Ts,f1,f2,0);
% Positive synchronous reference frame current
[fft_is_pos,vec_frec_is_pos] = ...
    FFT_Complex_Norm(is_pos(2*Te/Ts+1:end-1),Ts,f1,f2,0);
% Filtered positive synchronous reference frame current
[fft_is_pos_filt,vec_frec_is_pos_filt] = ...
    FFT_Complex_Norm(is_pos_filt(2*Te/Ts+1:end-1),Ts,f1,f2,0);
% Negative synchronous reference frame current
[fft_is_neg,vec_frec_is_neg] = ...
    FFT_Complex_Norm(is_neg(2*Te/Ts+1:end-1),Ts,f1,f2,0);

%% Plot results
```

```
figure('Name','3ph magnitudes','NumberTitle','off');
subplot(211);
plot(t(1:2*Te/Ts+1),vas(1:2*Te/Ts+1),...
    t(1:2*Te/Ts+1),vbs(1:2*Te/Ts+1),...
    t(1:2*Te/Ts+1),vcs(1:2*Te/Ts+1),...
    'LineWidth',1);
grid on;
set(gca,'XLim',[0 0.4]);
set(gca,'XTick',0:0.05:0.4);
set(gca,'YLim',[-1.5 1.5]);
set(gca,'YTick',-1.5:0.5:1.5);
legend('v_{as}','v_{bs}','v_{cs}','Location','West');
ylabel('V_s[V]');
subplot(212);
plot(t(1:2*Te/Ts+1),ias(1:2*Te/Ts+1),...
    t(1:2*Te/Ts+1),ibs(1:2*Te/Ts+1),...
    t(1:2*Te/Ts+1),ics(1:2*Te/Ts+1),...
    'LineWidth',1);
grid on;
set(gca,'XLim',[0 0.4]);
set(gca,'XTick',0:0.05:0.4);
set(gca,'YLim',[-4 4]);
set(gca,'YTick',-4:2:4);
legend('i_{as}','i_{bs}','i_{cs}','Location','West');
ylabel('I_s[A]');
xlabel('Time[s]');

figure('Name','Stationary qd magnitudes','NumberTitle','off');
subplot(211);
plot(t(1:2*Te/Ts+1),vqds_s(1,1:2*Te/Ts+1),...
    t(1:2*Te/Ts+1),vqds_s(2,1:2*Te/Ts+1),...
    'LineWidth',1);
grid on;
set(gca,'XLim',[0 0.4]);
set(gca,'XTick',0:0.05:0.4);
set(gca,'YLim',[-1.5 1.5]);
set(gca,'YTick',-1.5:0.5:1.5);
legend('v_{qs}^s','v_{ds}^s','Location','West');
ylabel('V_s[V]');
subplot(212);
plot(t(1:2*Te/Ts+1),iqds_s(1,1:2*Te/Ts+1),...
    t(1:2*Te/Ts+1),iqds_s(2,1:2*Te/Ts+1),...
    'LineWidth',1);
grid on;
set(gca,'XLim',[0 0.4]);
set(gca,'XTick',0:0.05:0.4);
set(gca,'YLim',[-4 4]);
set(gca,'YTick',-4:2:4);
legend('i_{qs}^s','i_{ds}^s','Location','West');
ylabel('I_s[A]');
xlabel('Time[s]');

figure('Name','Polar trajectory','NumberTitle','off');
subplot(121);
polarplot(vs(1:2*Te/Ts+1),'LineWidth',1);
grid on;
hold on;
polarplot(vs(1),'g*','MarkerSize',12);
polarplot(vs(2*Te/Ts+1),'r*','MarkerSize',12);
ax = gca;
ax.RLim = [0 ceil(max(abs([vs is])))];
ax.ThetaTick = 0:15:360;
title('v_{qds}');
subplot(122);
polarplot(is(1:2*Te/Ts+1),'LineWidth',1);
grid on;
hold on;
polarplot(is(1),'g*','MarkerSize',12);
```

```
polarplot(is(2*Te/Ts+1),'r*','MarkerSize',12);
ax = gca;
ax.RLim = [0 ceil(max(abs([vs is])))];
ax.ThetaTick = 0:15:360;
title('i_{qds}');

figure('Name','FFT','NumberTitle','off');
[~,ind_fft_vs]=sort(abs(fft_vs));
[~,ind_fft_is]=sort(abs(fft_is));
subplot(211);
stem(vec_frec_vs,abs(fft_vs),'r','LineWidth',1,'Marker','none');
grid on;
hold on;
text(vec_frec_vs(ind_fft_vs(end)),...
    1.1*abs(fft_vs(ind_fft_vs(end))),...
    sprintf('%d',vec_frec_vs(ind_fft_vs(end))),...
    'Color',[1 0 0],'HorizontalAlignment','center','FontWeight','bold');
set(gca,'XLim',[-1500 1500]);
set(gca,'XTick',-1500:500:1500);
set(gca,'YLim',[0 1.5]);
set(gca,'YTick',0:0.5:1.5);
ylabel('V_s[V]');
subplot(212);
stem(vec_frec_is,abs(fft_is),'r','LineWidth',1,'Marker','none');
grid on;
hold on;
text(vec_frec_is(ind_fft_is(end)),...
    1.1*abs(fft_is(ind_fft_is(end))),...
    sprintf('%d',vec_frec_is(ind_fft_is(end))),...
    'Color',[1 0 0],'HorizontalAlignment','center','FontWeight','bold');
text(vec_frec_is(ind_fft_is(end-1)),...
    1.25*abs(fft_is(ind_fft_is(end-1))),...
    sprintf('%d',vec_frec_is(ind_fft_is(end-1))),...
    'Color',[1 0 0],'HorizontalAlignment','center','FontWeight','bold');
set(gca,'XLim',[-1500 1500]);
set(gca,'XTick',-1500:500:1500);
set(gca,'YLim',[0 4]);
set(gca,'YTick',0:1:4);
ylabel('I_s[A]');
xlabel('Frequency[Hz]');

figure('Name','Stationary qd magnitudes','NumberTitle','off');
subplot(211);
plot(t(1:2*Te/Ts+1),iqds_pos(1,1:2*Te/Ts+1),...
    t(1:2*Te/Ts+1),iqds_pos(2,1:2*Te/Ts+1),...
    'LineWidth',1);
grid on;
set(gca,'XLim',[0 0.4]);
set(gca,'XTick',0:0.05:0.4);
set(gca,'YLim',[-4 4]);
set(gca,'YTick',-4:2:4);
legend('i_{qs}^{pos}','i_{ds}^{pos}','Location','SouthEast');
ylabel('I_s^{pos}[A]');
subplot(212);
plot(t(1:2*Te/Ts+1),iqds_pos_filt(1,1:2*Te/Ts+1),...
    t(1:2*Te/Ts+1),iqds_pos_filt(2,1:2*Te/Ts+1),...
    'LineWidth',1);
grid on;
set(gca,'XLim',[0 0.4]);
set(gca,'XTick',0:0.05:0.4);
set(gca,'YLim',[-4 4]);
set(gca,'YTick',-4:2:4);
legend('i_{qs\_filt}^{pos}','i_{ds\_filt}^{pos}','Location','SouthEast');
ylabel('I_{s\_filt}^{pos}[A]');
xlabel('Time[s]');

figure('Name','Polar trajectory','NumberTitle','off');
subplot(121);
```

```
polarplot(is_pos(1:2*Te/Ts+1),'LineWidth',1);
grid on;
hold on;
polarplot(is_pos(1),'g*','MarkerSize',12);
polarplot(is_pos(2*Te/Ts+1),'r*','MarkerSize',12);
ax = gca;
ax.RLim = [0 ceil(max(abs([vs is])))];
ax.ThetaTick = 0:15:360;
title('i_{qds}^{pos}');
subplot(122);
polarplot(is_pos_filt(1:2*Te/Ts+1),'LineWidth',1);
grid on;
hold on;
polarplot(is_pos_filt(1),'g*','MarkerSize',12);
polarplot(is_pos_filt(2*Te/Ts+1),'r*','MarkerSize',12);
ax = gca;
ax.RLim = [0 ceil(max(abs([vs is])))];
ax.ThetaTick = 0:15:360;
title('i_{qds\_filt}^{pos}');

figure('Name','FFT','NumberTitle','off');
[~,ind_fft_is_pos]=sort(abs(fft_is_pos));
[~,ind_fft_is_pos_filt]=sort(abs(fft_is_pos_filt));
subplot(211);
stem(vec_frec_is_pos,abs(fft_is_pos),'r','LineWidth',1,'Marker','none');
grid on;
hold on;
text(vec_frec_is_pos(ind_fft_is_pos(end)),...
    1.1*abs(fft_is_pos(ind_fft_is_pos(end))),...
    sprintf('%d',vec_frec_is_pos(ind_fft_is_pos(end))),...
    'Color',[1 0 0],'HorizontalAlignment','center','FontWeight','bold');
text(vec_frec_is_pos(ind_fft_is_pos(end-1)),...
    1.25*abs(fft_is_pos(ind_fft_is_pos(end-1))),...
    sprintf('%d',vec_frec_is_pos(ind_fft_is_pos(end-1))),...
    'Color',[1 0 0],'HorizontalAlignment','center','FontWeight','bold');
set(gca,'XLim',[-1500 1500]);
set(gca,'XTick',-1500:500:1500);
set(gca,'YLim',[0 4]);
set(gca,'YTick',0:1:4);
ylabel('I_s^{pos}[A]');
subplot(212);
stem(vec_frec_is_pos_filt,abs(fft_is_pos_filt),...
    'r','LineWidth',1,'Marker','none');
grid on;
hold on;
text(vec_frec_is_pos_filt(ind_fft_is_pos_filt(end)),...
    1.1*abs(fft_is_pos_filt(ind_fft_is_pos_filt(end))),...
    sprintf('%d',vec_frec_is_pos_filt(ind_fft_is_pos_filt(end))),...
    'Color',[1 0 0],'HorizontalAlignment','center','FontWeight','bold');
set(gca,'XLim',[-1500 1500]);
set(gca,'XTick',-1500:500:1500);
set(gca,'YLim',[0 1]);
set(gca,'YTick',0:0.2:1);
ylabel('I_{s\_filt}^{pos}[A]');
xlabel('Frequency[Hz]');

figure('Name','Stationary qd magnitudes','NumberTitle','off');
plot(t(1:2*Te/Ts+1),iqds_neg(1,1:2*Te/Ts+1),...
    t(1:2*Te/Ts+1),iqds_neg(2,1:2*Te/Ts+1),...
    'LineWidth',1);
grid on;
set(gca,'XLim',[0 0.4]);
set(gca,'XTick',0:0.05:0.4);
set(gca,'YLim',[-4 4]);
set(gca,'YTick',-4:2:4);
legend('i_{qs}^{neg}','i_{ds}^{neg}','Location','SouthEast');
ylabel('I_s^{neg}[A]');
xlabel('Time[s]');
```

```
figure('Name','Polar trajectory','NumberTitle','off');
title('Is,neg');
polarplot(is_neg(1:2*Te/Ts+1),'LineWidth',1);
grid on;
hold on;
polarplot(is_neg(1),'g*','MarkerSize',12);
polarplot(is_neg(2*Te/Ts+1),'r*','MarkerSize',12);
ax = gca;
ax.RLim = [0 ceil(max(abs([vs is])))];
ax.ThetaTick = 0:15:360;
title('i_{qds}^{neg}');

figure('Name','FFT','NumberTitle','off');
[~,ind_fft_is_neg]=sort(abs(fft_is_neg));
stem(vec_frec_is_neg,abs(fft_is_neg),'r','LineWidth',1,'Marker','none');
grid on;
hold on;
text(vec_frec_is_neg(ind_fft_is_neg(end)),...
    1.1*abs(fft_is_neg(ind_fft_is_neg(end))),...
    sprintf('%d',vec_frec_is_neg(ind_fft_is_neg(end))),...
    'Color',[1 0 0],'HorizontalAlignment','center','FontWeight','bold');
set(gca,'XLim',[-1500 1500]);
set(gca,'XTick',-1500:500:1500);
set(gca,'YLim',[0 1]);
set(gca,'YTick',0:0.2:1);
ylabel('I_s^{neg}[A]');
xlabel('Frequency[Hz]');
```

A.4 Saliency tracking

```
%% Clear workspace
close all;
clear;
clc;

%% Parameters
Loqs = 0.14e-3; % q-axis stator transient inductance [H]
Lods = 0.10e-3; % d-axis stator transient inductance [H]
h = 8; % Harmonic number of saliency
fe = 5; % Rotor electrical frequency
fc = 500; % Carrier frequency [Hz]
fs = 10e3; % Sample frequency [Hz]
ffilter = 5; % Filter frequency [Hz]
Kp_PLL = 200; % PLL proportional gain
Ki_PLL = 100; % PLL integral gain

%% Time vector computation
Te = 1/fe; % Rotor electrical period [s]
Ts = 1/fs; % Sample period [s]
Tc = 1/fc; % Carrier period [s]
t = 0:Ts:5*Te; % Time vector [s]
we = 2*pi*fe *... % Rotor electrical frequency [rad/s]
    [ones(1,round(0.7/Ts)) 2*ones(1,length(t)-round(0.7/Ts))];
wc = 2*pi*fc; % Carrier frequency [rad/s]
Oe_vec=zeros(1,length(t)); % Rotor electrical position vector [rad]
for cc1=2:length(t)
    % Integrator
    Oe_vec(cc1) = Ts/2*(we(cc1)+we(cc1-1)) + Oe_vec(cc1-1);
end

%% Voltage computation
vas = cos(wc*t);        % Phase a
vbs = cos(wc*t-2*pi/3); % Phase b
vcs = cos(wc*t+2*pi/3); % Phase c
```

```
a = exp(1j*2*pi/3);            % 2*pi/3 rotation
vs = 2/3*(vas+a*vbs+a^2*vcs);  % Complex voltage
vqds_s = [real(vs);-imag(vs)]; % Voltage in stationary qd axis

%% Inductance matrix with saliency and current computation
sum_Los = (Loqs+Lods)/2;   % Mean stator transient inductance
delta_Los = (Loqs-Lods)/2; % Differential stator transient inductance

is = complex(zeros(1,length(Oe_vec))); % Reserve memory for complex current

% Current computation
for cc = 1:length(Oe_vec)
    % Actual rotor electrical position
    Oe = Oe_vec(cc);

    % Inductance matrix
    Los = sum_Los*eye(2)...
        + delta_Los*[ cos(h*Oe)   -sin(h*Oe) ;...
                     -sin(h*Oe)  -cos(h*Oe) ];
    % Inverse inductance matrix
    Los_inv = 1/(sum_Los^2-delta_Los^2) *...
        ( sum_Los*eye(2)...
          - delta_Los*[ cos(h*Oe)   -sin(h*Oe) ;...
                       -sin(h*Oe)  -cos(h*Oe) ] );
    % Complex current
    is(cc) = 1/(1j*wc) *...
        complex( Los_inv(1,:)*vqds_s(:,cc) ,...
                -Los_inv(2,:)*vqds_s(:,cc) );
end

iqds_s = [real(is);-imag(is)]; % Current in stationary qd axis

ias = real(is);                          % Phase a
ibs = -1/2*real(is)+sqrt(3)/2*imag(is); % Phase b
ics = -1/2*real(is)-sqrt(3)/2*imag(is); % Phase c

%% Filtering of positive sequence component
% Positive synchronous reference frame current
is_pos = is.*exp(-1j*(wc*t));
iqds_pos = [real(is_pos);-imag(is_pos)];

% High-pass filter function
[b_filter,a_filter] = butter(2,2*ffilter/fs,'high');
%b_filter = fir1(20,2*ffilter/fs,'high'); a_filter = 1;

% Filtering of positive sequence component
is_pos_filt = filter(b_filter,a_filter,is_pos);
iqds_pos_filt = [real(is_pos_filt);-imag(is_pos_filt)];

%% Negative synchronous reference frame current computation
% Negative synchronous reference frame current
is_neg = is_pos_filt.*exp(-1j*(h*Oe_vec-2*wc*t));
iqds_neg = [real(is_neg);-imag(is_neg)];

%% PLL computation
% PLL transfer function
b_PLL = [Kp_PLL*(Ts/(2/Ki_PLL)+1) Kp_PLL*(Ts/(2/Ki_PLL)-1)];
a_PLL = [1 -1];

% Integrator transfer function (Trapezoidal)
b_INT = Ts/2*[1 1];
a_INT = [1 -1];

% Reserve memory for computation vectors
is_pos_PLL = complex(zeros(length(b_filter),1));
is_pos_filt_PLL = complex(zeros(length(a_filter),1));
iqds_neg_filt_PLL = zeros(length(b_PLL),2);
```

```
we_est = zeros(length(a_PLL),1);
Oe_est = zeros(length(a_INT),1);

% Reserve memory for storage vectors
is_pos_PLL_vec = complex(zeros(1,length(t)));
is_pos_filt_PLL_vec = complex(zeros(1,length(t)));
is_neg_PLL_vec = complex(zeros(1,length(t)));
we_est_vec = zeros(1,length(t));
Oe_est_vec = zeros(1,length(t));

% Control loop
for cc1=1:length(t)
    % Positive synchronous reference frame current
    is_pos_PLL(1) = is(cc1).*exp(-1j*(wc*t(cc1)));

    % Filtered positive synchronous reference frame current
    is_pos_filt_PLL(1) = ...
        ( b_filter*is_pos_PLL ...
          - a_filter(2:end)*is_pos_filt_PLL(2:end) ) ...
        /a_filter(1);

    % Negative synchronous reference frame current
    is_neg_PLL = is_pos_filt_PLL(1).*exp(-1j*(h*Oe_est(1)-2*wc*t(cc1)));
    iqds_neg_filt_PLL(1,:) = ...
        [real(is_neg_PLL) -imag(is_neg_PLL)];

    % Electrical frequency computation (PLL)
    if t(cc1)>=0.4 % Start control at 0.4s
        we_est(1) = ...
            ( b_PLL*-iqds_neg_filt_PLL(:,1) ...
              -a_PLL(2:end)*we_est(2:end)   )...
            /a_PLL(1);
    end

    % Electrical position (Integrator)
    Oe_est(1) = ...
        ( b_INT*we_est ...
          -a_INT(2:end)*Oe_est(2:end) )...
        /a_INT(1);

    % Update computation vectors
    for cc2=length(b_filter):-1:2
        is_pos_PLL(cc2) = is_pos_PLL(cc2-1);
    end
    for cc2=length(a_filter):-1:2
        is_pos_filt_PLL(cc2) = is_pos_filt_PLL(cc2-1);
    end
    iqds_neg_filt_PLL(2,:) = iqds_neg_filt_PLL(1,:);
    we_est(2) = we_est(1);
    Oe_est(2) = Oe_est(1);

    % Update storage vectors
    is_pos_PLL_vec(cc1) = is_pos_PLL(1);
    is_pos_filt_PLL_vec(cc1) = is_pos_filt_PLL(1);
    is_neg_PLL_vec(cc1) = is_neg_PLL;
    we_est_vec(cc1) = we_est(1);
    Oe_est_vec(cc1) = Oe_est(1);
end

% Update storage vectors
iqds_pos_PLL_vec = ...
    [real(is_pos_PLL_vec);-imag(is_pos_PLL_vec)];
iqds_pos_filt_PLL_vec = ...
    [real(is_pos_filt_PLL_vec);-imag(is_pos_filt_PLL_vec)];
iqds_neg_PLL_vec = ...
    [real(is_neg_PLL_vec);-imag(is_neg_PLL_vec)];

%% Plot results
```

```
figure('Name','3ph magnitudes','NumberTitle','off');
subplot(211);
plot(t,vas,t,vbs,t,vcs,'LineWidth',1);
grid on;
set(gca,'XLim',[0 1.0]);
set(gca,'XTick',0:0.1:1.0);
set(gca,'YLim',[-1.5 1.5]);
set(gca,'YTick',-1.5:0.5:1.5);
legend('v_{as}','v_{bs}','v_{cs}','Location','West');
ylabel('V_s[V]');
subplot(212);
plot(t,ias,t,ibs,t,ics,'LineWidth',1);
grid on;
set(gca,'XLim',[0 1.0]);
set(gca,'XTick',0:0.1:1.0);
set(gca,'YLim',[-4 4]);
set(gca,'YTick',-4:2:4);
legend('i_{as}','i_{bs}','i_{cs}','Location','West');
ylabel('I_s[A]');
xlabel('Time[s]');

figure('Name','Stationary qd magnitudes','NumberTitle','off');
subplot(211);
plot(t,vqds_s(1,:),t,vqds_s(2,:),'LineWidth',1);
grid on;
set(gca,'XLim',[0 1.0]);
set(gca,'XTick',0:0.1:1.0);
set(gca,'YLim',[-1.5 1.5]);
set(gca,'YTick',-1.5:0.5:1.5);
legend('v_{qs}^s','v_{ds}^s','Location','West');
ylabel('V_s[V]');
subplot(212);
plot(t,iqds_s(1,:),t,iqds_s(2,:),'LineWidth',1);
grid on;
set(gca,'XLim',[0 1.0]);
set(gca,'XTick',0:0.1:1.0);
set(gca,'YLim',[-4 4]);
set(gca,'YTick',-4:2:4);
legend('i_{qs}^s','i_{ds}^s','Location','West');
ylabel('I_s[A]');
xlabel('Time[s]');

figure('Name','Polar trajectory','NumberTitle','off');
subplot(121);
polarplot(vs,'LineWidth',1);
grid on;
hold on;
polarplot(vs(1),'g*','MarkerSize',12);
polarplot(vs(end),'r*','MarkerSize',12);
ax = gca;
ax.RLim = [0 ceil(max(abs([vs is])))];
ax.ThetaTick = 0:15:360;
title('v_{qds}');
subplot(122);
polarplot(is,'LineWidth',1);
grid on;
hold on;
polarplot(is(1),'g*','MarkerSize',12);
polarplot(is(end),'r*','MarkerSize',12);
ax = gca;
ax.RLim = [0 ceil(max(abs([vs is])))];
ax.ThetaTick = 0:15:360;
title('i_{qds}');

figure('Name','Stationary qd magnitudes','NumberTitle','off');
subplot(211);
plot(t,iqds_pos_PLL_vec(1,:),t,iqds_pos_PLL_vec(2,:),'LineWidth',1);
grid on;
```

```
set(gca,'XLim',[0 1.0]);
set(gca,'XTick',0:0.1:1.0);
set(gca,'YLim',[-4 4]);
set(gca,'YTick',-4:2:4);
legend('i_{qs}^{pos}','i_{ds}^{pos}','Location','SouthEast');
ylabel('I_s^{pos}[A]');
subplot(212);
plot(t,iqds_pos_filt_PLL_vec(1,:),t,iqds_pos_filt_PLL_vec(2,:),...
    'LineWidth',1);
grid on;
set(gca,'XLim',[0 1.0]);
set(gca,'XTick',0:0.1:1.0);
set(gca,'YLim',[-4 4]);
set(gca,'YTick',-4:2:4);
legend('i_{qs\_filt}^{pos}','i_{ds\_filt}^{pos}','Location','SouthEast');
ylabel('I_{s\_filt}^{pos}[A]');
xlabel('Time[s]');

figure('Name','Polar trajectory','NumberTitle','off');
subplot(121);
polarplot(is_pos_PLL_vec);
grid on;
hold on;
polarplot(is_pos_PLL_vec(1),'g*','MarkerSize',12);
polarplot(is_pos_PLL_vec(end),'r*','MarkerSize',12);
ax = gca;
ax.RLim = [0 ceil(max(abs([vs is])))];
ax.ThetaTick = 0:15:360;
title('i_{qds}^{pos}');
subplot(122);
polarplot(is_pos_filt_PLL_vec);
grid on;
hold on;
polarplot(is_pos_filt_PLL_vec(1),'g*','MarkerSize',12);
polarplot(is_pos_filt_PLL_vec(end),'r*','MarkerSize',12);
ax = gca;
ax.RLim = [0 ceil(max(abs([vs is])))];
ax.ThetaTick = 0:15:360;
title('i_{qds\_filt}^{pos}');

figure('Name','Stationary qd magnitudes','NumberTitle','off');
plot(t,iqds_neg_PLL_vec(1,:),t,iqds_neg_PLL_vec(2,:),'LineWidth',1);
grid on;
set(gca,'XLim',[0 1.0]);
set(gca,'XTick',0:0.1:1.0);
set(gca,'YLim',[-4 4]);
set(gca,'YTick',-4:1:4);
legend('i_{qs}^{neg}','i_{ds}^{neg}','Location','SouthEast');
ylabel('I_s^{neg}[A]');
xlabel('Time[s]');

figure('Name','Polar trajectory','NumberTitle','off');
polarplot(is_neg_PLL_vec(round(0.4/Ts)+1:end));
grid on;
hold on;
polarplot(is_neg_PLL_vec(round(0.4/Ts)+1),'g*','MarkerSize',12);
polarplot(is_neg_PLL_vec(end),'r*','MarkerSize',12);
ax = gca;
ax.RLim = [0 ceil(max(abs([vs is])))];
ax.ThetaTick = 0:15:360;
title('i_{qds}^{neg}');

figure('Name','we','NumberTitle','off');
plot(t,we,t,we_est_vec,'LineWidth',1);
grid on;
set(gca,'XLim',[0 1.0]);
set(gca,'XTick',0:0.1:1.0);
set(gca,'YLim',[-10 70]);
```

```
set(gca,'YTick',-10:10:70);
hdl=legend('$\omega_e$','$\widehat{\omega_e}$','Location','South');
hdl.Interpreter='LaTeX';
ylabel('\omega_e[rad/s]');
xlabel('Time[s]');

figure('Name','Oe','NumberTitle','off');
plot(t,180/pi*angle(exp(1j*Oe_vec)),...
    t,180/pi*angle(exp(1j*Oe_est_vec)),...
    'LineWidth',1);
grid on;
set(gca,'XLim',[0 1.0]);
set(gca,'XTick',0:0.1:1.0);
set(gca,'YLim',[-180 180]);
set(gca,'YTick',-180:60:180);
hdl=legend('$\theta_e$','$\widehat{\theta_e}$','Location','South');
hdl.Interpreter='LaTeX';
ylabel('\theta_e[deg]');
xlabel('Time[s]');
```

Appendix B

Simulink Models

```
function [R,L,W] = Matrices(Rs,Rr,Lls,Llr,Lm,wr,Lsal,h,Or,phi)

% Stator resistance matrix
RsM = Rs*eye(2);
% Rotor resistance matrix
RrM = Rr*eye(2);
% Total resistance matrix
R = [RsM zeros(2);...
     zeros(2) RrM];

% Saliency inductance matrix
LsalM = Lsal*...
        [ cos(h*(Or+phi))   -sin(h*(Or+phi)) ;...
          -sin(h*(Or+phi))  -cos(h*(Or+phi)) ];
% Stator inductance matrix
LsM = (Lls+Lm)*eye(2)+LsalM;
% Rotor inductance matrix
LrM = (Llr+Lm)*eye(2)+LsalM;
% Stator-Rotor inductance matrix
LsrM = Lm*eye(2);
% Rotor-Stator inductance matrix
LrsM = LsrM.';
% Total inductance matrix
L = [ LsM LsrM ;...
      LrsM LrM ];

% Frequency matrix (stationary reference frame)
W = [0  0   0   0  ;...
     0  0   0   0  ;...
     0  0   0  -wr ;...
     0  0   wr  0  ];
```

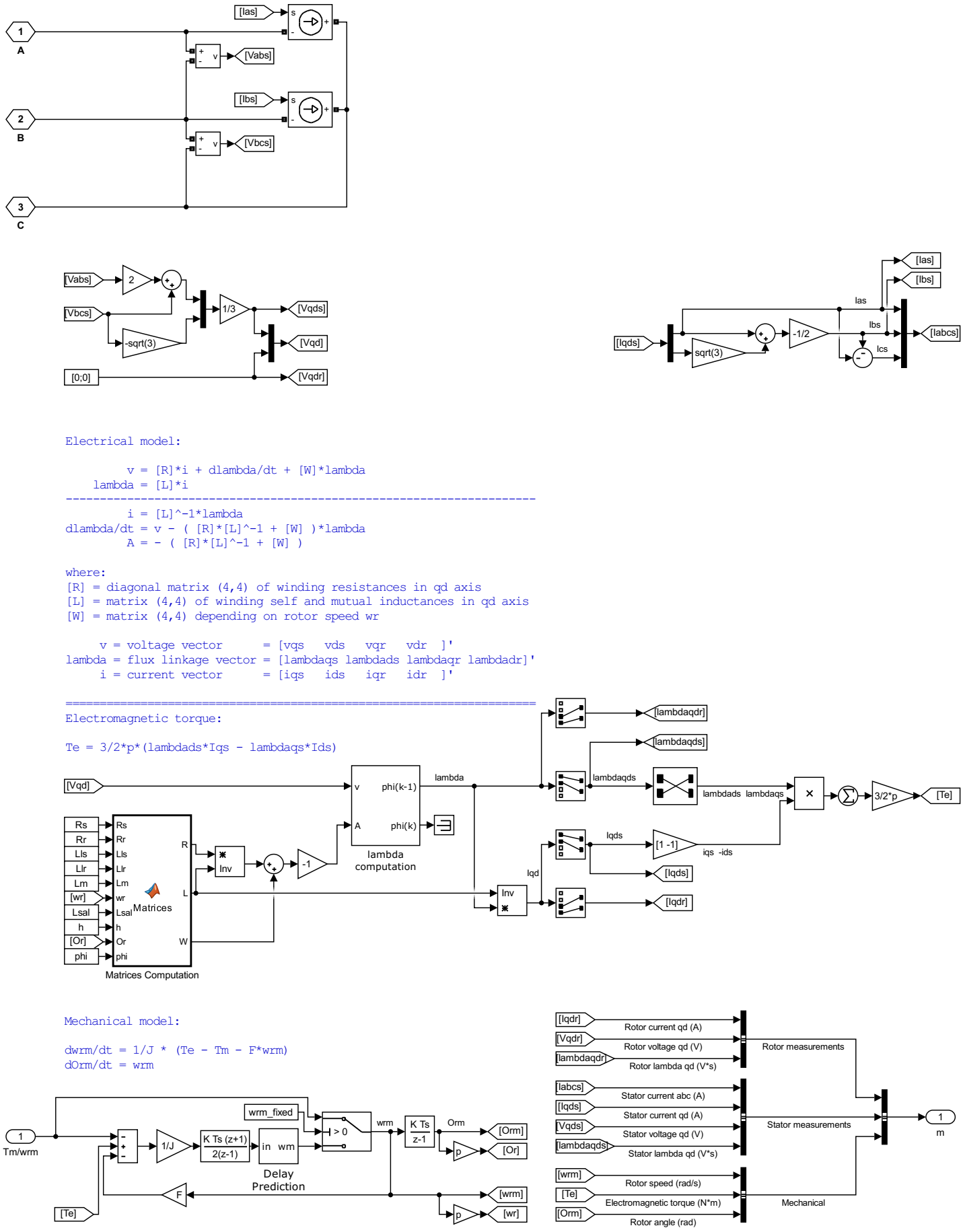

Figure B-1: Machine model with saliency.

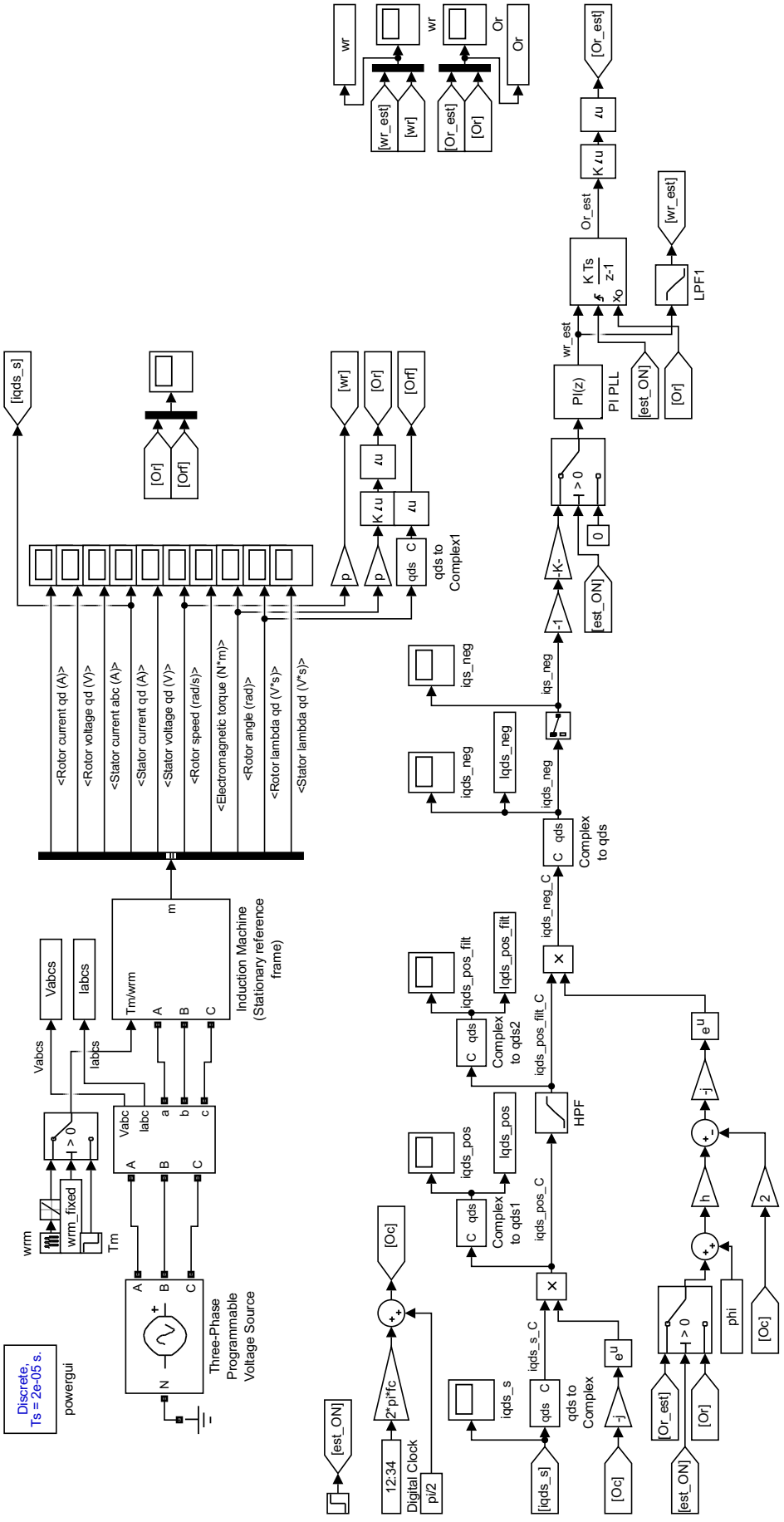

Figure B-2: Open loop simulation with pure carrier frequency excitation.

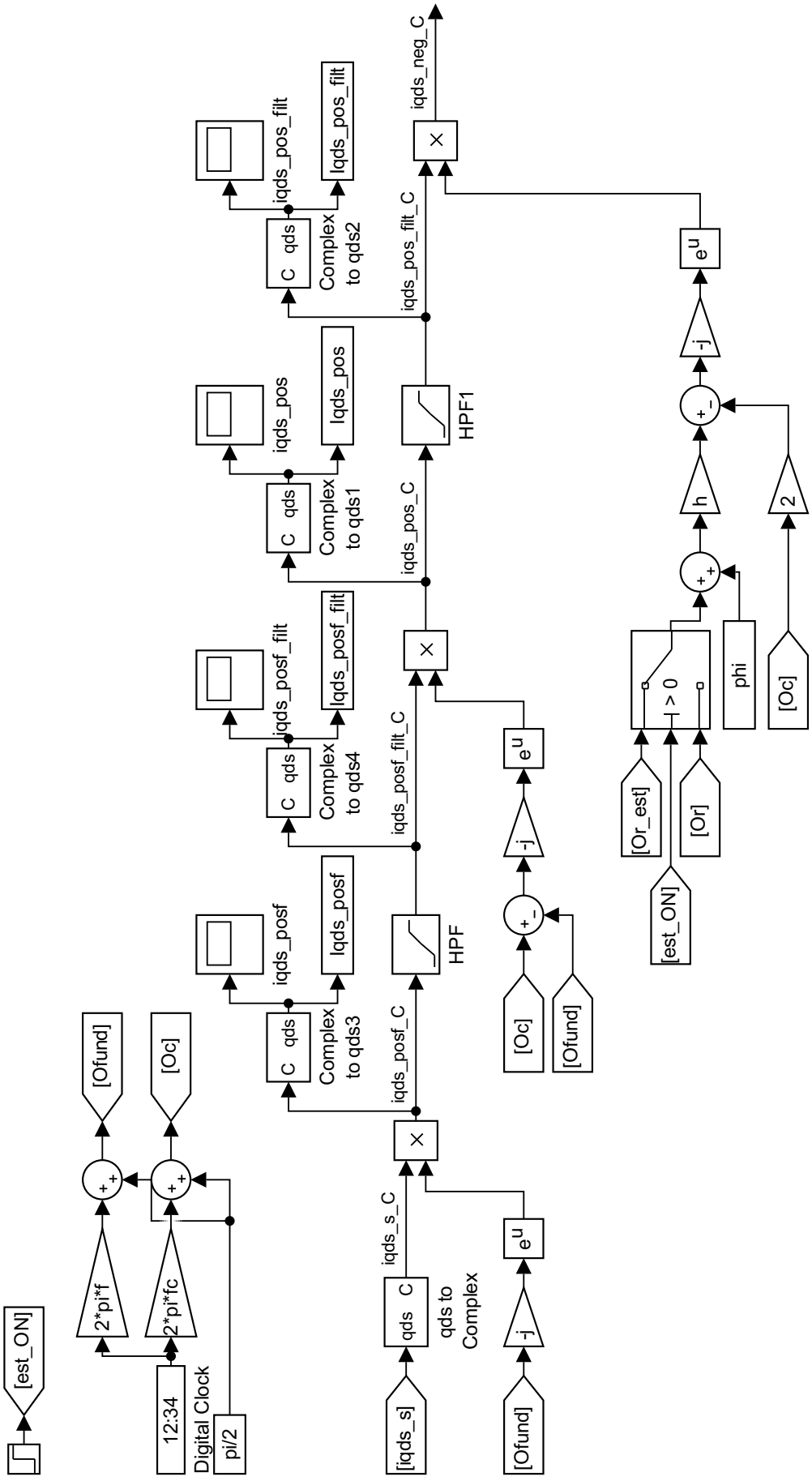

Figure B-3: Modification for open loop simulation including fundamental excitation.

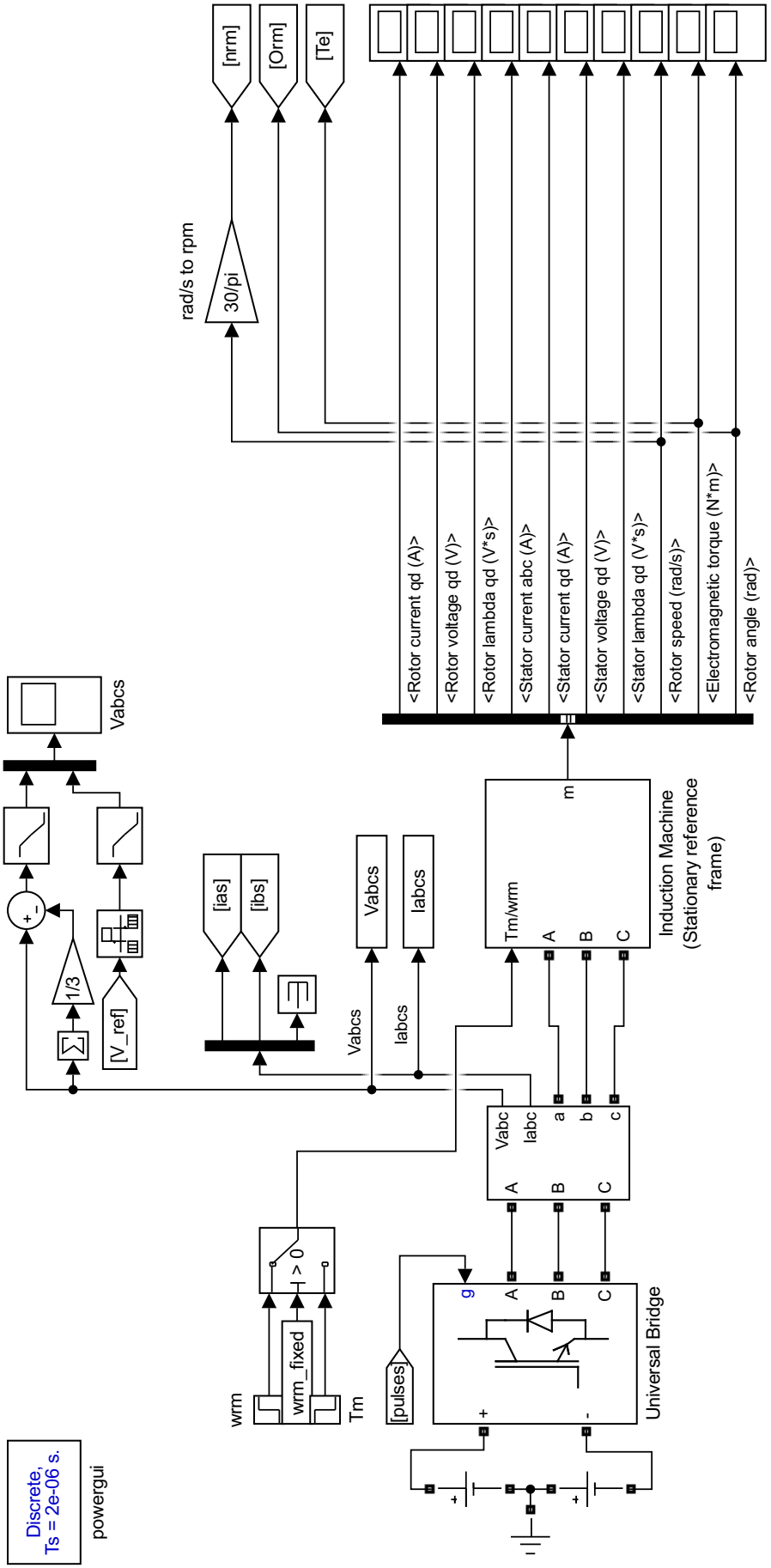

Figure B-4: Power system.

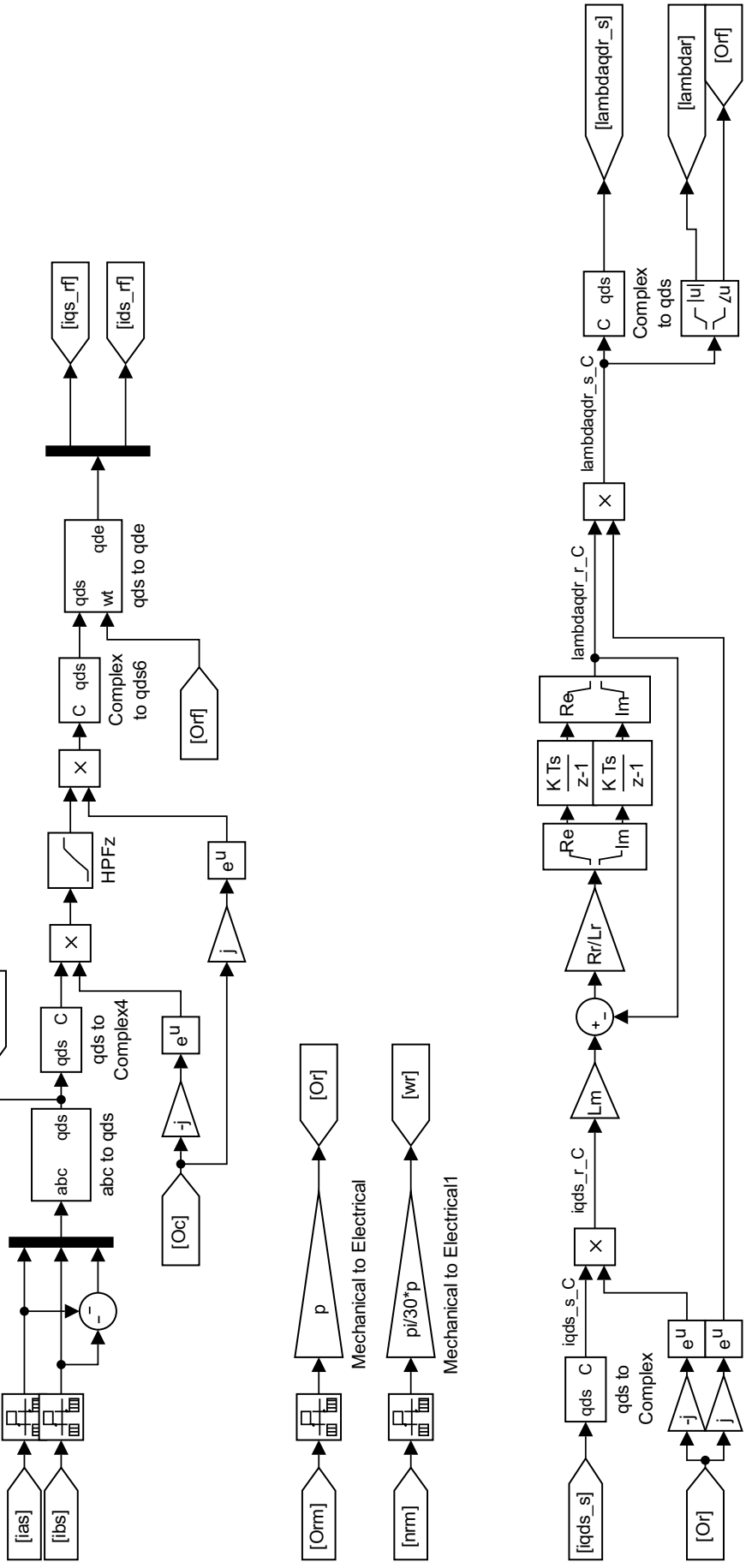

Figure B-5: Measurements and rotor flux observer.

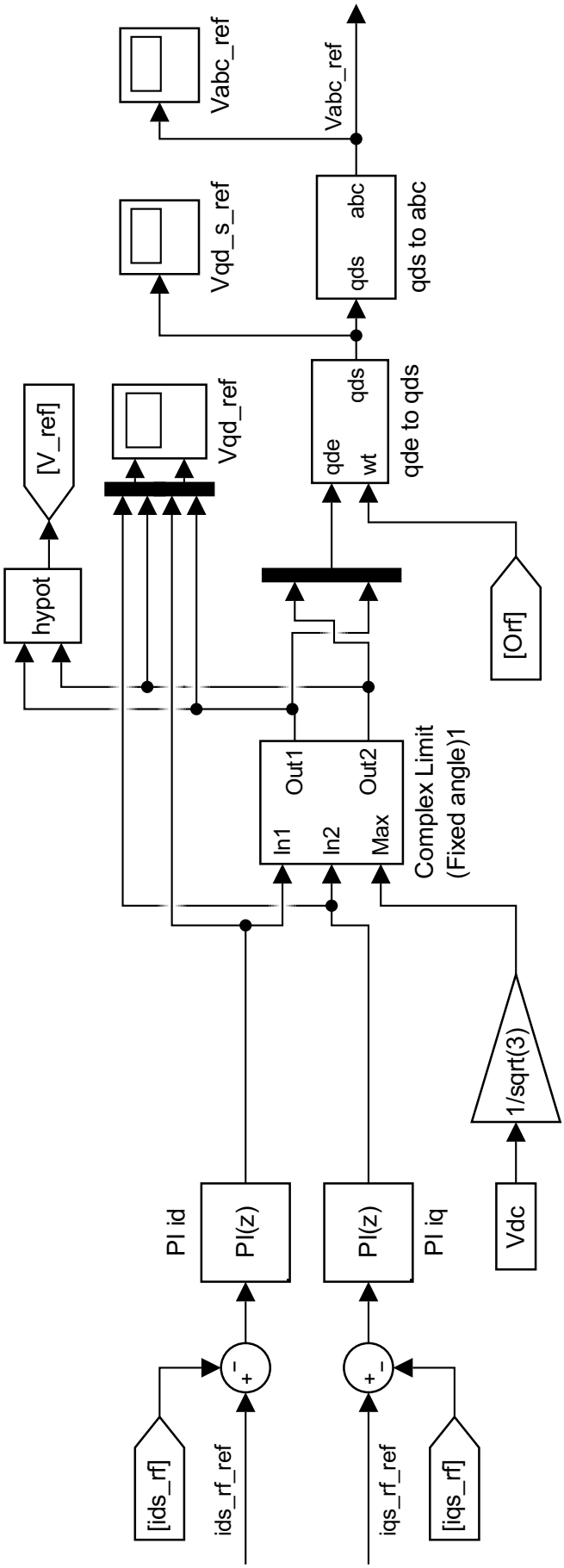

Figure B-6: Current control loop.

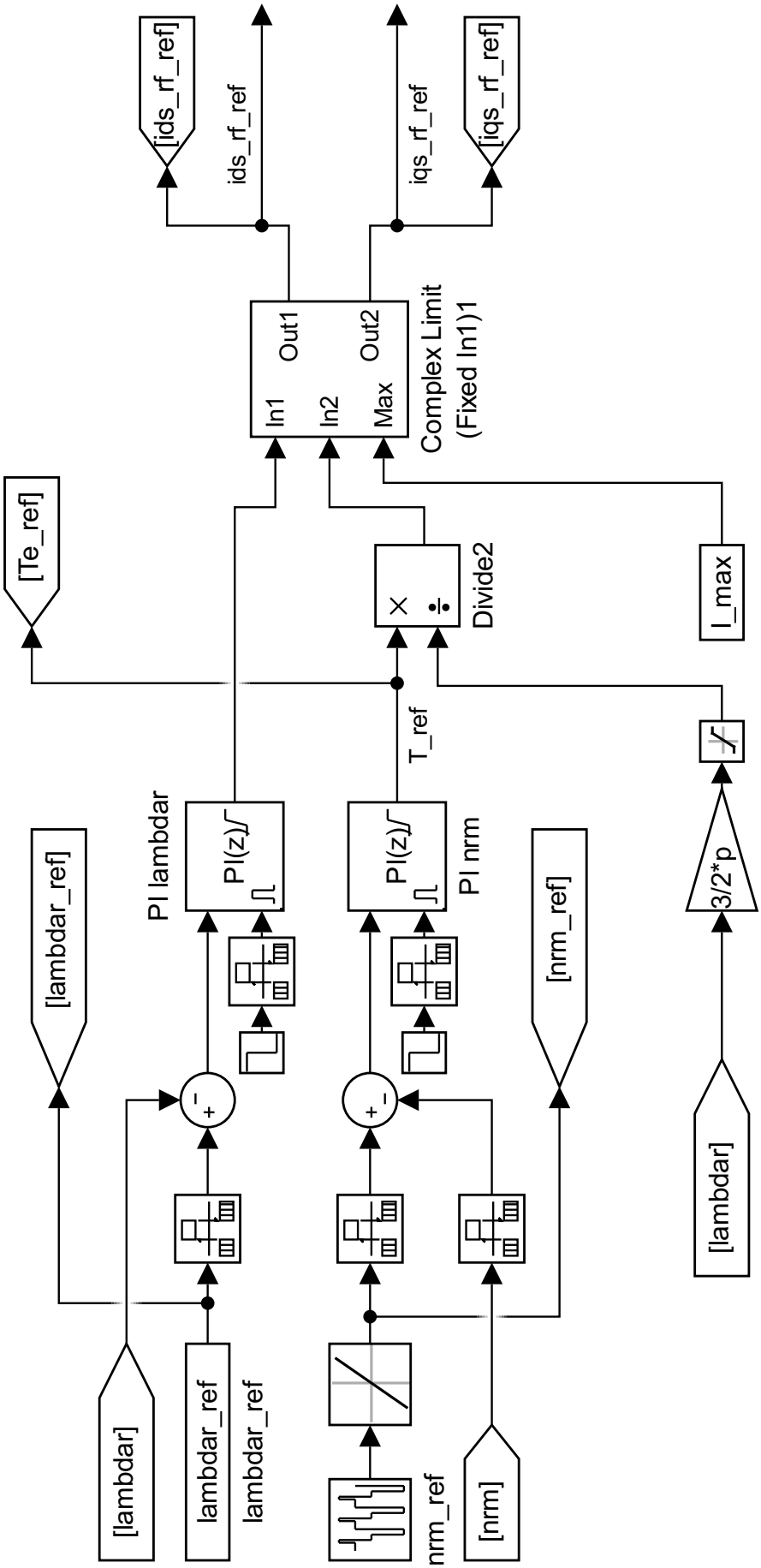

Figure B-7: Flux/speed control loop.

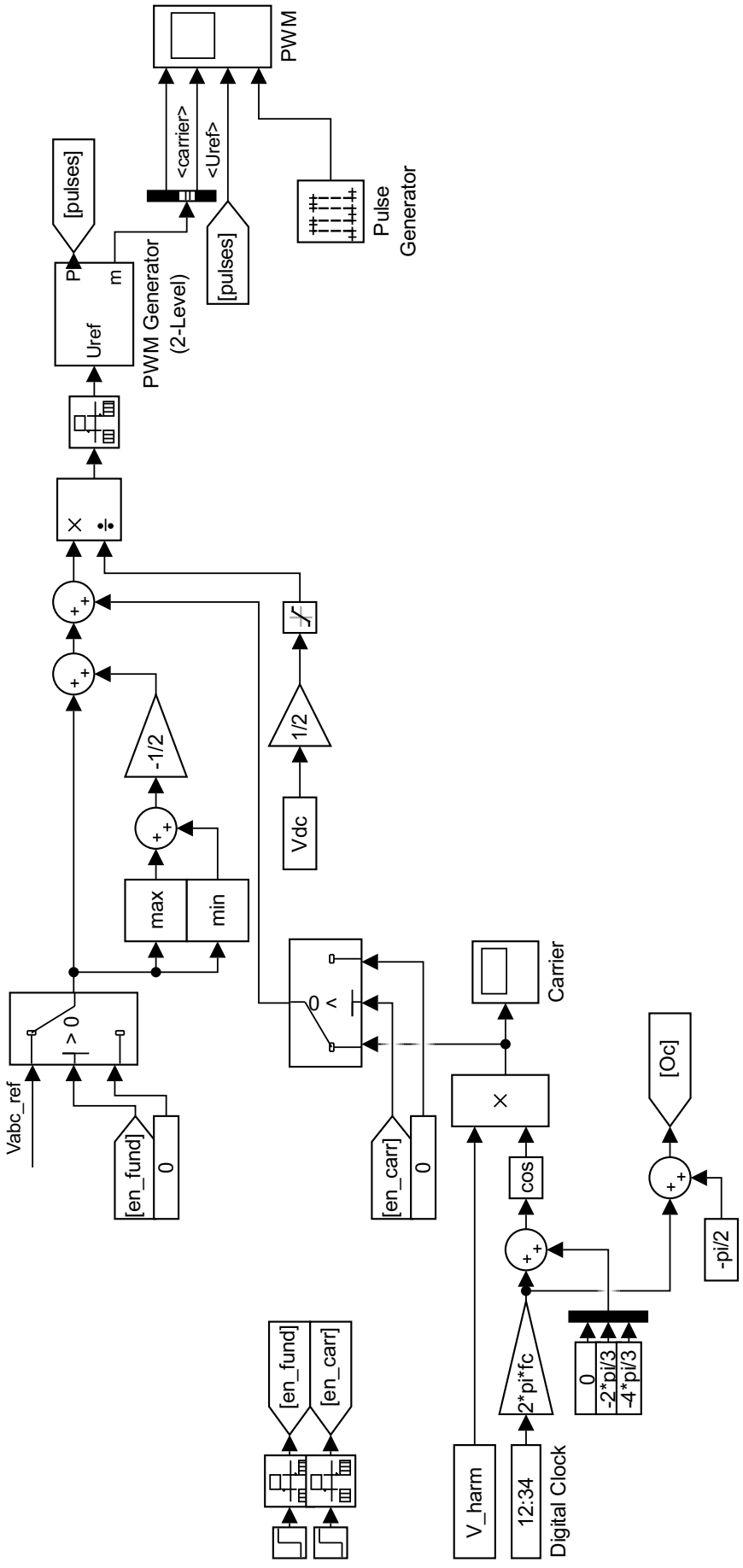

Figure B-8: Pulses generator.

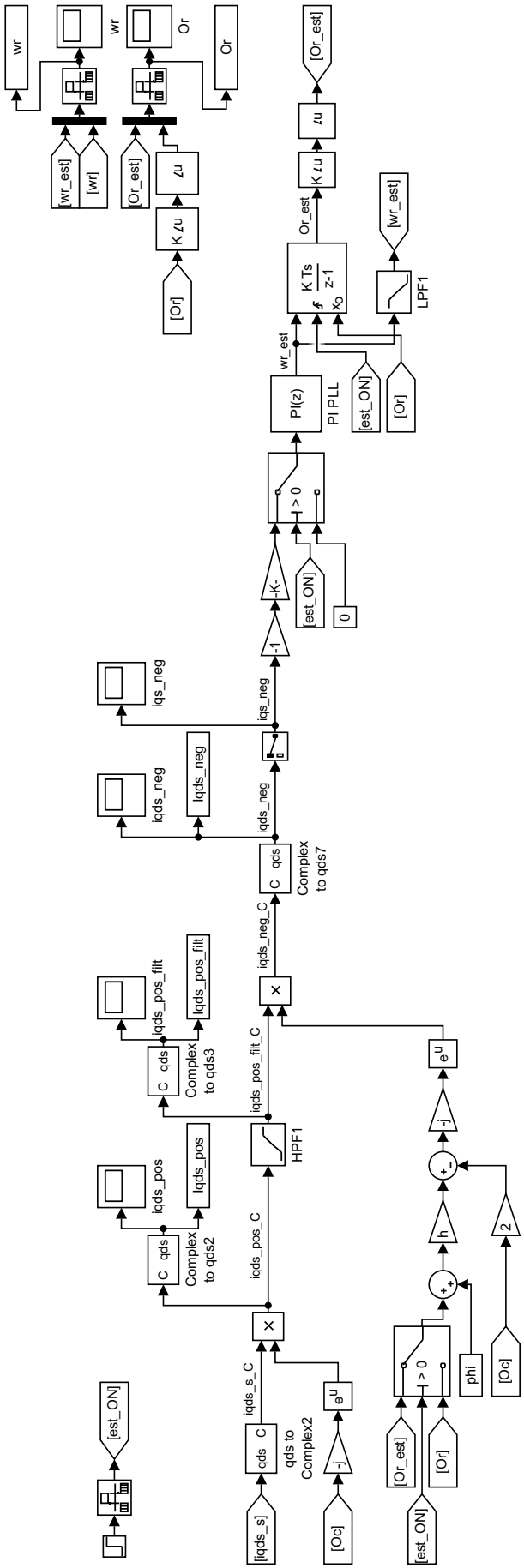

Figure B-9: Rotor angle estimator for FOC simulation with pure carrier frequency excitation.

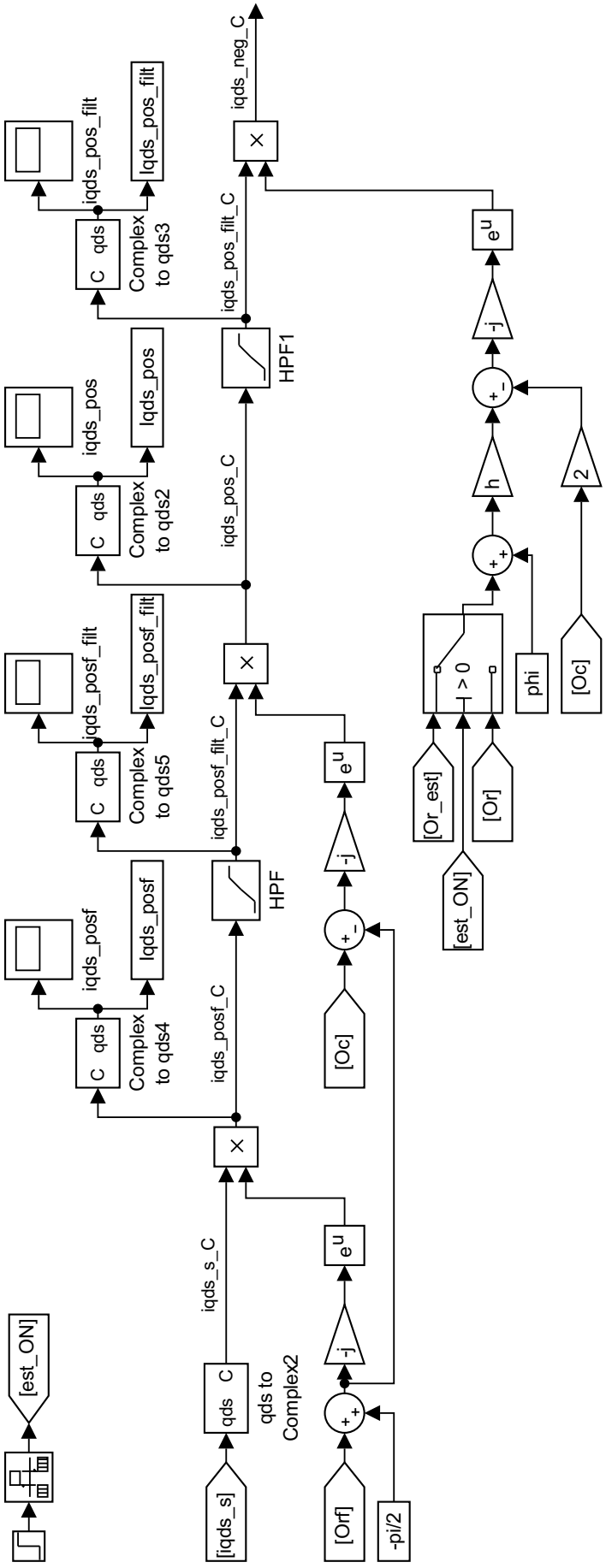

Figure B-10: Modification of rotor angle estimator for FOC simulation including fundamental excitation.

Bibliography

[1] M. W. Degner and R. D. Lorenz. Using multiple saliencies for the estimation of flux, position, and velocity in ac machines. *IEEE Transactions on Industry Applications*, 34(5):1097–1104, Sep 1998.

[2] M. W. Degner and R. D. Lorenz. Position estimation in induction machines utilizing rotor bar slot harmonics and carrier-frequency signal injection. *IEEE Transactions on Industry Applications*, 36(3):736–742, May 2000.

[3] Michael W. Degner. *Flux, position, and velocity estimation in AC machines using carrier signal injection*. PhD thesis, University of Wisconsin-Madison, 1998.

[4] Pablo García Fernández. *Control y diagnóstico de máquinas de alterna mediante el rastreo de asimetrías espaciales*. PhD thesis, Universidad de Oviedo, 2006.

[5] P. García, D. Reigosa, F. Briz, C. Blanco, and J. M. Guerrero. Sensorless control of surface permanent magnet synchronous machines using the high frequency resistance. In *2011 IEEE Energy Conversion Congress and Exposition*, pages 2709–2716, Sept 2011.

[6] K. D. Hurst, T. G. Habetler, G. Griva, and F. Profumo. Speed sensorless field-oriented control of induction machines using current harmonic spectral estimation. In *Industry Applications Society Annual Meeting, 1994., Conference Record of the 1994 IEEE*, pages 601–607 vol.1, Oct 1994.

[7] M. Ishida and K. Iwata. A new slip frequncy detector of an induction motor utilizing rotor slot harmonics. *IEEE Transactions on Industry Applications*, IA-20(3):575–582, May 1984.

[8] P. L. Jansen and R. D. Lorenz. Accuracy limitations of velocity and flux estimation in direct field oriented induction machines. In *1993 Fifth European Conference on Power Electronics and Applications*, pages 312–318 vol.4, Sept 1993.

[9] P. L. Jansen and R. D. Lorenz. A physically insightful approach to the design and accuracy assessment of flux observers for field oriented induction machine drives. *IEEE Transactions on Industry Applications*, 30(1):101–110, Jan 1994.

[10] D. W. Novotny and T. A. Lipo. *Vector Control and Dynamics of AC Drives*. Oxford University Press, 1996.

[11] M. Schroedl. Sensorless control of ac machines at low speed and standstill based on the inform method. In *Industry Applications Conference, 1996. Thirty-First IAS Annual Meeting, IAS '96., Conference Record of the 1996 IEEE*, volume 1, pages 270–277 vol.1, Oct 1996.